Core Photoelectron Spectroscopy and Chemical Reactivity of a Series of Aliphatic Alkenes and Alkynes

Alf Holme

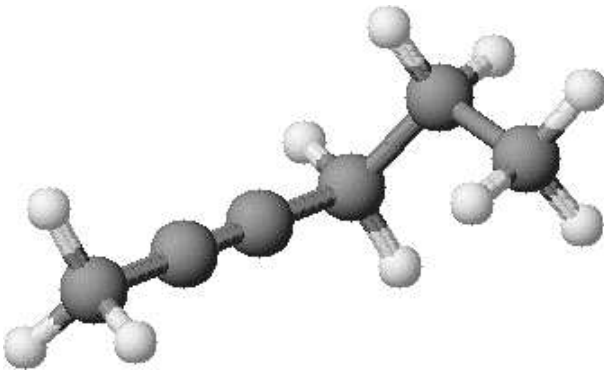

Cand. Scient. Thesis
Department of Chemistry
University of Bergen, Norway

December 2002

Acknowledgements

The experimental data of the thesis was acquired at the MAX-II ring at MAX-lab in Lund, Sweden. The theoretical calculations and data analysis were performed at the Chemistry Department at the University of Bergen.

I want to thank for financial support from the EC Access to Research Infrastructure Program (ARI) and computing time from the Programme for Supercomputing, which was financed by the Research Council of Norway (NFR).

I wish to give a special thank to my supervisor Prof. Leif J. Sæthre for all his assistance and guidance through this thesis. He has always been willing to answer questions and help me whenever needed. With his support, knowledge, enormous enthusiasm, and everlasting cheerful mood, working with him has been nothing but a pure pleasure and a really good experience.

I also want to thank Prof. Knut J. Børve for all his assitance related to the theoretical and computational part of this thesis. He has always been willing to discuss problems and answer questions.

I wish to thank Karoline Wiesner for a great time and great assistance at beamline I411 at MAX-lab. Many thanks to Prof. Svante Svensson and Prof. T. Darrah Thomas for fruitful and interesting discussions. I also wish to thank the staff at MAX-lab for their hospitality and service.

Finally, I wish to thank all fellow students, friends at the Chemistry Department, all my friends elsewhere, my father and mother, my three sisters, and especially my brother Frank for all support during the work with this thesis.

Bergen, December 2002

Alf Holme

Contents

Chapter 1

1 Introduction

The first chapter will give a brief description of electrophilic addition reactions and some of its reaction mechanisms, photoelectron spectroscopy, and the connections between these. In addition, ab initio molecular orbital calculations are used to aid in the analysis of the data and in the interpretation of the results.
Electrophilic additions to alkenes and alkynes have been of considerable interest among chemists for many decades. Some of the questions focused on throughout the years are:

- What are the reaction mechanisms in the electrophilic additions to alkenes and alkynes?
- How reactive are the alkenes compared to the alkynes in electrophilic addition reactions?
- What are the rates of the reactions, regiochemistry, stereochemistry, rearrangements, side products etc. in this class of reactions?

In this thesis, attention will be focused on the question in the middle. As will be seen, the reactivity difference between alkenes and alkynes in acid-catalyzed hydration reactions vanishes as the carbon chain length increases. For the shorter carbon chain lengths, the alkenes turns out to be the most reactive ones in the same type of electrophilic addition reactions. The data indicate what kind of reaction mechanism the alkenes are following in hydration reactions. The Ad_E2[1] mechanism is the one which is the most probable. This is also the most probable reaction mechanism for the alkynes with the longest carbon chains. For alkynes with shorter carbon chains, it is hard to tell because of the possibility of an Ad_E3 mechanism to occur (see section 1.1.1 for further information on the Ad_E2 and Ad_E3 mechanisms). The starting point of this thesis was the discussion of the electrophilic addition to alkynes by H. M. Weiss and T. T. Tidwell published in references [1] and [2], respectively. H. M. Weiss presents different evidence in support of an Ad_E3 mechanism to be dominating in the electrophilic addition to alkynes, and suggests that it is time for our textbooks to drop the (unstabilized) vinyl cation as the predominant intermediate.

[1] The term Ad is an abbreviation for addition, E for electrophilic, and the last number is the order of the reaction (the number of reactants in the rate determining step).

T. T. Tidwell discusses each argument presented in reference [1]. Tidwell suggests that the main features of electrophilic additions to alkenes and alkynes are very similar. He emphasizes the fact that vinyl cations are *not* difficult to form, and there are no major differences in the reaction mechanisms of alkenes and alkynes with electrophiles.
In these articles, the authors confine their discussion to the *reaction mechanisms* in electrophilic additions to alkenes and alkynes. One is arguing for the Ad_E3 mechanism instead of Ad_E2 in electrophilic additions to alkynes, while the other is arguing for a similarity between alkenes and alkynes with respect to reaction mechanisms. There is thus a clear disagreement between these two authors. This will be discussed further in the following.

1.1 Electrophilic addition reactions to aliphatic alkenes and alkynes

The electrophilic addition reaction is one of the most general and useful reaction of alkenes and alkynes for synthetic purposes. In this chapter, it is focused on reactions that proceed through polar intermediates or transition states. The reason for this, is the correlation to results from photoelectron spectroscopy. This will be further discussed in section 1.2.2.

1.1.1 The Ad_E2 and Ad_E3 reaction mechanisms

Two very important reaction mechanisms in electrophilic addition reactions are the Ad_E2 and Ad_E3 mechanisms [3], [4]. The symbol Ad_E2 signifies that the mechanism is a bimolecular second order reaction with respect to the alkene/alkyne and electrophile. This mechanism goes through a carbocation intermediate illustrated in figure 1 and figure 2. In this case an alkene is used in the reaction as an example.
In the three-step reaction, there is a prior dissociation step of the electrophilic reagent. This step does not appear in the two-step reaction.
The Ad_E3 mechanism is a termolecular third order reaction with respect to the alkene/alkyne and two reagents. This mechanism is illustrated in figure 3 with an alkene used as an example.
In this reaction, two reagents orient around the alkene/alkyne and react simultaneously with the double or triple bonded carbon atoms *without* making a carbocation. As will be seen, this is a very important difference between an Ad_E2 and Ad_E3 mechanism.
There are many factors determining which mechanism to follow. The stereochemistry and substituents of the alkenes/alkynes, reaction conditions (temperature and pressure), reagents, and concentrations of reagents are some of the factors. In section 1.1.6, the stereochemistry of electrophilic addition to aliphatic alkenes and alkynes will be discussed. What about the substituent effects of the alkenes and alkynes?
If an alkene or alkyne carry a strong electron withdrawing substituent situated close to the double or triple bond, the carbocation intermediate in an eventual Ad_E2 mechanism is expected to be relatively unstable. In order to

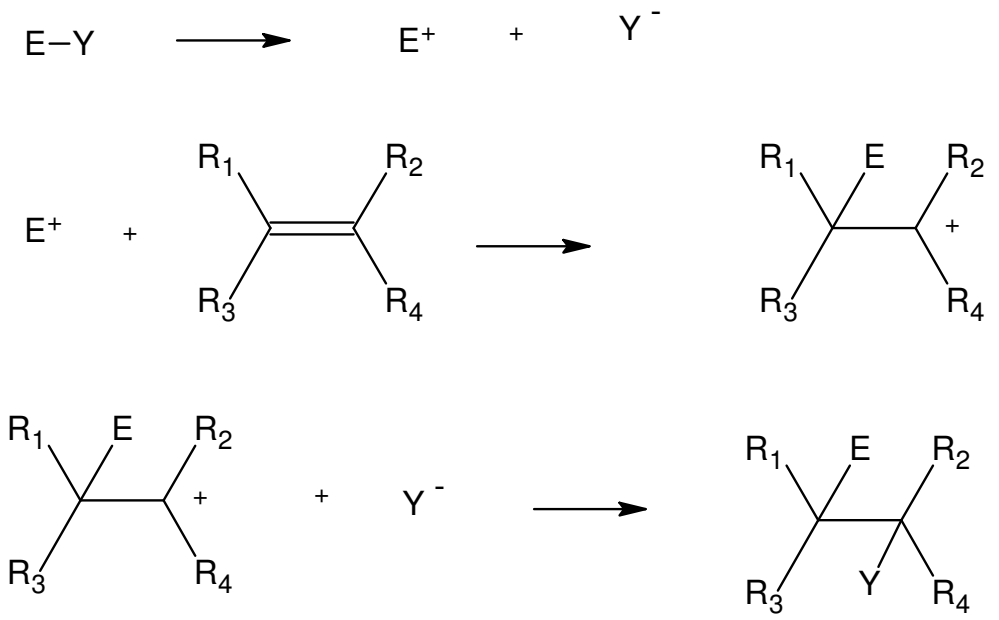

Figure 1: A three step illustration of the Ad_E2 mechanism where E is the electrophile and Y is the nucleophile.

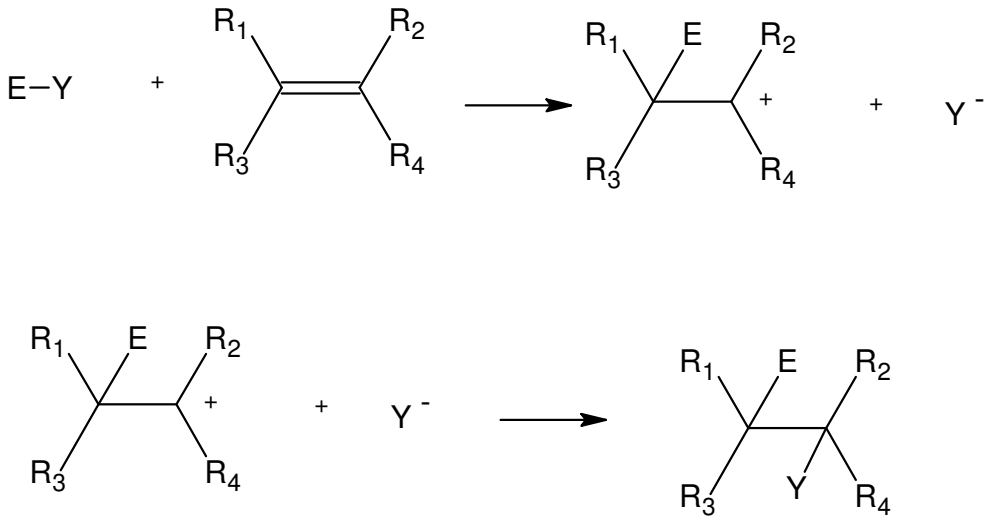

Figure 2: A two step illustration of the Ad_E2 mechanism where E is the electrophile and Y is the nucleophile.

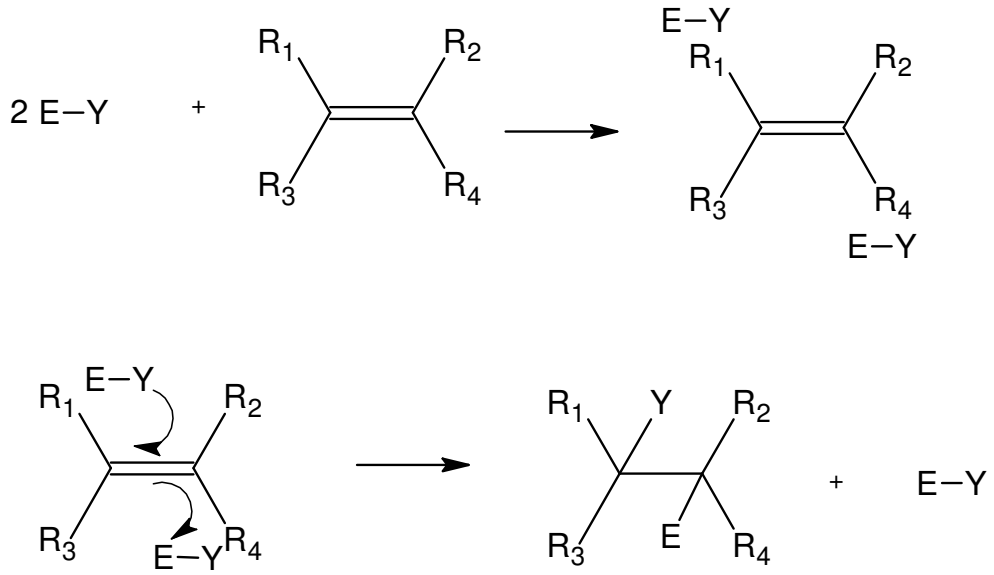

Figure 3: A two step illustration of the Ad_E3 mechanism where E is the electrophile and Y is the nucleophile.

stabilize this intermediate, it is necessary to orient a nucleophile to the carbocation at the same time as the electrophile is added to the alkene or alkyne. This is the Ad_E3 mechanism and is expected to be the dominating mechanism in this case. This is not necessarily the case in all electrophilic addition reactions to alkenes and alkynes with strong electron withdrawing substituents, because the influence of many other factors like those mentioned above can give a quite different result. This is just mentioned as a general example. In general, the alkenes are expected to follow the Ad_E2 mechanism while the alkynes are expected to follow the Ad_E3 mechanism. This can be explained in the same way. The carbocation (vinyl cation) intermediate of an alkyne in an Ad_E2 mechanism is more unstable than a sp^2 hybridized carbocation of an alkene following the same mechanism. Because of this, we can expect that the alkyne will follow an Ad_E3 mechanism while the alkene follows the Ad_E2 mechanism. Again, this is not necessarily the case if the alkyne for instance has a very good electron donating substituent which can stabilize a vinyl cation intermediate in an Ad_E2 reaction. Thus, the choice of mechanism is definitely not obvious.

1.1.2 The Markovnikov rule

An electrophilic addition reaction can be *regioselective, regiospecific, stereoselective* or *stereospecific*. A regioselective reaction is a reaction where one product is formed in greater amount than other possible products. The term *regio* is pointing towards the reactive atom(s) of the molecule. A regiospecific reaction gives exclusively only one product. The words selective and specific have the same meaning for stereoselective and stereospecific reactions, but in this case it is focused on the different stereoisomers formed in

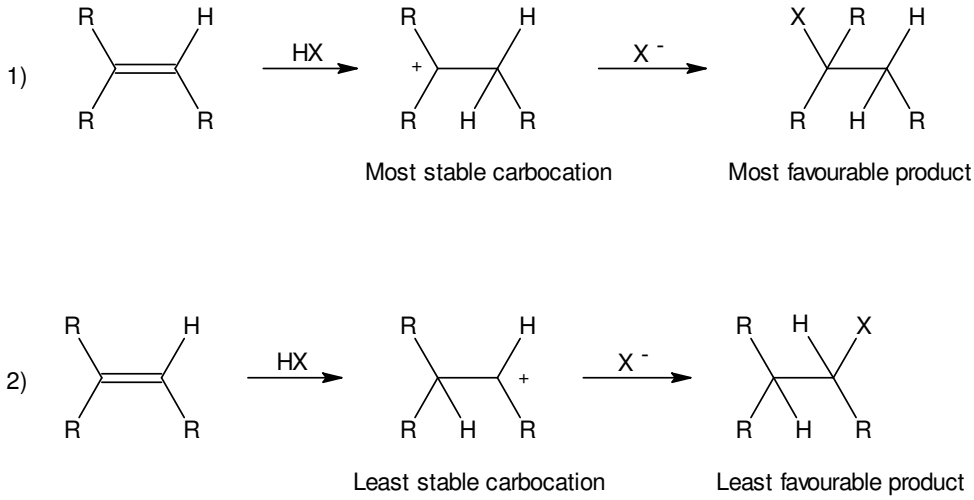

Figure 4: Two possible reaction paths in which path 1 is favoured due to the Markovnikov rule.

a chemical reaction. If the R-stereoisomer is formed in a greater amount than the S-isomer, this is a stereoselective reaction. If the R-isomer is formed exclusively, this is a stereospecific reaction[2].
In electrophilic additions to alkenes and alkynes, it is generally found that a regioselective reaction takes place. For instance, the major product formed in additions of hydrogen halides, HX, to an unsymmetrical alkene, is the one where X^- is bonded to the most substituted carbon atom. This can be explained by comparing the stabilities of the two different carbocation intermediates. The carbocation with the positive charge located at the carbon atom with the largest substituents turns out to be the most favourable. In addition to the electron donating effect, the reason for this is the bigger possibility of delocalizing the positive charge in the carbocation. This reaction has followed the *Markovnikov rule* which states the following:

In additions of hydrogen halides to unsymmetrical alkenes, the halide is attached to the carbon atom with the smallest number of hydrogen atoms.

This rule is illustrated in figure 4 where reaction path 1 gives the most favourable product.
In the next few sections, different types of electrophilic addition reactions will be discussed.

1.1.3 Electrophilic addition of hydrogen halides, HX

As mentioned earlier, the addition of hydrogen halides is generally found to follow the Markovnikov rule. Some of the mechanisms involved in this type of

[2]The R, S (R=rectus and S=sinister) convention is a scheme to denote configuration about a chiral centre in a molecule. A chiral molecule cannot be superimposed on its mirror image.

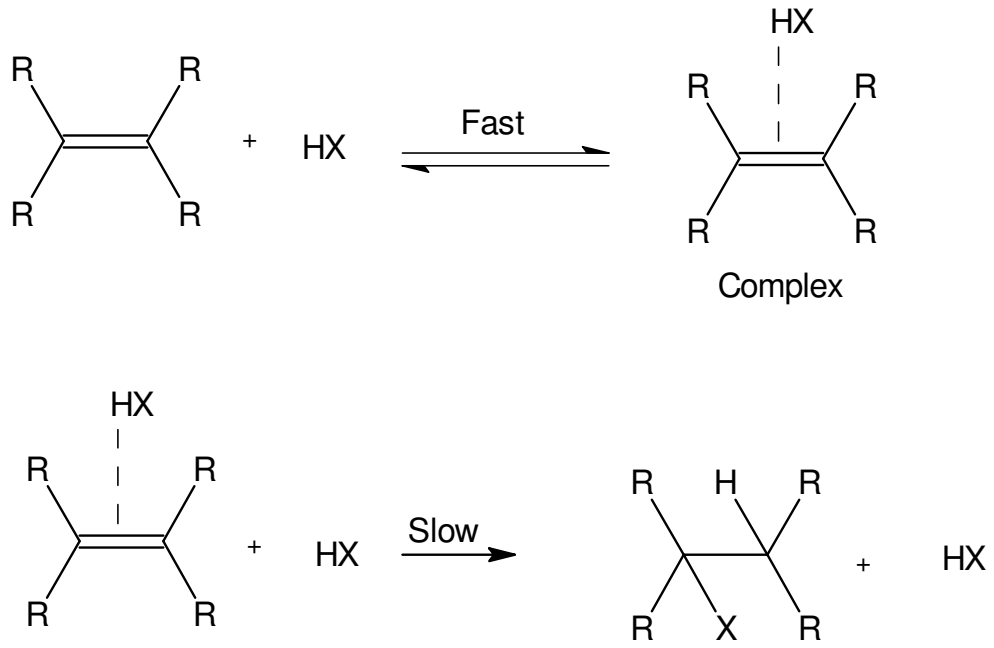

Figure 5: A termolecular addition reaction (Ad_E3) between a hydrogen halide-alkene complex and a second hydrogen halide.

addition reactions, are the Ad_E2 and Ad_E3 mechanisms. If these second and third order reactions are irreversible, we can write the respective rate expressions as follows:

$$\frac{d[alkene]}{dt} = -k[alkene][HX] \tag{1}$$

$$\frac{d[alkene]}{dt} = -k[alkene][HX]^2 \tag{2}$$

In these expressions, k is the rate constant and gives information about how fast a chemical reaction occurs. Because of this property, this parameter can be correlated to chemical reactivity. This will be further discussed in section 1.2.2.

There are other possible mechanisms in which free-radical chain addition occurs in competition with the ionic addition. These reactions are often initiated by peroxide impurities or by light and leads to the anti-Markovnikov addition product. These reactions will not be further discussed in this thesis.

In Ad_E3 additions to alkenes, a complex is formed between the alkene and hydrogen halide with the second hydrogen halide molecule. This happens because of the little likelihood of productive termolecular collisions. This is illustrated in figure 5. This figure has similarities with the reaction shown in figure 3.

In additions of hydrogen halides to alkenes, they can add *syn* or *anti*. When they add *syn*, the hydrogen halide molecules add to the alkene on the same side. When they add *anti*, the hydrogen halide molecules add to the alkene on

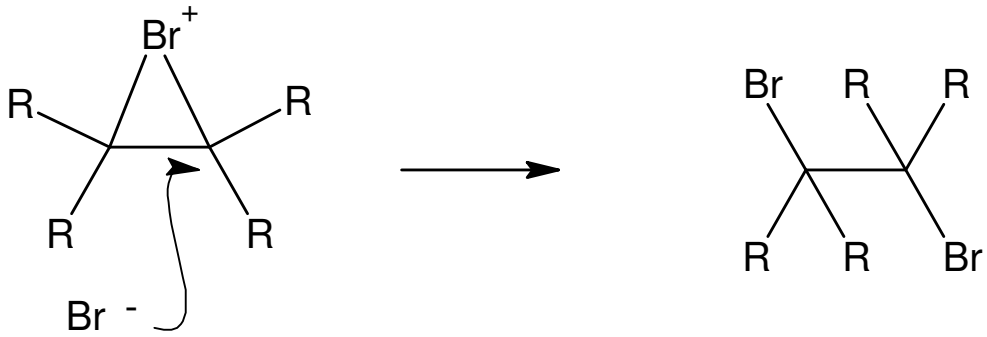

Figure 6: An illustration of an *anti* addition that proceeds through a bromonium ion.

both sides of the double bond. *Anti* additions occur in Ad_E3 reactions as illustrated in figures 3 and 5. The *anti* addition is dominating in the addition of hydrogen halides to unconjugated alkenes.

1.1.4 Electrophilic addition of halogens, X_2

Chlorinations and brominations of alkenes are among the most general of organic reactions. Two important questions have been raised in this connection:

- Is there a discrete positively charged intermediate, or is the addition concerted?
- If there is a positively charged intermediate, is it a carbocation or a cyclic halonium ion?

The results of numerous stereochemical studies support an *anti* addition in the brominations of alkenes that contain substituents that weakly stabilize a carbocation intermediate. The extent of *syn* addition becomes much larger (can become the dominant pathway) when the alkene is conjugated with an aryl group. Chlorinations tend to follow the same pattern.
The *anti* stereochemistry can be explained by taking a closer look at the bridged bromonium ion intermediate that is created in the addition of Br^+ to the alkene. As can be seen in figure 6, the nucleophilic Br^- attacks one of the carbon atoms on the "back-side" of the bromonium ion. This ruptures one of the C-Br bonds which finally gives the *anti* addition. This is the case of the more stable bridged intermediates. However, if the bridged intermediate is very unstable, the intermediate exists in a shorter time period than the Br^- needs to orientate to the back-side of the bromonium ion and react. Because of this, the *syn* additions will predominate. This structure is also called a σ *complex* because the valence bond representation implies a full or partial σ bond between the olefinic carbon atoms and the bromonium atom [5].
On the other hand, a freely rotating open carbocation is expected to give both *syn* and *anti* addition products. If the intermediate were an ion pair that

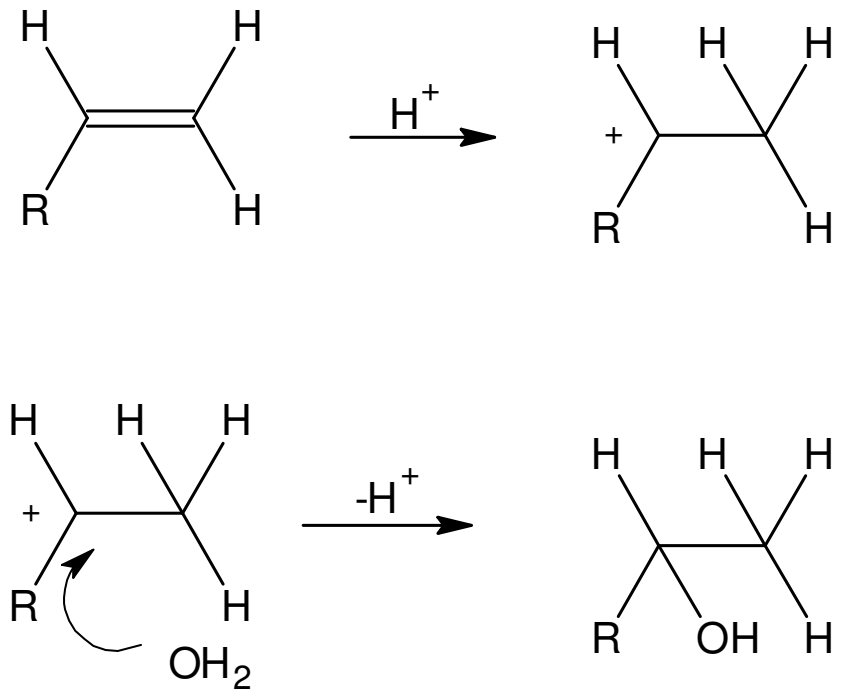

Figure 7: An illustration of acid-catalyzed hydration of an alkene.

collapsed faster than rotation about the C-C bond, *syn* addition could predominate. Aliphatic systems normally go through the bridged intermediate, while styrenes are the borderline cases. The stability of the bridged intermediate increases with increasing halide cation, X^+ (increasing atomic weight). The reason for this trend is the halides' increasing polarizability and ability to carry a positive charge.

1.1.5 Acid catalyzed hydration reactions

In addition to the gas phase basicities (GB) and proton affinities (PA) (further discussed in chapter 7), the reactivity data used in this thesis is based on acid-catalyzed hydration reactions. This is a group of electrophilic additions to alkenes and alkynes where alcohols (R-OH) and ketones (R-CO-R) are formed. This can be viewed as an Ad_E2 reaction involving a carbocation intermediate. The alkene is protonated and the carbocation is then captured by water. This is shown in figure 7.
When an alkyne is protonated and hydrated, we end up with *tautomerism*. This is dynamic isomerism in which two isomers are directly interconvertible. There is an equilibrium between the alcohol and ketone isomer. These reactions are summarized in figure 8.
The observed products from these reactions support the Markovnikov rule. The rate determining step in these reactions is observed to be the protonation step which gives the carbocation intermediate. The addition of the water molecule is evidently fast compared to the deprotonation of the carbocation

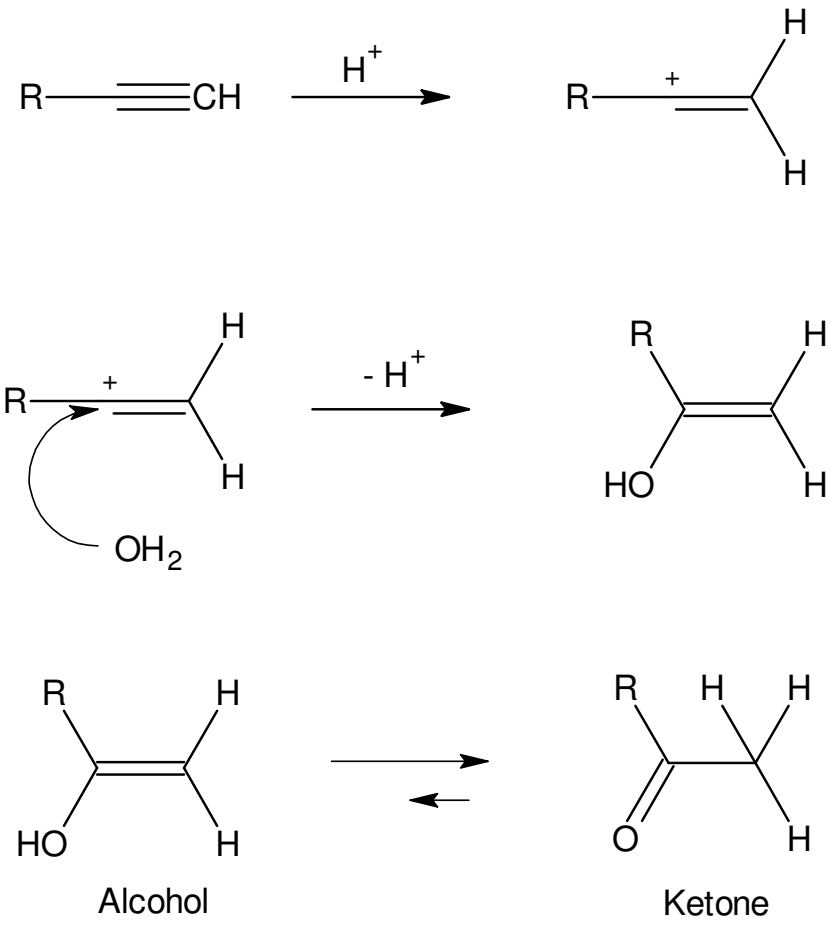

Figure 8: An illustration of acid-catalyzed hydration of an alkyne.

intermediate. Therefore, the products in the hydration reactions are mainly alcohols and ketones.

In addition to the Ad_E2 mechanism, it is also a possibility for an Ad_E3 mechanism to occur where one water molecule is reacting with the alkene/alkyne at the same time as the proton does. An alternative mechanism in alkene hydrations, is the water attack on an alkene-proton complex. The reaction mechanism in this case is Ad_E3, and is illustrated in figure 9.

Because of the tautomerism shown in figure 8, we have to be careful in the interpretation of the rate constant k. In many published articles (including the ones previously referred to), the rates of the hydrations to some of the alkynes are measured by UV spectroscopy by observing the appearance of the carbonyl (R-CO-R) absorption. Because of the equilibrium between the alcohol and ketone, the rate constant k will be somewhat affected in the measurements. The rates of the hydrations of the alkenes and some of the alkynes are often measured by observing the decrease in the alkene/alkyne absorption, and will therefore be unaffected by any structural isomerism equilibrium.

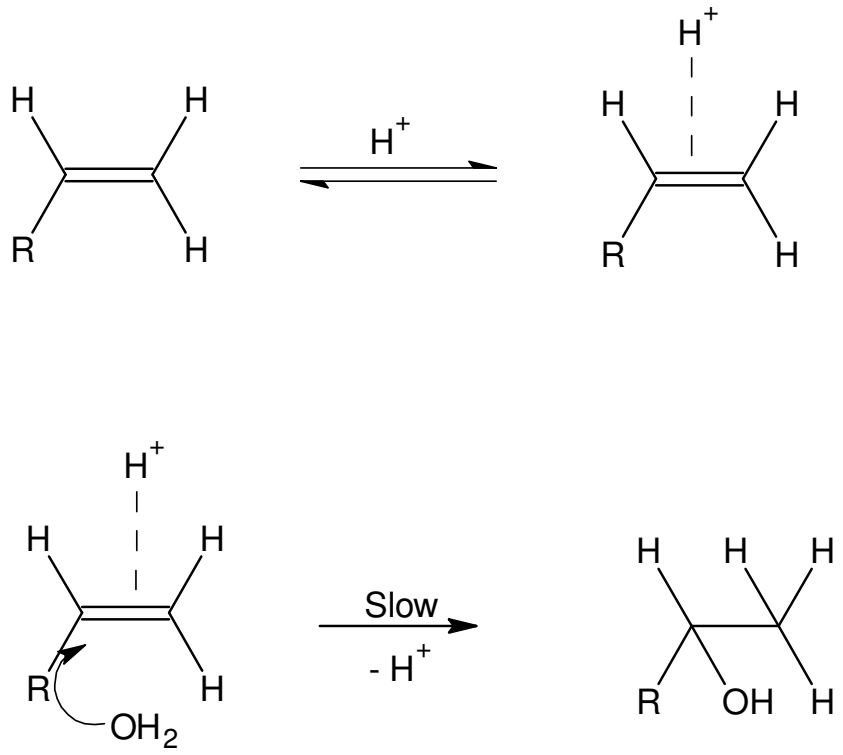

Figure 9: An illustration of a water attack on an alkene-proton complex.

1.1.6 The stereochemistry of electrophilic addition to aliphatic alkenes and alkynes

The term *stereochemistry* refers to the three-dimensional nature of molecules and to their space-filling properties. Our physical models (sticks and balls) and many of our computer models give a perception of the three dimensions and how the molecules really look like. The stereochemistry is important in order to understand reaction mechanistic patterns better. What is the energy involved in the change of stereochemistry of the molecules during a reaction? As we will see in chapter 7, correlations between reactivity data from acid-catalyzed hydration reactions and results from *photoelectron spectroscopy* are only fairly good. The results from photoelectron spectroscopy does not take into account the stereochemical changes that take place in an acid-catalyzed hydration reaction. This may be one of the reasons for the bad correlations. However, the gas phase basicities (GB) and proton affinities (PA) were well correlated to the data from photoelectron spectroscopy.

1.2 Photoelectron spectroscopy (PES)

What is photoelectron spectroscopy, and how can we use this technique to investigate chemical reactivity? These questions will be discussed in this and the following sections.
In photoelectron spectroscopy, the sample (gas, liquid, or a solid) is irradiated

with monochromatic photons. The expelled photoelectrons are then analyzed by means of an electron spectrometer/analyzer which is often combined with a preretardation electron lens. The energies and intensities of the photoelectrons are recorded, and also in many cases their angular distributions. The recorded kinetic energies of the electrons can be used to find the binding or ionization energies of the electrons. The ionization energy (IE) is related to the photon energy (E = hν) and kinetic energy (E_{KIN}) of the photoelectrons:

$$IE = h\nu - E_{KIN} \tag{3}$$

Here, h is Planck's constant (h = 6.626×10^{-34} Js) and ν is the frequency (s^{-1}) of the light. Both core and valence electrons can be ionized and measured. Photoelectron spectroscopy is not only used to study chemical reactivity, but also different physical processes taking place in the photoionization of the molecules (or atoms). These can be processes like *vibronic coupling*, *shake up*, and *post collision interaction (PCI)*. In addition, different types of *vibrations* of the molecules can be studied. These physical processes are further described in chapter 3.
Photoelectron spectroscopy was essentially developed during the 1950's and 1960's [6]. Earlier attempts following the discovery of the photoelectric effect (discussed in section 1.2.1) were too crude, and it was largely impossible to use photoelectron spectra to study atoms, molecules, and solids. In the beginning, the light (photons) was generated using sources like Al(Kα), Mg(Kα), He^I, and He^{II} etc (these are still used).
Nowadays, the experiments in photoelectron spectroscopy are carried out with light mainly generated from *synchrotrons* (further discussed in chapter 2). In this case, the light is generated from charged particles spiraling around magnetic-field lines in space. Natural synchrotron radiation is as old as the stars! For instance, the light we can see from the Crab Nebula is synchrotron radiation [7].
Usable synchrotron radiation is only a half-century old. The first observation came at the General Electric Research Laboratory in Schenectady, New York, on April 24, 1947. Since that time, synchrotron radiation has become a premier research tool for the study of matter as the facilities around the world constantly have evolved to provide this light in ever more useful forms.

1.2.1 The photoelectric effect

Since photoelectron spectroscopy and all the other spectroscopies using synchrotron radiation is based on the *photoelectric effect*, it is natural to give some information about it.
In 1887, during electromagnetic-wave experiments, Heinrich Hertz discovered the *photoelectric effect* [8]. When light struck a metal surface, some electrons near the surface absorbed enough energy to overcome the attraction of the positive ions in the metal and escape into the surrounding space.
Experiments carried out by the German physicists Wilhelm Hallwachs and Philipp Lenard during the years 1886-1900, showed that when monochromatic light fell on the metal plate shown in figure 10 [9], no photoelectrons at all

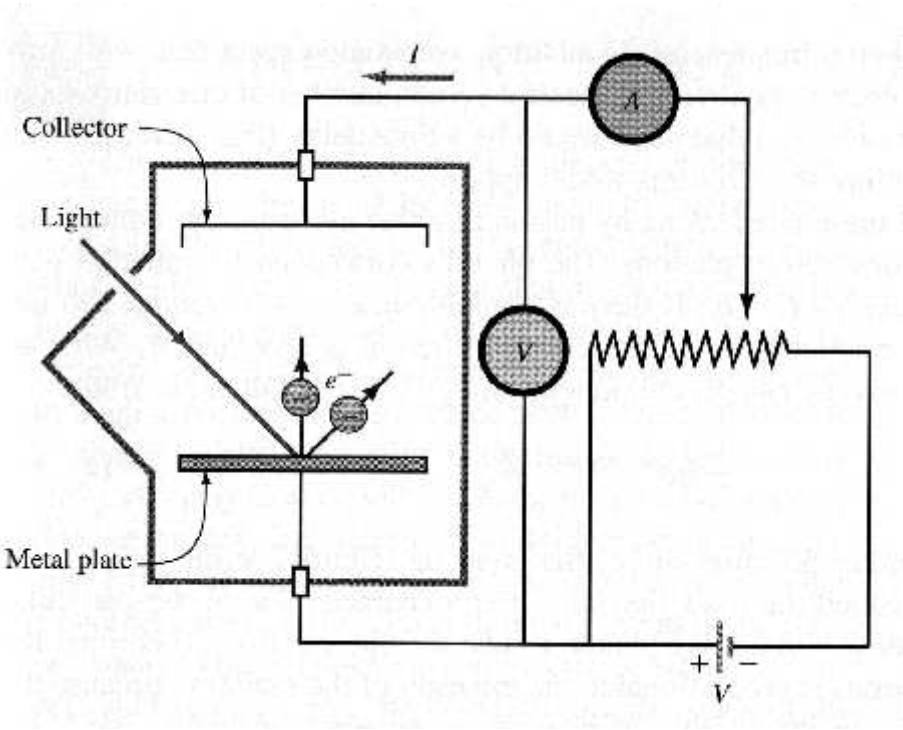

Figure 10: Schematic diagram of the experimental setup for measurement of the photoelectric effect.

were emitted unless the frequency of the light was greater than some minimum value called the **threshold frequency**. When the frequency ν was greater than the threshold frequency, some electrons were emitted from the metal plate with substantial initial speeds. If the intensity of the light was increased while its frequency was constant, the current leveled off at a higher value which showed that more electrons were emitted per time unit while the kinetic energies of the photoelectrons were the same. However, when the frequency of the monochromatic light was increased, the kinetic energies of the photoelectrons increased proportionally. These observations could not be explained by classical mechanics and electrodynamics.

The observed phenomena result from the *quantum* nature of radiation. Electromagnetic radiation has both wave and particle properties. The energy in an electromagnetic wave is always emitted and absorbed in packages called *photons* or *quanta*, with energy proportional to the frequency of the radiation ($\nu = c/\lambda$). This correct analysis was developed by Albert Einstein in 1905 (which he won the Nobel prize in physics for) building on an assumption made 5 years earlier by Max Planck. The energy E of a photon is equal to a constant h (Planck's constant) times it's frequency ν (c is the speed of light (2.998×10^8 m/s) and λ is the wavelength of the light):

$$E = h\nu = \frac{hc}{\lambda} \tag{4}$$

A photon arriving at the surface of the metal plate is absorbed by an electron. This energy transfer is an all-or-nothing process. The electron gets all the energy of the photon or none at all. If this energy is greater than the **work function** ϕ, the electron may escape from the surface. The excess energy is conserved in the electron as kinetic energy, E_{KIN}. The relationship between the energy of the photon, the work function, and the kinetic energy of the electron is expressed in the following equation (m is the mass of the electron, and v_{max} is the velocity of the electron):

$$E_{KIN} = \frac{1}{2}mv_{max}^2 = h\nu - \phi \tag{5}$$

1.2.2 Photoelectron spectroscopy and chemical reactivity of aliphatic alkenes and alkynes

In photoelectron spectroscopy, molecules and atoms are core or valence ionized making them positively charged. For the same atom or molecule, the core ionization energy is higher than the valence ionization energy. The reason for this is the more strongly electrostatic attraction between the core electrons and the positively charged nucleus. The valence electrons are more shielded from the nucleus by the inner electrons which results in lower ionization energies.
In chemistry, chemical reactivity is a wide concept. There are many types or classes of chemical reactions that can take place in nature or in the laboratory. Some of these classes of reactions can be nucleophilic substitutions (S_N1, S_N2), electrophilic additions (Ad_E2, Ad_E3), elimination reactions (E1, E1cb, E2), aromatic substitutions, concerted reactions, and free-radical reactions. All of these reactions follow their own characteristic reaction mechanisms with one or several reaction steps. To determine the reactivity of a compound following a specific reaction mechanism, we need to investigate each reaction step in a chemical reaction.
Chemical reactivity can be measured by the *rate* of a specific reaction. The faster a reaction occur, the more reactive are the molecules (atoms) acting in the reaction. The magnitude of the rate is measured by a rate constant k. Another parameters used to measure chemical reactivity are the changes in enthalpy (ΔH) and Gibbs free energy (ΔG). ΔH is related to ΔG through the equation $\Delta G = \Delta H - T\Delta S$ where T is the absolute temperature in Kelvin and ΔS is the entropy changes.
A chemical reaction may consist of several reaction steps. The slowest reaction step is the one which determines the rate of the overall reaction. This step is called the *rate determining step* and will therefore decide the reactivity of the compound(s) following a specific mechanism. The rate determining step has the highest activation energy (E_a) in a reaction. This can be rationalized from the Arrhenius equation:

$$k = A \times e^{-\frac{E_a}{RT}} \tag{6}$$

In this equation, k is the rate constant, A is the Arrhenius constant, R is the

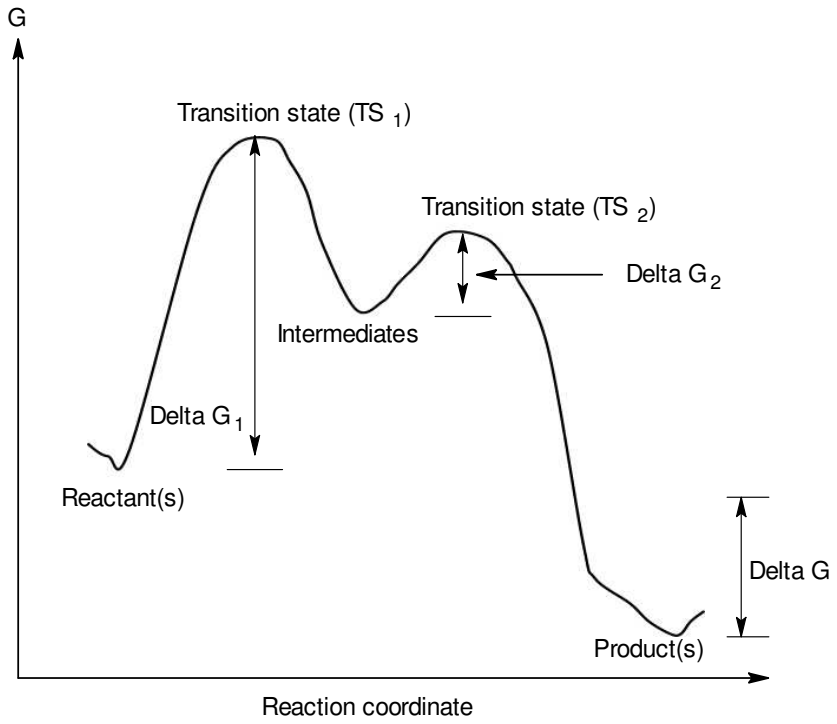

Figure 11: Potential energy diagrams for a two-step reaction.

gas constant, and T is the absolute temperature in Kelvin. The rate constant k drops if the activation energy increases. In figure 11, a reaction coordinate of a two-step reaction is shown as an example.

As we can see, ΔG_1 is larger than ΔG_2 (Δ is expressed as Delta). This means that the first step is the one with the highest activation energy (or highest ΔG since ΔG is directly proportional to E_a), and will therefore be the rate determining step in the reaction.

The rate determining step is usually the step where carbocations are formed. Electrophilic addition reactions is an example of a class of reactions in which the rate determining step is the carbocation formation. At this point, we can see a similarity between reactivity in electrophilic addition reactions and photoelectron spectroscopy. In photoelectron spectroscopy, we need a certain amount energy to ionize a molecule or an atom to get a product with a positive charge. The star sign (*) by the ionized ethene molecule in figure 12 denotes the ionized carbon atom. Because of the electronegativity of the ionized carbon atom, it pulls the π electrons towards itself and creates an electron pair which is localized at the same carbon atom. This electron transfer make the other carbon atom positively charged. Likewise in electrophilic proton additions, we need a certain activation energy in order to get a carbocation intermediate with a positive charge. In both cases, there is a formation of species with positive charges, and the total number of non-bonding and bonding electrons is the same. In figure 12, ethene (C_2H_4) is used as an example.

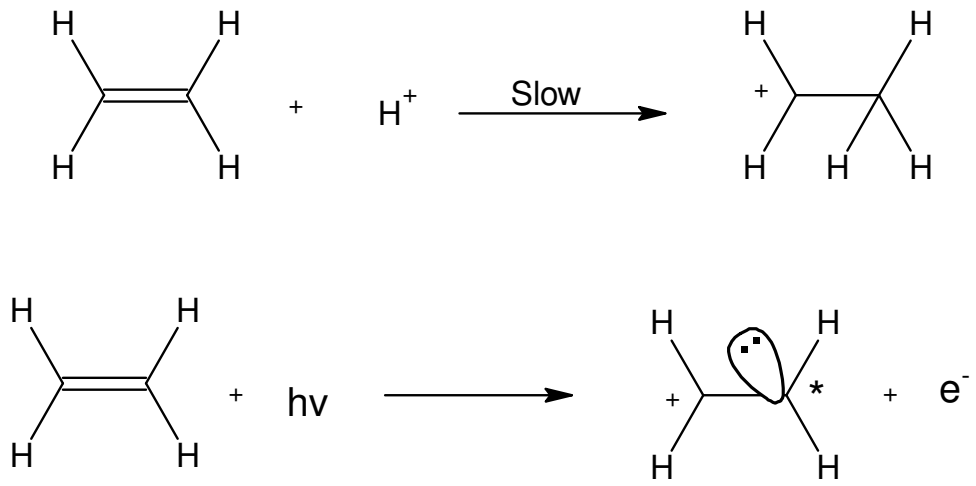

Figure 12: Rate determining protonation and core ionization of ethene.

Even though energies involved in rate determining protonations and core ionizations are not comparable, the *trend* in a series of molecules are comparable. In this thesis, this series will consist of alkenes and alkynes. As will be seen, the core ionization energies are used instead of the valence energies. The reason for this is the complexity of the valence spectra. In a hydrocarbon, there are molecular orbitals with different energies. These will all appear in the spectrum and give many peaks which are relatively difficult to analyze. It is more appropriate to core ionize the molecules. In this case, it is removed electrons from the 1s orbital in the carbon atoms. The result of this is a spectrum with fewer well defined peaks (the number of peaks is equivalent with the number of chemically inequivalent carbon atoms). These spectrums are more easy to analyze, and therefore the molecules are core ionized instead of valence ionized. In this case, we are not interested in the energy levels of the different valence orbitals. What we want, is to use the energies from the experimental spectrum in order to gain insight in chemical reactivity. In addition, different processes taking place in the molecules in the photoionization process are investigated. These processes, which are further described in chapter 3, have to be taken into account in the fitting procedure in order to get as good fitting as possible. The fitting procedure is further described in chapter 5.

1.2.3 Chemical shifts and chemical properties related to photoelectron spectroscopy

As we will see in chapter 5, the vibrational profiles of a specific molecule generated from a program called G2FC is fitted to an experimental spectrum in a fitting program called Igor Pro. The number of profiles is the same as the number of chemically inequivalent carbon atoms in the molecule. The ionization energy difference between the inequivalent carbon atoms in the molecule is called the *chemical shift* and is denoted ΔI.

The magnitude of ΔI gives us very important information. It gives us information about the reactivity of the carbon atoms within a molecule (intramolecular) and the reactivity of a specific carbon atom in one molecule compared to a carbon atom in a different molecule (intermolecular). On the basis of this, we are able to predict the reactivity within a series of molecules. As mentioned in section 1.2.2, there is a similarity between reactivity in electrophilic addition reactions and photoelectron spectroscopy. This similarity can be seen in the relative energies (not the absolute) involved in the creation of species with positive charge. In electrophilic addition reactions, the rate determining step is usually the formation of the carbocation intermediate. In some elimination reactions (E1) and nucleophilic substitutions reactions (S_N1), the rate determining step is also the formation of a carbocation intermediate. In this way, not only electrophilic addition reactions can be connected to photoelectron spectroscopy, but also elimination reactions and nucleophilic substitution reactions [10].

1.3 Ab initio calculations

As mentioned in the previous section, theoretical calculations were done in order to get the necessary information to calculate the chemical shift ΔI. These chemical shifts were calculated from the electronic energies of the initial and final (ionized) state of the molecules where zero point energies (ZPE) were taken into account. In addition, other parameters like orbital energies (ϵ), electrostatic potentials (U), and Gibbs free energies (G) were extracted from the calculations and used for different purposes. The *Gaussian 98* set of programs was used in the calculations. The *ab initio* calculations are further discussed in chapter 4.

Chapter 2

2 The experimental facility and experiment

This section will describe how the experimental facility is built up and how the experiment is done.

2.1 The instrument at the MAX-laboratory

There are many facilities in the world that produce synchrotron radiation. One of these is the MAX-laboratory located in Lund, Sweden. In the following sections, a closer description of this facility will be given. Figure 13 shows an overview of the MAX-laboratory. There is a third MAX-ring under construction that is not shown in this figure.

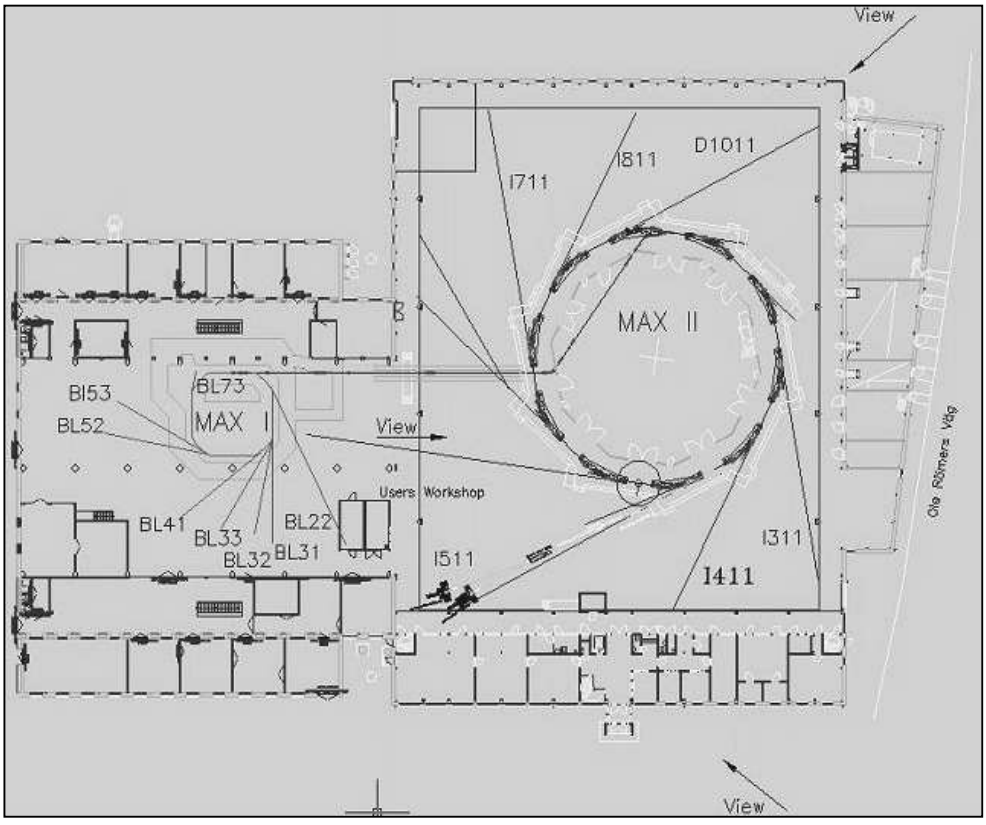

Figure 13: An overview of the MAX-laboratory.

The light is generated in a process which consists of several steps. First, the electrons are generated from an electron source called the electron gun. These electrons must be accelerated to a speed near the speed of light. To achieve

this, a racetrack mikrotron accelerator (similar to a LINAC) is used. Then the electrons are injected into MAX I, the first MAX-ring. Here the electrons are sent through undulators and bending magnets at different beamlines to produce light with many wavelengths. This light is monochromatized and used in different experiments.
The accelerated electrons in the MAX I-ring can also be injected into the larger MAX II-ring. Here the electrons are further accelerated to a higher energy. These electrons are sent through undulators or wigglers to produce a very intense light beam that goes through a monochromator to give light with specific wavelengths. This light is ending up at the end station where it can be used for experiments.
The electron gun, racetrack mikrotron, LINAC, MAX I, MAX II, and beamline I411 are further described in the following sections.

2.1.1 The electron gun

The source which produces the electrons is the electron gun [11]. This device also accelerates the electrons by using a steady electric field. Figure 14 on the facing page shows an example of an electron gun.
In the electron gun, the cathode is heated to a certain temperature to cause emission of electrons from the surface of the cathode. The cathode consists of a metal or compounds like barium oxide, BaO, or lantanium hexaborane, LaB_6. Because of a voltage between the cathode and anode, the electrons are accelerated towards the anode. In this way, a beam of electrons is produced. The energy of the electrons is increased by increasing the voltage between the cathode and anode. If accelerating gaps and/or rapidly alternating fields are used, we can get even higher energies of the electrons.
A different way of releasing electrons from the surface of the cathode, is to use photoemission where the cathode is irradiated by a strong laser pulse.

2.1.2 The linear accelerator (LINAC) and racetrack mikrotron

LINAC is an abbreviation for linear accelerator and is an instrument which accelerates particles in a straight line [11], [12]. In order to reach high energies, it is necessary to alter the voltage inside the LINAC. The necessary frequencies are high, and because of this, one often talks about radio frequency accelerators.
The timing is one problem at this point. When the electrons accelerates and gain a non-relativistic velocity, the time varying electric field must be controlled properly to achieve an optimal interaction between the field and the particles.
The structure of the Wideröe LINAC is shown in figure 15. This device consists of a series of cylindrical tubes which are placed along the longitudinal axis of an evacuated glass cylinder. Alternate tubes are connected to opposite terminals of an rf generator. By selecting the rf voltage and frequency, a variety of heavy ions can be accelerated across the gaps and bunched simultaneously.

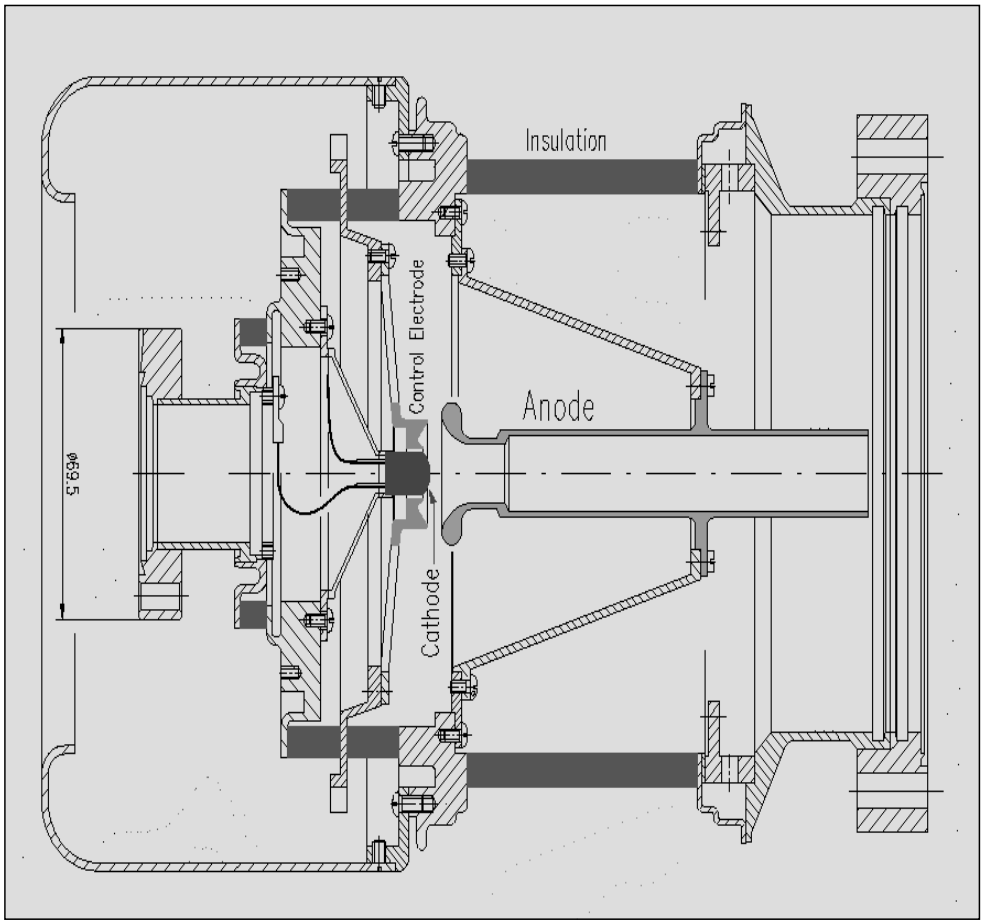

Figure 14: An example of an electron gun.

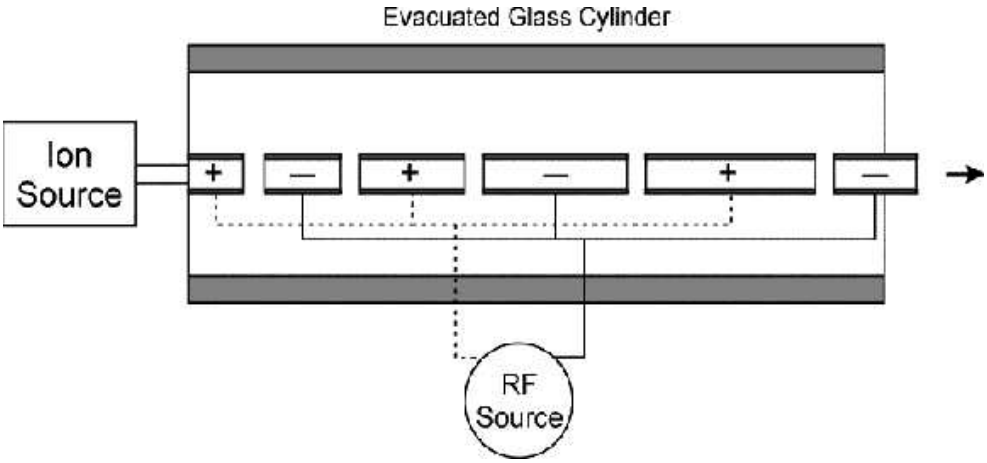

Figure 15: The Wideröe linear accelerator.

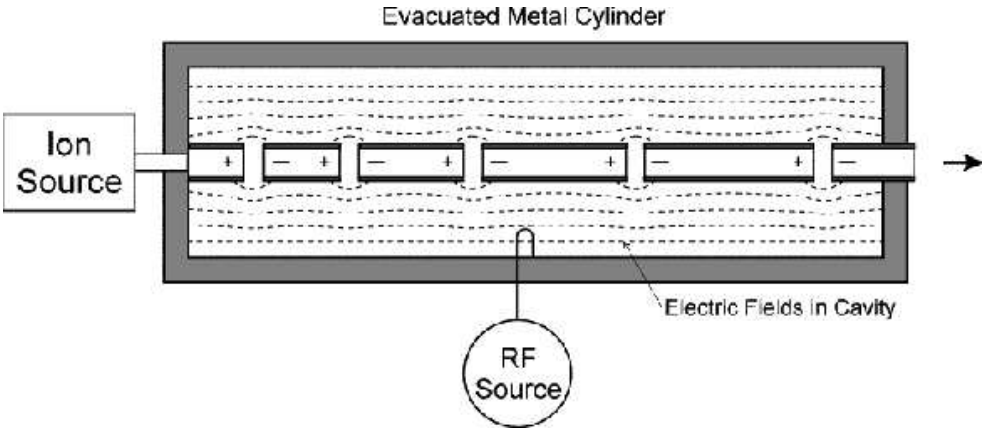

Figure 16: The Alvarez linear accelerator.

At a moment when the rf voltages are maximum on each electrode, acceleration takes place in every gap. After crossing these gaps, the particles enter the metallic cyllindrical electrodes which act as a shield to the electric fields. These particles then exit the electrode after the field in the next gap has changed polarity. The reason why the length of the cylindrical electrodes gets longer as the particles are accelerated, is that the particle beam must arrive at the next gap when the rf voltages at that gap are appropriate for accelerating. In figure 16 we can see the structure of the Alvarez linear accelerator. This device was developed in 1946 by Dr. L. Alvarez and his coworkers. This LINAC is based on a somewhat different principle. A similar series of cylindrical metal electrodes were used, but mounted along the longitudinal axis of an evacuated metallic cylinder. The field is accelerating forward for one half of the rf cycle, and deaccelerating backward for the next half cycle. Each metallic electrode shields the particles from the electric fields when they travel in the wrong direction (same as for the Wideröe structure).
The racetrack mikrotron has a magnet which is split into two halfs, and the accelerating cavity is enlarged into a LINAC. The principle is the same, but larger energies can be given to the electron in each turn and accelerate the electrons up to a few 100 MeV (see figure 17 on the facing page).

2.1.3 MAX I and MAX II storage rings

In figure 13 on page 21 both MAX I and MAX II storage rings are shown. The two rings support research in accelerator physics, nuclear physics using energetic electrons, and research using synchrotron radiation. These research areas include disciplines like surface science, semiconductor physics, materials science, atomic and molecular physics, chemistry, biology and medicine [13]. MAX I is an electron storage ring which receives the electrons from a racetrack miktrotron accelerator with an energy of about 100 MeV. The diameter of this ring is about 10 m. In the MAX I ring, the electrons are further accelerated to an energy of about 500 Mev before they leave the ring to a beamline or the MAX II ring. The lifetime of the beam is around 3-5

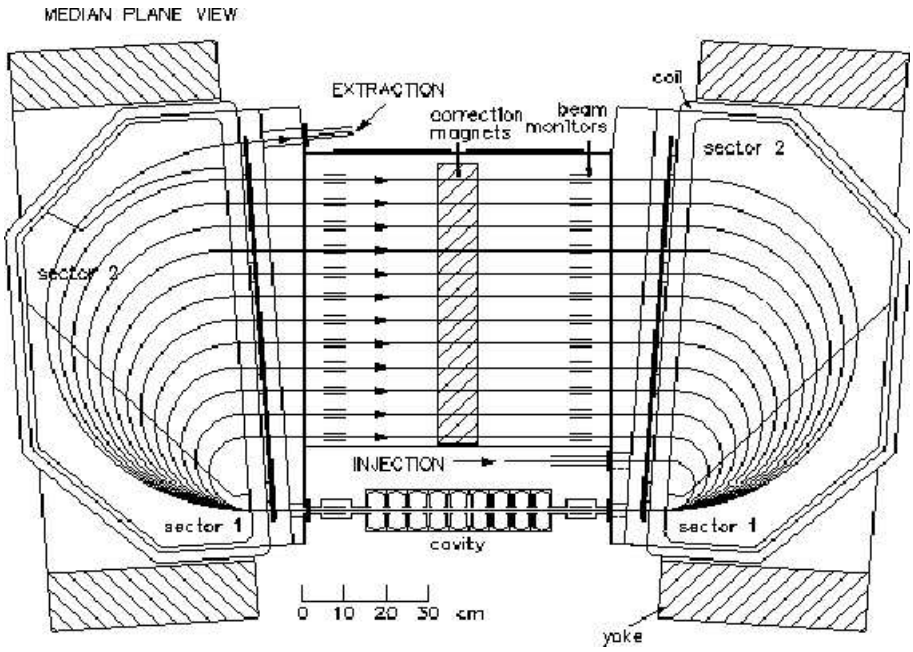

Figure 17: The racetrack mikrotron.

hours, which means that the ring has to be refilled after each 4^{th} hour.
MAX II is an electron storage ring which receives the electrons from MAX I with an energy of about 500 MeV. The diameter of this ring is about 29 m. In the MAX-II ring, the electrons are further accelerated to a maximum energy of about 1.5 GeV. This energy is more preserved in this ring compared to MAX I, so the lifetime of the beam is longer. This means that one injection per day is enough.
Both of the rings produce *synchrotron radiation*. An accelerated particle traveling on a curved trajectory emits radiation. When moving at relativistic speeds, this radiation is emitted as a narrow cone tangent to the path of the particle [14]. This is illustrated in figure 18 on the following page [15]. Synchrotron radiation is generated when relativistic electrons or positrons are accelerated and undergoes a change of direction in a magnetic field. This means that the particles and the magnetic field are acting together in a synchronous manner.

2.1.4 Beamline I411

Figure 19 on the next page shows schematically how beamline I411 is constructed [13].
The first device of I411 is the undulator. An undulator has periodic magnetic structures with relatively weak magnetic fields. The periodicity causes the electron to experience a harmonic oscillation as it moves in the axial direction. This results in a motion which is characterized by small angular excursions called undulations. Because of these weak magnetic fields, the amplitude of this undulation is forced to be small. This results in a narrow radiation cone.

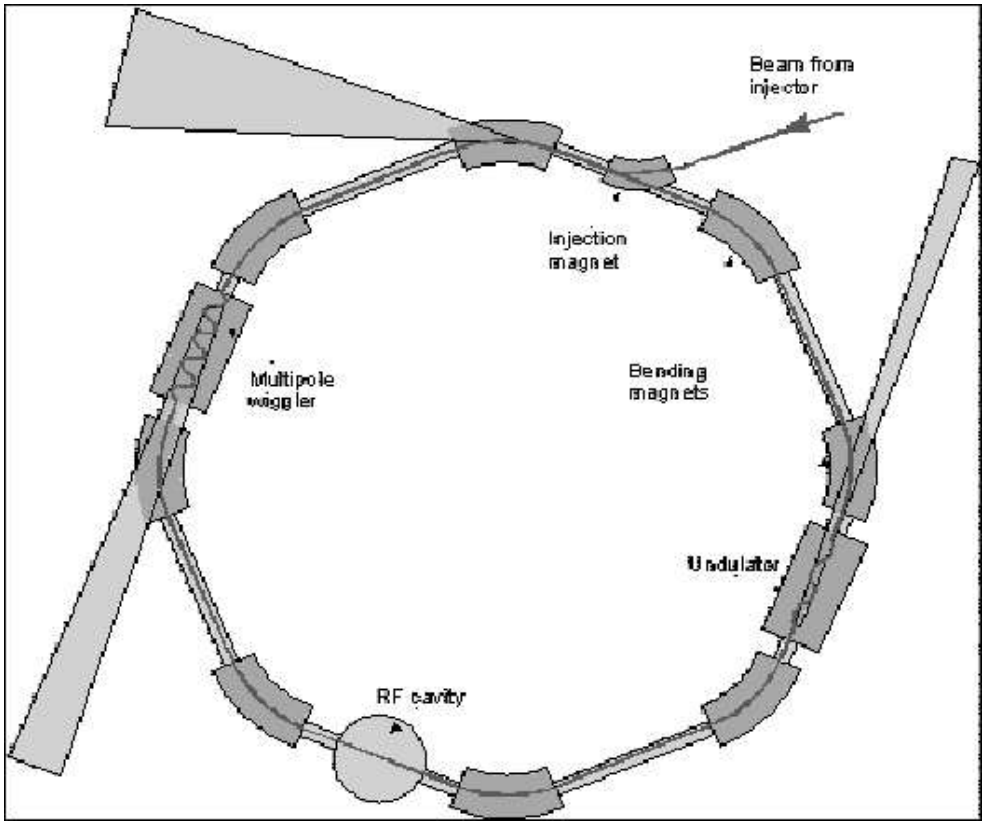

Figure 18: An illustration of a storage ring.

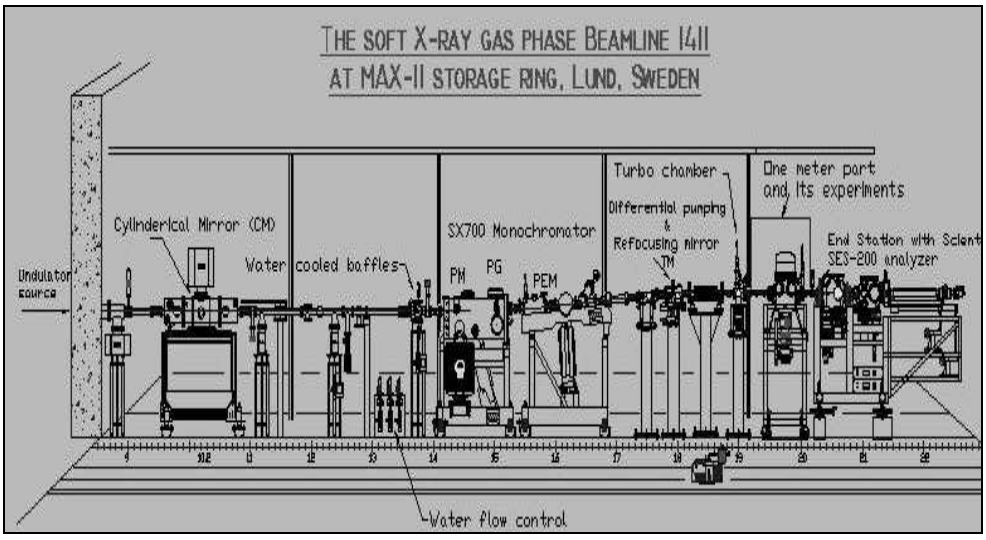

Figure 19: Beamline I411 at MAX-lab.

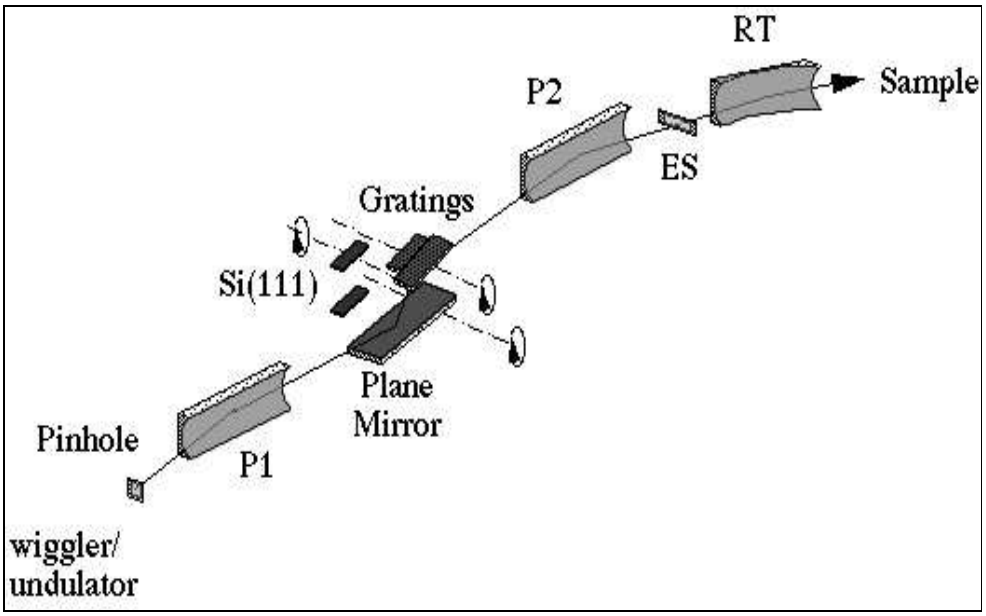

Figure 20: An optical layout of a modified SX700 plane grating monochromator.

This leads to radiation with small angular divergence and relatively narrow spectral width.

Synchrotron radiation is produced as the electrons pass through the undulators. The energy loss of the electron beam to synchrotron radiation is replenished with a radio-frequency accelerator. This is a cavity with an axial electric field oscillating at the frequency of arrival of sequential electron bunches.

The radiation coming out of an undulator must then be spectrally filtered by a monochromator to further narrow the relative spectral bandwidth to a suitable value of $\frac{\Delta\lambda}{\lambda}$ where λ is the wavelength of the incoming light. In addition, the monochromator filters out all the unwanted wavelengths and lets through the wavelengths that are used in the experiment. The monochromator at I411 is the SX700 plane grating monochromator (PGM) (there are other kinds of monochromators like the spherical grating monochromator(SGM)) [16].

Figure 20 shows a modified version of the SX700 monochromator [17]. The figure is showing two plane gratings in the monochromator while it should be only one for an SX700, but the principle is the same.

The SX700 is the current and most popular of the many versions of monochromators. From the figure we can see that the incoming radiation travels through a pinhole before it is collimated by a paraboloidal mirror (P1). This collimated light is reflected by a plane mirror and a plane grating before the monochromatized light is focused by a new paraboloidal mirror (P2) and lead into a vertically adjustable exit slit (ES). Finally, the diverging beam is re-focussed by a toroidal mirror (RT) before it is ending up in the sample.

At the end of the beamline, we find the end station (see figure 21 on the next page) [18], [19]. Here the experiments are carried out.

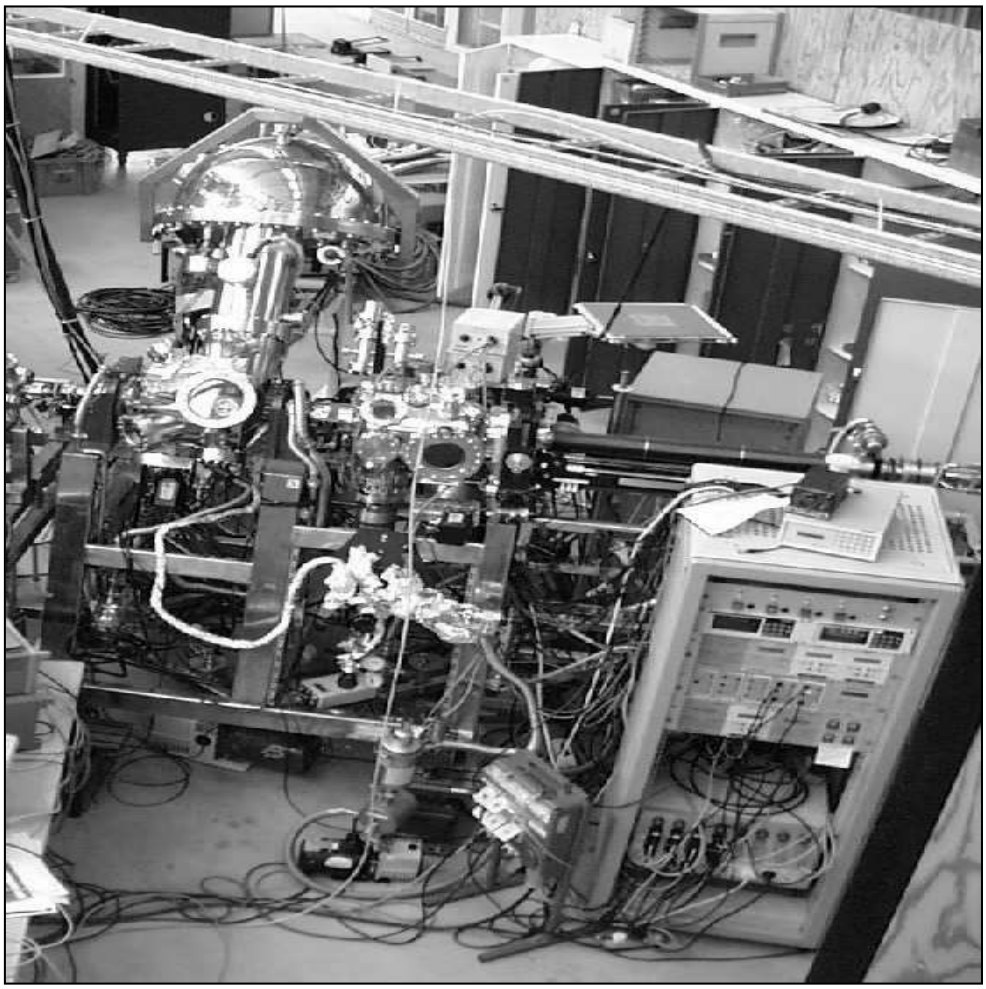

Figure 21: The end station.

This end station is equipped with an angle resolved Scienta SES-200 hemispherical analyzer [20]. This is produced by Scienta Instruments AB, Uppsala, Sweden, and designed for gas phase, solid state, liquids, and thin film studies.
The end station consists of three parts (for solid samples and not used by us) in addition to the SES-200 analyzer; the introduction chamber, the preparation chamber, and the analysis chamber. The introduction chamber is designed in order to make a rapid change of solid samples. A transfer rod system is used to introduce the sample "holders" into the preparation chamber where the samples are attached a cryostat with a good thermal contact. The cryostat is mounted into a computer controlled manipulator used for transferring the samples to a measurement position. The introduction chamber is evacuated by a turbo pump. The preparation and analysis chambers are pumped by turbo pumps and cryopumps.
In experiments based on gas phase photoelectron spectroscopy, the sample is introduced differently than the solid sample. The sample is in most cases a liquid which has a vapor pressure which is sufficiently high for the measurement. Pumps are also used in this case to create a very low pressure inside the manifold, gas cell and analyzer. The next section will give more details of how this is done.
The SES-200 analyzer is a versatile analyzer which is suitable of experiments in which the energy of charged particles is analyzed[3]. Primarily it is developed for X-ray photoelectron spectroscopy (XPS), ultraviolet photoelectron spectroscopy (UPS), and synchrotron radiation experiments. Figure 22 on the following page shows an example of how a modern hemispherical electron energy analyzer is constructed [22], [23].
The analyzer consists of two entrance lenses that focus incoming electrons onto the entrance aperture, hemispherically-shaped electrodes, and finally an electron detector. The electron trajectory is between two metallic hemispheres, where the entrance and exit apertures are circular, producing a circular image. The electrons that converge, are the ones that are deflected through an angle of 180^0. The following equation tells us that the energy resolution is dependent on the analyzer:

$$\frac{\Delta E}{E} = \frac{x_1 + x_2}{2r} + \alpha^2 \tag{7}$$

The variable r equals $\frac{a+b}{2}$ where a and b are the radii of the hemispheres. x_1 and x_2 are the radii of the entrance and exit aperatures. The angle α is the maximum deviation of the electron trajectory with respect to the normal to the entrance aperature.
The electrons passing the entrance aperature, experience immediately a change in the electric field when they enter the hemispherical part of the analyzer. The hemispherically-shaped electrodes have a negative and a positive charge which repulses and attracts, respectively, the incoming

[3]SES is an abbreviation for Scienta Electron Spectrometer, and the SES-200 electron spectrometer has a Scienta type II lens and a full-hemispherical analyzer of mean radius 200 mm [21].

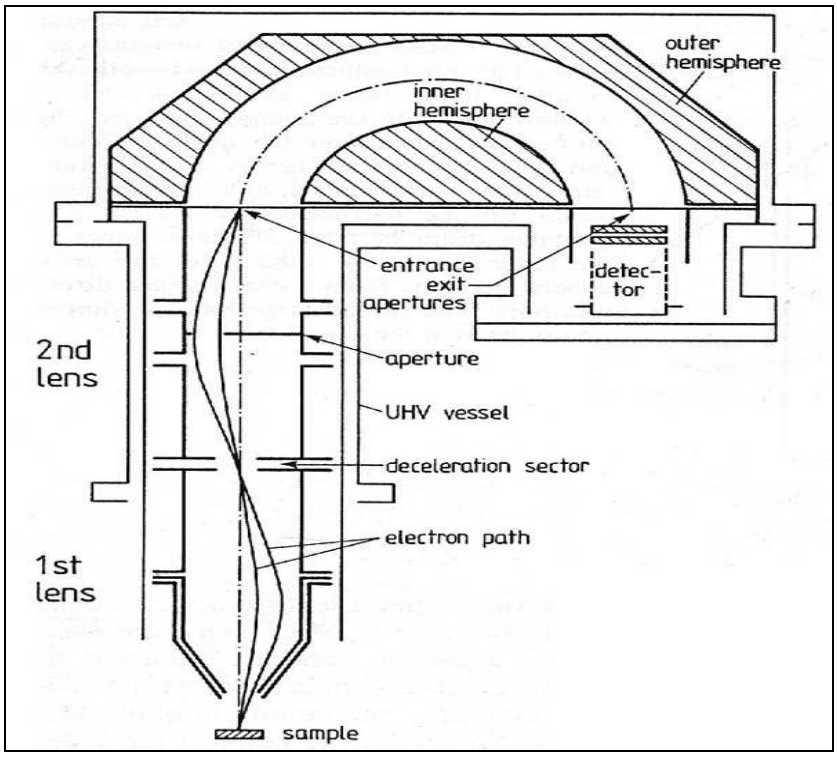

Figure 22: A layout of a hemispherical electron energy analyzer.

electrons. The electrode nearest the centre of the hemisphere has a positive charge, while the other one farthest away has a negative charge. The result of this is that the electrons with the highest kinetic energies will not be affected by the electric field to the same extent as the electrons with lower kinetic energies. This means that the high-energy electrons will travel longer than the low-energy electrons in the hemisphere. Thus, the low-energy electrons will be detected close to the centre of the hemisphere, while the high-energy electrons will be detected farther away from the centre. In this way, when the electron signal intensity is plotted against the kinetic energy of the electrons, a photoelectron spectrum is generated.

2.2 The experiment

In the beginning of the experiment, the experimental settings or parameters are adjusted to get an optimal spectrum (more about this in the next section). Then a manifold is mounted on the frame on the end station right beside the analyzer. The manifold is used to introduce our samples into the gas cell. Often a test measurement of CH_4 is done to see how well the instrument responds. If the spectrum looks fine and as expected, the measurements of the different compounds can be started.
The samples (in most cases a liquid) are usually obtained commercially. 2-3 mL of the liquid sample is transferred to a glass tube which can be mounted to the manifold described above. It is important to get rid of the air inside the

glass tube and manifold because this contamination will affect the resultant spectrum. This problem is solved by pumping. The pumps are connected to the analyzer and manifold in such a way that they remove gas from the analyzer, the tube from the manifold to the gas cell, the manifold, and the sample glass tube, efficiently.
The sample mounted to the manifold is frozen to a solid sample by using liquid nitrogen. By doing this (at least twice), we can remove the air inside the glass tube. After heating the solid sample to liquid, the vapor pressure of the sample is enough to create a measurable pressure inside the analyzer (10^{-6} Torr). One of the reasons why it is necessary with such a low pressure, is the improvement of the resolution of the spectrum. A relatively high pressure in the gas cell will give a higher intensity, but because of the scattering effect and charge accumulation in the gas cell, this will affect the resolution of the spectrum.
The sample molecules are moving from the glass tube to the manifold, and from the manifold through a tube to the gas cell. The pressure inside the manifold and gas cell can be controlled by valves. When the wanted pressure inside the gas cell is achieved, the spectrum can be recorded by the Scienta computer. This is repeated until enough counts is collected, where the counts are directly proportional to the intensity in the spectrum.
When we have finished a sample, we have to prepare the instrument for a new run. The gas inside the manifold and the analyzer is removed by pumping. In addition we are warming up (baking out) the manifold and the tube from the manifold to the analyzer to remove as much sample as possible that is attached to the walls inside the manifold and tube. Afterwards we let the system cool down to the room temperature. The instrument is now ready for a new sample.

2.2.1 Experimental settings

There are many parameters to adjust in an XPS-experiment. This can be parameters like the pass energy (Ep), the SES-slit opening, the energy range, the step energy, the time per step, the number of sweeps per experiment run, the energy of the incoming monochromatized light, the undulator gap, the monochromator slit opening, and the pressure inside the analyzer. The pass energy is the energy of the electrons as they pass through the analyzer. The SES-slit of 900 is a specific magnitude of the entrance slit of the analyzer. The step energy is the energy interval in which the electron intensity is not recorded at the detector. For each 10 meV in the scanning through the whole energy range, the intensity is recorded (see table 1). The undulator gap is the distance between the two permanent magnets in the undulator. The mono-slit is the exit-slit of the monochromator.
The settings used in a typical carbon 1s measurement are shown in table 1 on the next page. From measurement to measurement, often some of these parameters need to be adjusted.
In order to get as correct energies as possible from the spectrum, a *calibration* is necessary. The next and last section in this chapter will tell more about

Table 1: Settings used in a typical measurement

Pass energy (Ep)(eV)	20
SES-slit	900
Energy range (eV)	287.0 - 291.5
Step energy (meV)	10
Time per step (sec)	0.2
Number of sweeps	10
Energy of light (hv)(eV)	330
Undulator gap (mm)	30.76
Mono-slit (μm)	5
Pressure (Torr)	$5x10^{-6}$

how this is done.

2.2.2 Energy calibration

With synchrotron radiation, the accuracy with which the photon energy is known is not high [24]. This means that the apparent photon energy may change from one day to another with a given setting of the monochromator. This happens due to instabilities or imperfections of the instrument. One effect that give measurement errors, is charge accumulation in the gas cell during a measurement. Thus, for finding accurate ionization energies, it is necessary to include an internal standard (calibrant) for which the ionization energy is well known. This calibrant is measured together with the sample (mixed together) to get the spectra of both the calibrant and the sample in the same spectrum.
A good calibrant should have its peak close to the compound of interest, but not overlapping. A good calibrant should also be available at a low cost. In carbon 1s measurements both CO_2 and CF_4 meet these requirements.
The calibrants mentioned in table 2 on the facing page, were calibrated earlier by *V. Myrseth et al.* [25] by using the argon $2p_{3/2}$ line. Argon is a monatomic gas, and has no vibrational excitation. The result of this is that the vertical and adiabatic energies are identical. The reported ionization energy of Ar $2p_{3/2}$, 248.629 eV, is well known in the literature and lies 40-50 eV away from the carbon 1s ionization energies. In the same way as described above, the calibrant (Ar) was measured together with the compound of interest which includes all the compounds shown in table 2 on the next page.

[4] Unweighted average for the $^2\sum_g$ and $^2\sum_u$ states.

Table 2: Adiabatic carbon 1s ionization energies (eV) of different small molecules

Molecule	**Adiabatic energy**
Methane, CH_4	290.689
Ethane, C_2H_6	290.545
Ethene, C_2H_4	290.695
Ethyne, C_2H_2	291.128(avg)[4], 291.179($^2\sum_g$)
Carbon monoxide, CO	296.069
Carbon dioxide, CO_2	297.664
Tetrafluoromethane, CF_4	301.898
Fluoromethane, CH_3F	293.478
Trifluoromethane, CHF_3	299.143

Chapter 3

3 Physical processes affecting the lineshape in a photoelectron spectrum

Each line in a spectrum has a given lineshape. In core photoelectron spectroscopy, this lineshape is influenced by several physical processes. This chapter will describe these processes.

3.1 Post collision interaction (PCI) and different broadening factors

When core photoelectron spectroscopy is carried out on light elements such as carbon, the Auger process dominates the secondary decay [26]. A normal Auger process is illustrated in (a) in figure 23 on the following page [27]. In the normal Auger process, a core electron is ejected into continuum by an incoming photon. This is followed by a decay of a valence electron into the core, which causes an ejection of a valence electron into continuum. This second-ejected electron is called an Auger electron.
If the second-ejected Auger electron is moving faster than the photoelectron, the Auger electron will catch up with the photoelectron and pass it (in the Auger process, the decay of the valence electron into the core happens *simultaneously* with the ejection of the highly energetic Auger electron). When this happens, the photoelectron "feels" an effective charge of +2 from the ionized atom or molecule which is left behind, and is retarded to a higher degree compared with an effective charge of +1. The Auger electron will go from "feeling" a charge of +2 to +1 after the passage of the photoelectron. This speeds the Auger electron even more. This process is called *post-collision interaction* and is illustrated in (b) in figure 23 on the next page. This PCI-effect gives an asymmetric line which is amplified on the low-kinetic-energy side (or the high-ionization-energy side) of the spectrum.
There are three different broadening factors worth mentioning. The first one is called the *lifetime broadening* (ΔE), which is expressed in the following equation: $\Delta E \Delta t \approx \hbar/2$. This equation is known as the Heisenberg's uncertainty principle where Δt is the decay time or life time of the core hole. $\hbar$ is equal to $h/2\pi$ where h is Planck's constant. A common lifetime broadening of a carbon 1s line is 100 meV. If we put this value into the equation, we get a lifetime of the core hole of about $3\text{x}10^{-15}$ seconds or 3 femtoseconds.
A second broadening factor is the broadening due to the different components of the instrument. The energy analyzer is associated with an uncertainty in addtion to an energy distribution of the photons.
Doppler broadening [30] is a third kind of broadening factor which originates from the kinetic energy of the gas-phase atoms or molecules of the sample

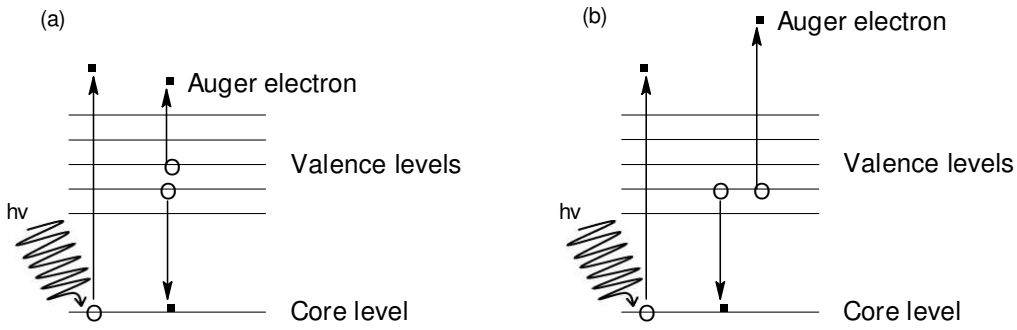

Figure 23: An illustration of a normal Auger transition (a) and a post collision interaction (PCI) (b).

having random motion. This factor has a relatively small influence on the broadening of the spectra.

3.2 The vibrational structure and Franck-Condon principle

The vibrational structure of an electronic transition is explained by the **Franck-Condon principle** [28]:

Because the nuclei are so much massive than the electrons, an electronic transition takes place very much faster than the nuclei can respond.

Because of the electronic transition, the electron density in the atom or molecule is rapidly removed from one specific region and built up in another. The initially stationary nuclei experience this new force field, and starts to vibrate by swinging forwards and backwards from their original position. The stationary equilibrium position of the nuclei in the initial electronic state is therefore a stationary turning point in the final electronic state. This means that the most intense vibronic transition is from the ground vibrational state to the vibrational state lying vertically above it (the arrow in figure 24 on the facing page). This is called the **vertical transition**, and the molecular geometry of the ground state is the same as for the excited state. Transitions to other vibrational levels also occur, but with lower intensity and is called **adiabatic transitions**. In this case, the molecular geometry of the ground state is different from that of the excited state.
The vibrational structure of the spectrum depends on the relative horizontal position of the two potential energy curves. The more the upper potential curve is displaced in the horizontal direction, the longer vibrational progression and more vibrational structure we get.
Figure 24 on the next page [29] shows the potential curves of the ground and excited states with different bond lenghts. The change in bond length can be explained by the change of the total antibonding character in the chemical

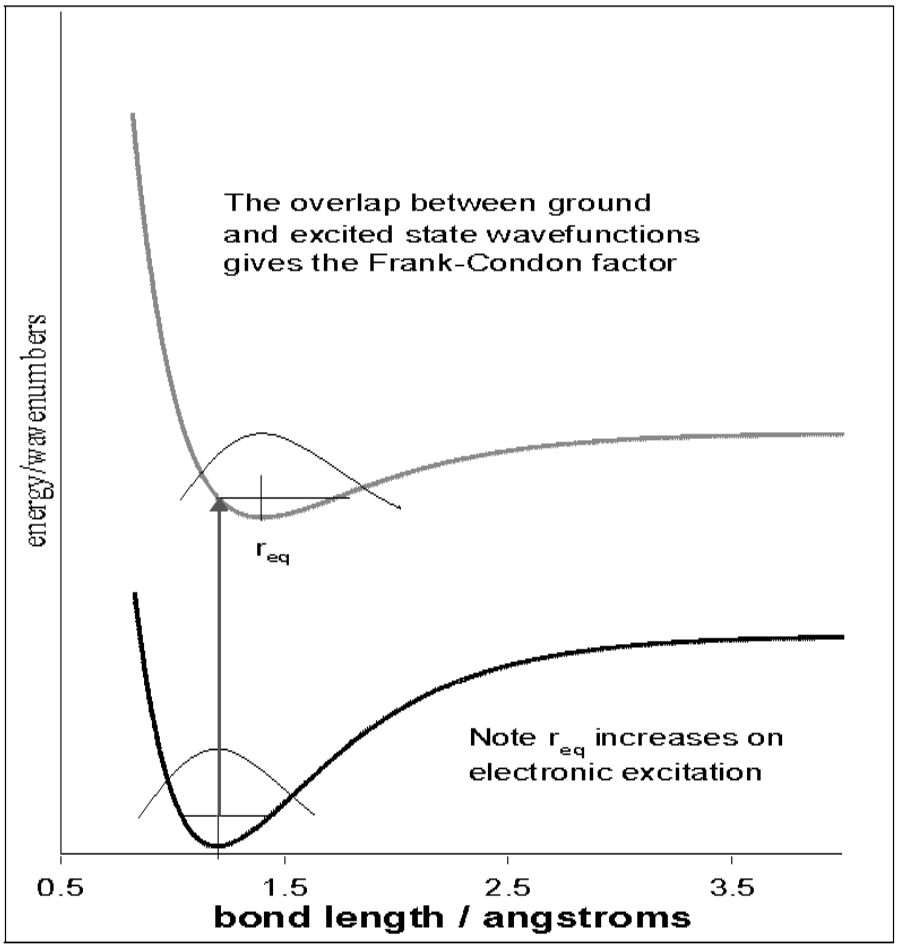

Figure 24: An illustration of the Franck-Condon principle with different ground and excited states.

bond. By increasing the antibonding character of the chemical bond, we also increase the bond length between two atoms. The antibonding character can be increased either by filling up the antibonding MO with electrons or removing electrons from the bonding MO. In this case, it is removed electrons from a specific MO. Since the equilibrium bond length increases in the electronic excitation, this specific MO must be a bonding MO.

A different type of electronic transition that may happen, is illustrated in figure 25. In this case the ground and excited state are similar. This means that the bond distance between the two atoms is unaffected of the electronic transition. In such kind of electronic transitions, the excited electron usually originates from a non-bonding MO.

Figure 26 on page 39 illustrates the difference between an electronic transition with similar ground and excited states and an electronic transition with different ones. This is shown by plotting the intensity against the difference in the potential surface of the ground and excited states.

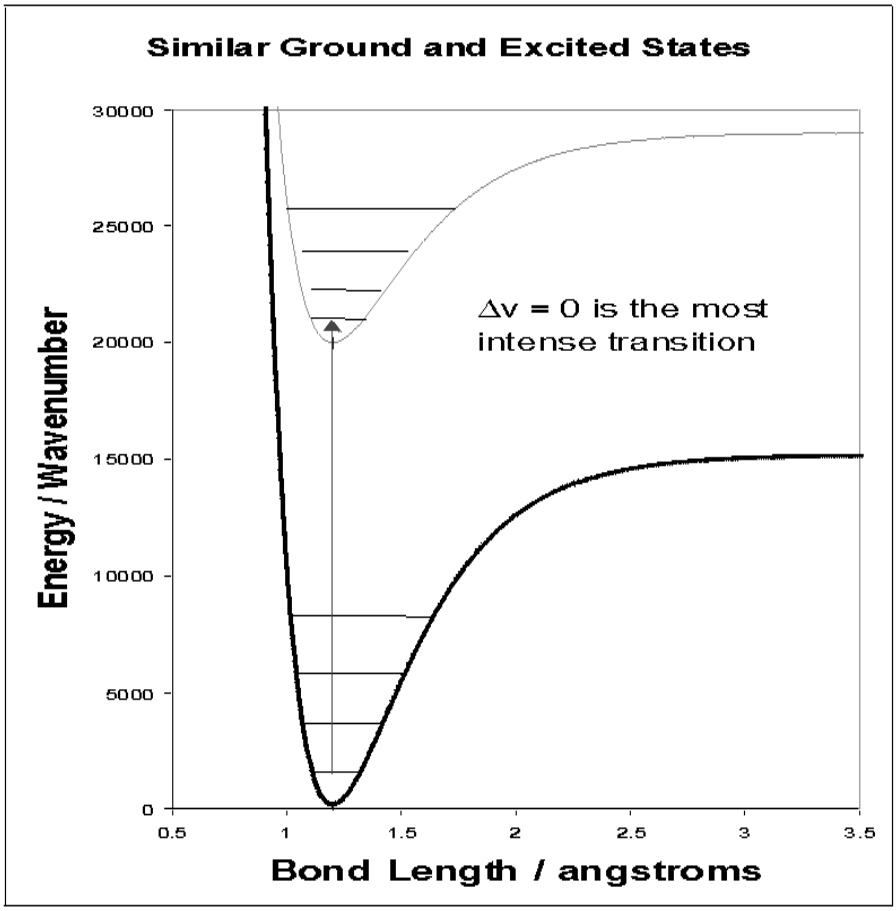

Figure 25: An illustration of the Franck-Condon principle with similar ground and excited states.

The Franck-Condon factor mentioned in figure 24, is the squared overlap integral between the ground and excited state.
The quantitative form of the Franck-Condon principle is derived from the expression for the transition dipole moment, $\mu_{fi} =< f|\mu|i >$. The dipole moment operator is a sum over all nuclei and electrons in the molecule shown in equation 8.

$$\mu = -e\sum_{i} r_i + e\sum_{I} Z_I R_I \tag{8}$$

In this equation, e is the electronic charge, r_i are the electronic coordinates, Z_I are the nuclear charges, and R_I are the nuclear coordinates. The vectors are the distances from the centre of charge of the molecule. The magnitude of the transition dipole moment is directly proportional to the intensity of the transition. The intensity of the transition is proportional to the square modulus of the overlap integral, $S(\nu_f, \nu_i)$, between the vibrational states of the initial and final electronic states. This is shown in equation 9.

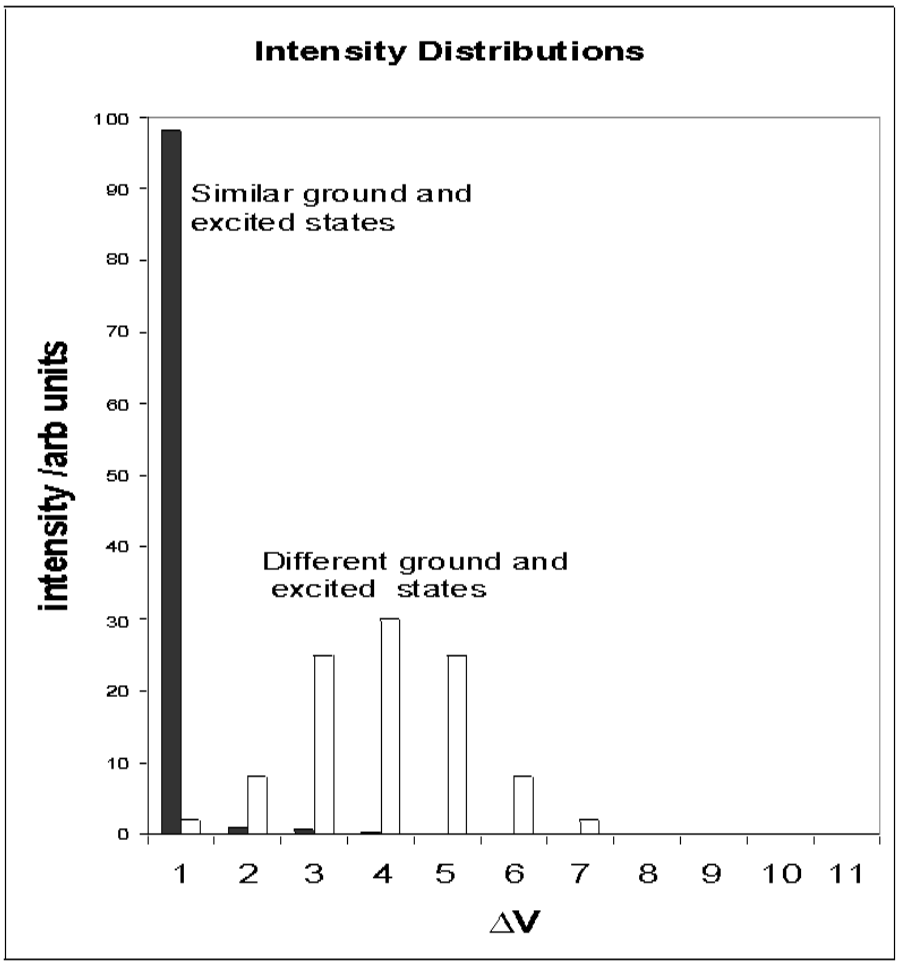

Figure 26: Plotting the intensity against the difference in the potential surface of the ground and excited states.

$$|\mu_{fi}|^2 = |\mu_{\epsilon_f,\epsilon_i} S(\nu_f, \nu_i)|^2 \tag{9}$$

The expression $|S(\nu_f, \nu_i)|^2$ is the squared overlap integral and known as the **Franck-Condon factor** for the transition. This means that the greater the overlap of the vibrational state wavefunction in the upper electronic state with the vibrational wavefunction in the lower electronic state, the greater the intensity of that particular simultaneous electronic and vibrational transition.

3.3 Vibronic coupling

To explain the vibronic coupling [31], an octahedral complex is used as an example. When a visible absorption spectrum of an octahedral complex is studied, one finds signals with very small intensity in the spectrum. We know that d-d transitions in octahedral complexes are symmetry forbidden (Laporte selection rule), so why do these small signals appear in the spectrum?

Centrosymmetric complexes like the octahedral ones, have a centre of inversion (i) as a symmetry operation. Molecules and atoms with this symmetry operation are included in the **Laporte selection rule**:

The only allowed transitions are transitions that are accompanied by a change of parity.

The result of this is that u[5]⟶g[6] and g⟶u transitions are allowed, while g⟶g and u⟶u transitions are symmetry forbidden. A forbidden transition can become allowed if the molecule (the octahedral complex in this case) gets out of the centrosymmetric geometry by an asymmetrical vibration. In this specific case, the selection rule does not apply, and the d-d transition becomes parity-allowed. This means that the $e_g \leftarrow t_{2g}$ transition becomes weakly allowed. This weak relaxation of the Laporte selection rule is known as vibronic transition or **vibronic coupling** because it arises from the interaction of *vibr*ational modes with the electr*onic* transition modes.
A work published in December 2000 by K. J. Børve et al. [32], describes the vibronic structure in the carbon 1s photoelectron spectra of the centrosymmetric acetylene, HCCH, and the deuterated acetylene, DCCD. This article explains, among other things, that vibronic coupling occur in a carbon 1s ionization of acetylene and d-acetylene.
As will be seen in this thesis, vibronic coupling occur in trans-2-butene, 2-butyne, trans-3-hexene, and 3-hexyne. As mentioned in section 4.4, trans-2-butene, trans-3-hexene, and 3-hexyne have the C_{2h} symmetry, while 2-butyne has the D_{3d} symmetry. Since these two point groups have the inversion symmetry element (i), the four molecules will be included in the Laporte selection rule and give vibronic coupling.

3.4 Shake-up

Figure 27 on the next page shows an illustration of the shake-up process. As we can see, an incoming photon excites a core electron to a valence level. This is followed by a deexcitation of a valence electron to the core orbital, which releases enough energy to excite a second valence electron to the continuum. In addition, the excited core electron absorbs enough energy to excite or **shake up** to an even higher valence level. This shake-up process is an electron transfer from the higest occupied molecular orbital (HOMO) to the lowest unoccupied molecular orbital (LUMO). The less the difference in energy (ΔE) between these two molecular orbitals, the easier and more frequently this electron transfer occur.

Core photoelectron shake-up spectra provide information on the electronic relaxation process accompanying the creation of a core vacancy. In the article written by C. Enkvist et al. [33], they have investigated the carbon 1s shake-up spectra of biphenyl and p-terphenyl. These molecules are

[5] u stands for ungerade (German word) and means uneven.
[6] g stands for gerade (German word) and means even.

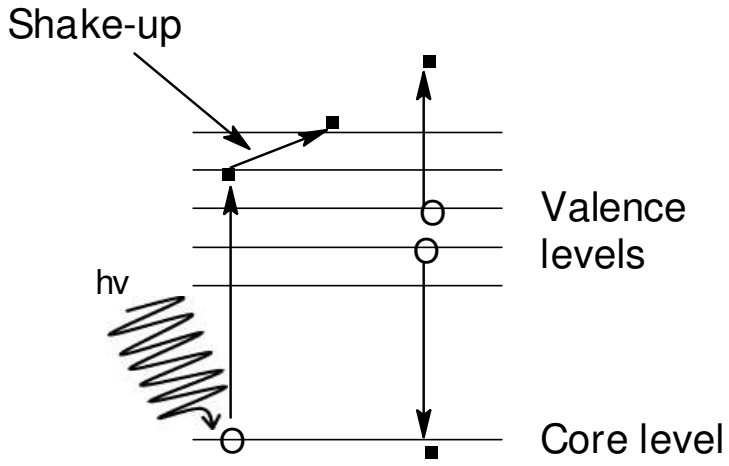

Figure 27: An illustration of the shake-up process.

unsaturated, and as will be seen in section 6.3, some of the unsaturated molecules in this thesis show a tendency of shake-up. Unsaturated molecules show a higher tendency of shake-up compared to saturated molecules because of the small difference in energy between the HOMO and LUMO in these molecules.
The effect of this process can be seen in the photoelectron spectra as a lower intensity peak. This means that the spectrum shows a peak with a lower intensity than predicted by theory (stoichiometrical determined). The reason for this lower intensity, is the involvement of the core electrons in the shake-up process instead of being ionized from the molecule and detected. Because it is the detected electrons that produces the intensity in the spectrum, we will get a peak with a lower intensity than expected. The shake-up electron will also give a certain intensity in the spectrum, but in an another energy region.

Chapter 4

4 Description of some theoretical aspects related to photoelectron spectroscopy

To analyze and interpret the data we get from a photoelectron spectroscopical experiment, we need tools to do this. One very important tool that helps us with this, is the ab inito calculation. This will be discussed more closely in this chapter. Initial and final state effects and Koopman's theorem will also be discussed.

4.1 Ab initio electronic structure calculations

Electronic structure methods use the law of quantum mechanics rather than classical physics as the basis for their computations [45]. Quantum mechanics states that the energy and other related properties of a molecule or an atom may be obtained by solving the *time-independent*[7] *Schrödinger equation*[8] [47]:

$$H\Psi = E\Psi \tag{10}$$

H is known as the energy operator and is called the Hamiltonian, while E is the energy of the system the equation is describing. Ψ is called the *wavefunction*, and all the information about a given system is encoded in this function. The Hamiltonian consists of a kinetic (T) and potential (V) energy operator:
$H = T + V$.
Exact solutions to equation 10 are not computationally practical for any but the smallest systems. Electronic structure methods are characterized by their various mathematical approximations to its solution.
The words "ab initio" have their origin from the Latin language, and can be translated into english as "from the beginning". This means that the computation is solely based on the laws of quantum mechanics and on the values of a small number of physical constants like the speed of light, the masses and charges of electrons and nuclei, and Planck's constant, *without* using parameters derived from experimental data to simplify the computation. However, an electronic structure method which is based on experimental data, is called a *semi-empirical method*.
Semi-empirical and ab initio methods differ in computational cost and accuracy of result. Semi-empirical calculations are relatively inexpensive and provide reasonable qualitative description of molecular systems and fairly

[7] In the time-dependent case, the Schrödinger equation has the form:
$H\Psi = i\hbar\frac{\partial\Psi}{\partial t}$ where $\hbar = \frac{h}{2\pi}$.

[8] This equation was first introduced by Erwin Schrödinger in 1926.

accurate quantitative predictions of energies and structures for systems where good parameter sets exist. In contrast, ab initio calculations provide high quality quantitative predictions for a broad range of systems. This means that they are not limited to any specific class of system.
The computational program used in this thesis is called *Gaussian 98* [46]. This program is capable of predicting many properties of molecules and reactions.
Each calculation starts out with an input file where the "guess" structure of the molecule is specified. Exact values of bonding lengths, three-atom angles, and torsional angles are given in a *z-matrix* in the input file (the structure of the molecule can also be specified in a Cartesian coordinate system).
Two other very important parameters that also have to be specified in the input file, are the *calculation method* and *basis set*. The Gaussian program contains many different theoretical procedures corresponding to different approximation methods (most often referred to as different *levels of theory*). The description of the different levels of theory used in this thesis can be found in section 4.1.1, 4.1.2, and 4.1.3.
A basis set is a mathematical representation of the molecular orbitals of a molecule. The basis set can be interpreted as restricting each electron to a particular region of space. Larger basis sets impose fewer constraints on electrons and more accurately approximate exact molecular orbitals. The larger basis sets require more computational resources and calculation time. More information about basis sets and the basis set used in this thesis, is given is section 4.1.4.

4.1.1 The Hartree-Fock (HF) level of theory

With experience from helium, it is hopeless to believe that one can find exact solutions for atoms with more than 2 electrons. It is more practical to approximate the atom as a system consisting of Z independent electrons in a potential $V(\vec{r})$ [48].
The potential $V(\vec{r})$ does not only consist of the electrostatic attraction to the nuclei, but also the average electrostatic repulsion to the other electrons. If electron i is in a one particle state (one *orbital*) $\psi_i(\vec{r})$, the charge density $-e|\psi_i(\vec{r_i})|^2$ will give a contribution to the potential that the other electrons "feel". The potential of electron k is the nucleus attraction plus the repulsion from the other electrons:

$$V(\vec{r}_k) = -\frac{Ze^2}{4\pi\epsilon_0 r_k} + \sum_{i(\neq k)} \int \frac{e^2|\psi_i(\vec{r_i})|^2}{4\pi\epsilon_0|\vec{r_k} - \vec{r_i}|} d^3r_i \tag{11}$$

The wave function of electron k will then satisfy a Schrödinger equation with this potential:

$$[-\frac{\hbar^2}{2m}\nabla_k^2 + V(\vec{r_k})]\psi_k(\vec{r_k}) = \epsilon_k\psi_k(\vec{r_k}) \tag{12}$$

The orbitals ψ_i which appears in the potential energy term, is not known. Therefore we have to seek a *self consistent* set of orbitals, hence the name

self-consistent field (SCF). This is done by putting the orbitals into the potential and let them reproduce themselves as solutions. In practice this equation is solved by *iteration*. The iteration process involves the following: An initial potential is chosen, the wavefunctions are calculated, and the new *effective* potential is calculated from the Z states with the lowest energy, until self-consistence is achieved.
To get an easier calculation, the effective potential $V(r)$ is averaged over the angles in each step such that a spherically symmetric potential $V(r)$ is achieved. This is called the *Hartree*[9]*-Fock*[10] *method*.
The Pauli exclusion principle[11] is also taken into account by putting all the electrons in different states (the spin is also in this state description). The main point is that the atomic structure is described by using one particle orbitals in a spherically symmetric effective potential $V(r)$. Of physical reasons, it is expected that this effective potential of an electron is approximately the same as the electron-nuclei potential $-Ze^2/4\pi\epsilon r$ for very small distances, while this potential is reduced at larger distances because of the *screening effect* of the other $Z-1$ electrons.
However good the wavefunction ψ may appear to be, it is not the "exact" wavefunction. This means that the Hartree-Fock method relies on *averages*. It does not consider the *instantaneous* electrostatic interactions between electrons. Neither does it take into account the quantum mechanical effects on electron distributions because the effect of $Z-1$ electrons on an electron of interest is treated in an average way. Because of these deficiencies, it is said that the HF method ignores **electron correlation**.
There are two types of Hartree-Fock calculations, **restricted (RHF) and unrestricted (UHF) Hartree-Fock**. In a restricted Hartree-Fock calculation, all the electrons except those occupying open-shell orbitals are forced to occupy doubly occupied spatial orbitals. In an open-shell unrestricted Hartree-Fock calculation, separate spatial orbitals for the spin up and spin down electrons are used.

4.1.2 The Becke3LYP (B3LYP) level of theory

B3LYP[12]is a hybrid functional based on *Density Functional*[13] *Theory* (DFT) [49]. DFT starts out with the concept of the electron probability density, $\rho(\vec{r})$:

$$\rho(\vec{r}) = |\psi(\vec{r})|^2 \tag{13}$$

DFT is a very popular calculation method because it is taking into account the electron correlation in addition to be less computationally demanding

[9]Douglas Rayner Hartree (1897-1958), a british physicist.
[10]Vladimir Aleksandrovitch Fock (1898-1974), a russian physicist.
[11]The Pauli exclusion principle: In any atom no two electrons can have all four quantum numbers the same.
[12]B3LYP: Becke's three-parameter formulation with Becke-style hybrid functionals. LYP is a gradient-corrected correlation functional by Lee, Yang, and Parr.
[13]A functional is defined in mathematics as a function of a function. In Density Functional Theory, functionals are functions of the electron density.

than many other calculation methods. It can do calculations on molecules with 100 or even more atoms in significantly less time than the HF-methods. DFT also give results that very frequently agree more closely with experiment than HF calculations do for systems involving d-block metals.
For a system of Z electrons, $\rho(\vec{r})$ denotes the total electron density at a particular point in space $\mathbf{r}$. The electronic energy E is said to be a **functional** of the electron density, and is denoted $E[\rho]$. DFT methods partition the electronic energy into several terms [50]:

$$E = E^T + E^V + E^J + E^{XC} \tag{14}$$

E^T is the kinetic energy term which is arising from the motion of the electrons, E^V includes the terms describing the potential energy of the electron-nuclear attraction and of the repulsion between pairs of nuclei, E^J is the electron-electron repulsion term which is also described as the Coulomb self-interaction of the electron density, and E^{XC} is the exchange-correlation term and includes the remaining part of the electron-electron interactions. All terms except the nuclear-nuclear repulsion are functions of $\rho(\vec{r})$, the electron probability density. The E^{XC} term accounts for the exchange energy arising from the antisymmetry of the quantum mechanical wavefunction in addition to dynamic correlation in the motions of the individual electrons.

4.1.3 The Möller-Plesset-2 (MP2) level of theory

Perturbation theory [51] (PT) provides an alternative systematic approach to finding the correlation energy. The application of PT to a system composed of many interacting particles, is generally called **many-body perturbation theory** (MBPT). Because it is a necessity to find the correlation energy of the ground state, one takes the zero-order hamiltonian from the Fock operators of the Hartree-Fock SCF method. This choice of $H^{(0)}$ was made in the early days of quantum mechanics in 1934 by C. Möller and M.S. Plesset, and the procedure is called Möller-Plesset perturbation theory (MPPT).
In MPPT, the zero-order hamiltonian $H^{(0)}$ (H_{HF}) is given by the sum of one-electron Fock operators:

$$H_{HF} = \sum_{i=1}^{n} f_i \tag{15}$$

The HF ground-state wavefunction ϕ_0 is an eigenfunction of H_{HF} with an eigenvalue E^0 given by the sum of the orbital energies of all the occupied spinorbitals.
The perturbation $H^{(1)}$ is given by:

$$H^{(1)} = H - \sum_{i=1}^{n} f_i \tag{16}$$

where H is the electronic hamiltonian. The HF energy E_{HF} associated with the normalized ground-state HF wavefunction ϕ_0 is the expectation value:

$$E_{HF} =< \phi_0|H|\phi_0 >=< \phi_0|H_{HF} + H^{(1)}|\phi_0 > \tag{17}$$

It is shown that:

$$E_{(0)} =< \phi_0|H_{HF}|\phi_0 > \tag{18}$$

$$E_{(1)} =< \phi_0|H^{(1)}|\phi_0 > \tag{19}$$

This gives the relation:

$$E_{HF} = E^{(0)} + E^{(1)} \tag{20}$$

Therefore, the first correction to the ground state energy is given by second-order perturbation theory as:

$$E^{(2)} = \sum_{J \neq 0} \frac{< \phi_J|H^{(1)}|\phi_0 >< \phi_0|H^{(1)}|\phi_J >}{E^{(0)} - E_J} \tag{21}$$

The inclusion of the second-order energy correction is designated **MP2**. In general, bond lengths based on MP2 are in excellent agreement with experiment for bonds involving hydrogen. However, MP2 is not that good predicting the bond length in the case of multiple bonds.

4.1.4 Basis sets. Dunning triple zeta with polarized functions (TZP)

A basis set is the mathematical description of the orbitals within a system used to perform the theoretical calculation [53]. The larger the basis sets gets, the more accurately the orbitals are approximated by imposing fewer restrictions on the locations of the electrons in space. In the quantum mechanical picture, electrons have a finite probability of existing anywhere in space.
A standard basis set for electronic structure calculations use linear combinations of gaussian functions to form the orbitals. Basis sets assign a group of *basis functions* to each atom within a molecule to approximate it's orbitals. These basis functions are composed of a linear combination of gaussian functions (*contracted functions*). The component gaussian functions are referred to as *primitives*, while a basis function consisting of a single gaussian function is called an *uncontracted* function.
The basis set which I have used in my thesis, is called TZP, which stands for Triple Zeta with Polarized functions. What does this mean?
The first way that a basis set can be made larger, is to increase the number of basis functions per atom. A split valence basis set have two or more sizes of basis function for each valence orbital. In the case of hydrogen and carbon, they will be represented as follows, having two sizes of basis function for each valence orbital (the primed and unprimed orbitals differ in size):

H: $1s, 1s'$
C: $1s, 2s, 2s', 2p_x, 2p_y, 2p_z, 2p'_x, 2p'_y, 2p'_z$

The *double zeta* basis sets form all molecular orbitals from linear combinations of two sizes of functions for each atomic orbital. The TZP basis set is a *triple split valence* basis set. The triple split valence basis set uses three sizes of contracted functions for each orbital-type.
Split valence basis sets allow orbitals to change *size*, but not to change *shape*. Polarized basis sets remove this limitation by adding orbitals with an angular momentum beyond what is required for the ground state to the description of each atom. In the case of TZP and the calculations of the hydrocarbons in this thesis, this basis set is polarized by adding a d-function to the carbon atom and a p-function to the hydrogen atom.

4.1.5 The effective core potential (ECP) in hole-state calculations

When an atom or molecule is core ionized, a core hole is created in a particular core orbital. By using the effective core potential (ECP), this localized core hole can be modeled [56] in a theoretical calculation. In this method, all core-valence interactions are approximated with l-dependent projection operators, and a totally symmetric screening type potential [54]. l is the angular momentum quantum number. A core hole ECP is different from an ordinary ECP.
ECP allow treatment of the core electrons as if they were some averaged potentials rather than actual particles [55]. ECP's are not orbitals, but modifications to a hamiltonian, and as such are very efficient computationally. The core potentials are usually specified for shells that are filled. However, for rare elements with partially filled f cores, the open shell cores are necessary. For the rest of the electrons, the valence electrons, basis functions are needed. These are special basis sets optimized for the use with specific ECP's.
The ECP are usually tabulated in the literature as parameters of the following expansion:

$$ECP(r) = \sum_{i=1}^{M} d_i \times r^{n_i} \times 10^{-\zeta_i \times r^2} \tag{22}$$

M is the number of terms in the expansion, d_i is a coefficient for each term, r denotes the distance from the nucleus, n_i is a power of r for the ith term, and ζ_i represents the exponent for the ith term.
To specify ECP for a given atomic center, you need to include the number of core electrons that are substituted by ECP, the largest angular momentum quantum number included in the potential, and number of terms in the "polynomial gaussian expansion" shown in equation 22.
However, there are some problems connected to ECP. The vibrational frequencies are higher than the observed experimental frequencies. This is corrected by scaling each frequency individually by empirical constants (see section 5.2 for further information). Secondly, the predicted changes in bond

lengths and bond angles are not accurate compared to experimental observations. It is important to notice that there are other reasons why these problems arise in addition to ECP.

4.2 Initial and final state effects on core ionization energies

To obtain further chemical insight (acidity, basicity, reactivity) from the chemical shifts (ΔI) in core photoelectron spectroscopy, it is necessary to separate the ionization energy into an initial state charge distribution represented by the potential energy difference, ΔV, and the electronic and geometric relaxation energy difference in the final state, ΔR [38]. These quantities are related through $\Delta I = \Delta V - \Delta R$ [39]. Let us take a closer look at this relation by considering figure 28.

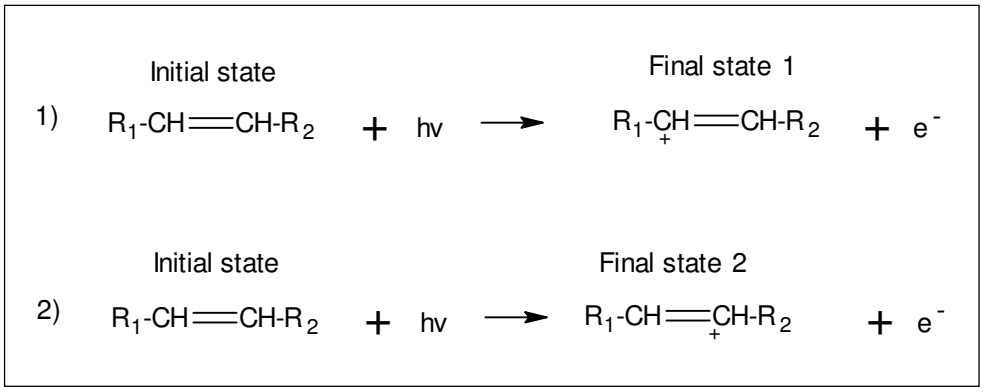

Figure 28: Carbon 1s ionizations of an alkene with two different final states where $R_1 \neq R_2$.

This figure shows a core ionization of an alkene which is core ionized at two chemically inequivalent carbon atoms. These carbon atoms are chemically inequivalent because of their different chemical environment. Due to this difference, we do not expect these two carbon 1s ionization energies to be the same. This difference in carbon 1s ionization energy, is called the *chemical shift* and is termed ΔI.
The ionization energy can be expressed as $I = V - R$. V represents the total effect of the initial state on the energy required to remove a core electron from a molecule in which the remainder of the electron structure remains unchanged from that of the neutral molecule. To express $I = V - R$ as a chemical shift, ΔI is expressed as $I_1 - I_2$. I_1 is the same as $V_1 - R_1$, and I_2 is the same as $V_2 - R_2$. If these relations are solved with respect to ΔI, we end up with the expression $\Delta I = \Delta V - \Delta R$. To illustrate the difference between the initial state charge distribution V and the geometric and electronic relaxation of the final state, R, an example is given in the following [58]. Imagine that all the four H-atoms in methane are substituted with flourine atoms, F. Because of the electronegativity of the fluorine atom, the electron density in the vicinity of the carbon atom in tetrafluoromethane is smaller than in the methane molecule. The result of this, is that it is "harder" for the

carbon atom in tetrafluoromethane to accept a positive charge than it is for the carbon atom in methane to do it (the carbon atom in tetrafluoromethane has a small positive charge before the carbon 1s ionization). Consequently, the ionization energy of the tetrafluoromethane molecule must be higher than for the methane molecule (this is shown in reference [57]). This result give evidence for the existence of the charge distribution in the initial state, V.
Other cases are not that simple. Instead of substituting all the four H-atoms with fluorine atoms, one of the H-atoms is substituted with a methyl group to give ethane. We know that the carbon atom is more electronegative than the H-atom, so we expect the ionization energy of ethane to be higher than in methane. This is not the case. It is shown that the carbon 1s ionization energy in ethane is 0.21 eV *less* than it is in methane [58]. This unexpected difference is better understood by recognizing that the ionization energy not only depends on the charge distribution in the initial state, but also on the geometric and electronic rearrangement in the resulting ion (final state) as a response to the removal of the core electron. This relaxation energy, R, is larger for the more polarizable methyl group than it is for hydrogen, and more than offsets the difference in the electronegativity-effect.
The ΔI values can be found by investigating the spectra. ΔV can be found from theoretical calculations using the *extended Koopmans' theorem* (see section 4.3). ΔR can finally be calculated by subtracting ΔI from ΔV:
$\Delta R = \Delta V(calc) - \Delta I(exp)$.

4.3 Koopmans' theorem and the extended Koopmans' theorem (EKT)

The accurate quantification of the initial-state contribution ΔV to the measured shift [58] can be done as shown in the following. One way to find the contribution from the initial state to the ionization energy, is to equate the initial-state effect V to the negative of the electrostatic energy of a core electron. This is an over-simplification because of the neglect of the kinetic energy and exchange interactions of the electrons.
An alternative way to estimate V, is to approximate the initial-state effect by the negative of the orbital energy of the core electron. Koopmans' theorem shows that within the Hartree-Fock approximation, the energy needed to remove an electron *without rearrangements of the spectator electrons* is given precisely by $-\epsilon_c$, where ϵ_c is the core orbital energy:

$$I = -\epsilon_c \tag{23}$$

We know that $I = V - R$. When the rearrangement of the spectator electrons is not taken into account, the R-term disappears, and we end up with $I = V$. This gives us the expression $V = -\epsilon_c$.
Koopmans' theorem (equation 23) is a one-electron model and is true under the condition that there are no relaxations of the spectator electrons during the ionization. This means that the same orbitals are describing both the final state and the ground state. Koopmans' theorem often give too high ionization

energies, and the difference between experiment and theory based on Koopmans' theorem has a tendency to increase with increasing ionization energies. The reason for this is the neglect of the final state effect R. Because it was shown that $-\Delta\epsilon_c$ provided estimates of unsatisfactory accuracy of ΔV due to the neglect of electron correlation in the initial state, it was necessary with an extension of Koopmans' theorem which took into account the influence of valence-electron correlation in addition to the wave nature of the core electrons. This extension was developed by Børve and Thomas [58] and is shown in equation 24:

$$\Delta V \approx -\Delta\epsilon_c + (\Delta U^{VCI} - \Delta U^{HF}) \tag{24}$$

In this equation, $\Delta\epsilon_c$ is the difference in initial-state core orbital energies, and ΔU is the difference in electrostatic energy of a unit positive charge at the two nuclei that are being compared. The superscripts HF and VCI denote Hartree-Fock and valence-correlated levels of theory respectively. Equation 24 is valid in the case of well-localized or close-to-degenerate inner-shell orbitals.

4.4 Computational details

All the theoretical calculations were done in the Gaussian 98 set of programs [46]. All the molecules were geometry optimized by using the hybrid density functional theory method B3LYP. In this density functional, exchange effects are modeled both by explicit Hartree-Fock exchange and by effective local and non-local density functionals. All calculations use atom-centered Gaussian-type functions contracted to triple-ξ quality [61] and augmented by polarization functions [62], leading to C[5s, 3p, 1d] and H[3s, 1p] and TZP as the default basis set. In addition to finding the equilibrium geometries, these calculations also generated harmonic vibrational frequencies and normal mode vectors which were used as input to the Franck-Condon analysis. In addition, the electric potentials from the B3LYP-calculation (U^{VCI}) were used to calculate ΔV and ΔR by using the extended Koopmans' theorem.
The B3LYP-optimized geometry of the molecules in the ground and final state were followed by calculations based on single point second order Möller-Plesset perturbation theory (MP2) with TZP as the default basis set. The idea of doing these calculations, was to improve the electronic energies to obtain more accurate theoretical chemical shifts, ΔI.
Restricted Hartree-Fock-calculations (RHF) were also carried out to calculate the carbon 1s orbital energies (ϵ_c) and the electric potentials (U^{HF}) which are used to calculate ΔV and ΔR using the extended Koopmans' theorem. The Hartree-Fock-calculations used optimized geometry from the B3LYP-calculations with TZP as the default basis set.
The symmetry of the molecules (in this thesis) in their ground state is generally the same. In the most cases, the molecules started out with containing one mirror plane leading to the point group C_s. During the optimization, however, many molecules chose to "destroy" this symmetry by twisting a little bit of the molecule ending up with no mirror plane and the

C_1-point group. 2-butyne (staggered conformation) has a D_{3d} symmetry while 3-hexyne, trans-2-butene, and trans-3-hexene have a C_{2h} symmetry.
The core of the ionized carbon atom was represented by Stevens and co-workers' effective core potential (ECP) [56]. This potential was scaled to account for only one electron in the 1s shell [40].

Chapter 5

5 The analysis of the data

This chapter will describe how the theoretical and experimental data is extracted and analysed. Three important programs in this process are the Scienta, G2FC, and Igor Pro programs.

5.1 The Scienta program

When the spectrum of a sample is recorded at MAX-lab, this recording has to be done several times to get enough *counts* (the number of counts is directly proportional to the intensity of the spectrum). These different recordings have to be summed to a final spectrum. This summation is carried out in the *Scienta program* [35]. This program is also used to control the recording of the data. A short introduction to how to use this program can be found in appendix A. The summed spectrum is now ready for the curve fitting process in Igor, which is described in section 5.3.

5.2 G2FC

As we shall see in section 5.3, we need theoretical calculated vibrational profiles in our curve fitting analysis. To get these profiles, we first have to do a calculation that gives us the necessary data. This is information like molecular geometries, normal modes, and vibrational frequencies of both the initial and core ionized state [36]. When this is done, the necessary data in the calculated output files has to be extracted in some way.
This is done by using a program made by Knut J. Børve [37]. This program is called G2FC and identifies the individual normal modes and their frequencies in the ground and final state. Gaussian output files for both the ground state and the different final states are used as an input. The program allows for individual scaling of the frequencies, perform Franck-Condon analysis for the totally symmetric modes, and provides computation of change in normal coordinate, Δq. Ionization of carbon 1s levels is accompanied by vibrational excitations, and the intensity of each vibrational line can be computed according to the Franck-Condon principle [38]. The present level of theory exaggerates the contraction in C-H bonds that takes place during the ionization of sp^3 carbons by 0.3 pm (1pm is 10^{-12}m) (in this thesis, this value was also used for the sp^2 carbon atoms). This value is taken from very accurate calculations of methane [40] and ethane [41]. Hence, when the Franck-Condon factors (see section 3.2) were computed, C-H bonds at the ionized carbon atoms were lengthened accordingly.
The calculated harmonic frequencies are slightly too high as compared with

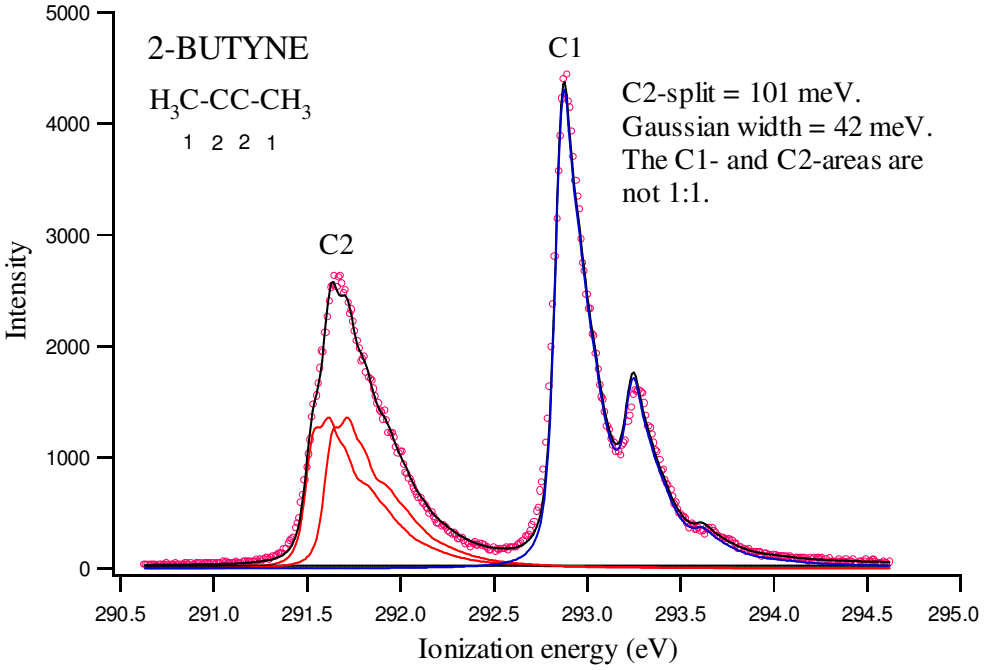

Figure 29: An Igor-fit of 2-butyne.

experimental frequencies. All the vibrational frequencies were therefore scaled by a factor of 0.99, except for the symmetric C-H stretching mode on the core ionized carbon atom which was scaled by a factor of 0.95.

5.3 Igor Pro

When all the spectra are summed in the Scienta program, and all the theoretical vibrational profiles generated in G2FC, we can try to fit the profiles to the experimental spectrum. The program we are using to do this fitting, is called Igor Pro [42]. An introduction to how to use this program is given in appendix B. An example of a 2-butyne spectrum fitted in Igor is shown in figure 29 (the analysis of this spectrum is done in section 6.1). The intensity is plotted along the ordinate while the carbon 1s ionization energy is plotted along the abscisse. The circles in the spectrum is the summed experimental data. The lines beneath the carbon 2 peak (C2) and carbon 1 peak (C1) are the theoretical calculated vibrational profiles. These profiles are added together to give a total profile shown by a line almost overlapping with the experimental data. As can be seen, the vibrational profile of each chemically inequivalent carbon atom is determining the shape of the spectrum.
The calculated chemical shifts are used to determine initial energies of the theoretical profiles. It is also assumed that the intensity areas of the different chemically inequivalent carbon atoms should be approximately equal. If these initial guesses are not totally in agreement with the experimental data, which they seldom are, the theoretical profiles have to be adjusted along the abscisse

and the ordinate to make them fit as much as possible without making it unreasonable. It is unreasonable when the resulting fitted chemical shifts and intensity area ratios are not what we expect them to be when we compare them to the theoretical results, and the fact that the number of ionized electrons from a specific carbon atom approximately should be equal to the number of ionized electrons from an another chemically inequivalent carbon atom in the molecule (the number of ionized electrons detected in the analyzer are directly proportional to the intensity areas).
The adjustments along the abscisse and ordinate are easily done in Igor. After a rough adjustment, the details are done in Igor by a *Fit* calculation. This calculation is focusing on making the χ^2 value as small as possible (χ^2 is the least squares fit goodness parameter). This means that the theoretical profiles are adjusted in the necessary direction along the abscisse and ordinate to make them overlap as much as possible under the restrictions I have specified in the Igor *Peaktable*. In this table, all the parameters of the theoretical profiles are controlled. These are parameters like Lorentzian widths[14], Gaussian widths[15], and the asymmetric parameter (the degree of asymmetry can be found from equation 25) in addition to the intensity, and ionization energy. The *Fit* calculation is followed by an *Auto* calculation to see if the fitting improves even more. These different calculations and the χ^2 value are further discussed in appendix B.

$$Asymmetry = \frac{1}{\sqrt{2}}\left(\frac{1}{\sqrt{\epsilon_{PE}}} - \frac{1}{\sqrt{\epsilon_{Auger}}}\right) \tag{25}$$

where $\epsilon_{PE} = \frac{E_{KIN}}{27.21}$ and $\epsilon_{Auger} = \frac{250}{27.21}$. E_{KIN} is the kinetic energy of the photoelectron ionized from the molecule in eV, while ϵ_{PE} is the kinetic energy of the photoelectron in atomic units (au). ϵ_{Auger} is the kinetic energy of the Auger electron in atomic units (au) [38]. This means that the asymmetry increases with decreasing kinetic energy of the photoelectron and increasing kinetic energy of the Auger electron (becomes zero when E_{KIN} is above or equal to 250 eV).
Equation 25 is an approach by van der Straten et al. [43] which models the effect of post collision interaction (PCI) (see section 3.1) with a Lorentzian lifetime width of 100 meV and a Gaussian width of 65 meV for the instrumental resolution.

[14]The Lorentzian width is related to the life time of the core hole.
[15]The Gaussian width depends on the analyzer, the light source, and the Doppler effect.

Chapter 6

6 Results and discussion

The molecules are presented in order of the increasing numbers of carbon atoms in the molecule in the first sections. In addition, a closer description of the chemical reactivity and ground and final state effects of the alkenes and alkynes is given in the two final sections.

6.1 The butenes and butynes

In this section all the experimental and theoretical results of 1-butene, (cis+trans)-2-butene, 1-butyne, and 2-butyne are given. A schematic structure of these molecules can be seen in figure 30:

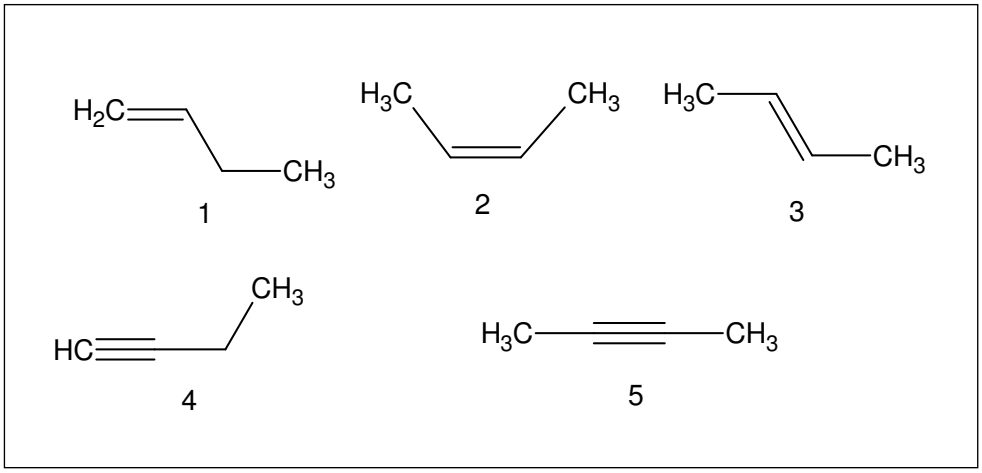

Figure 30: The structures of 1-butene (1), cis-2-butene (2), trans-2-butene (3), 1-butyne (4), and 2-butyne (5).

All of these molecules were measured at a photon energy of 330 eV[16] and an undulator gap of 30.76 mm. Cis- and trans-2-butene was measured experimentally as a mixture, and not individually. 1-butene and (cis+trans)-2-butene were measured at MAX-lab in Lund in Sweden with a passing energy (Ep) of 20 eV, an 800 SES-slit, and a step energy of 10 meV. 1-butyne and 2-butyne were measured at the Advanced Light Source (ALS) in Berkeley (California) in USA under comparable conditions.
Ab initio calculations were carried out on all these molecules, whereas the trans-2-butene results were used in the analysis instead of the cis-2-butene results. Trans-2-butene was chosen because of its higher ground state stability

[16] The photon energy is approximately 40 eV above the ionization energy of the C1s level.

Table 3: Theoretical calculated and experimental intramolecular chemical shifts (ΔI) of 1-butene, 1-butyne, trans-2-butene, and 2-butyne.

Molecule	**Atom**	ΔI_{calc} **(eV)**	ΔI_{exp} **(eV)**
1-butene	C1	0	0
	C2	0.416	0.410
	C3	0.485	0.547
	C4	0.301	0.366
1-butyne	C1	0	0
	C2	0.510	0.496
	C3	1.297	1.352
	C4	0.559	0.615
Trans-2-butene	C1	0	0
	C2	-0.312	-0.411
2-butyne	C1	0	0
	C2	-1.223	-1.337

compared to cis-2-butene. The ground state stabilities were measured and compared from the electronic and zero point energies based on B3LYP and MP2 calculations.
1-butene exists in three possible conformations; a "trans"-conformation, a "cis"-conformation, and a skew-conformation. Second-order Möller-Plesset theory showed that the skew-conformation was the most stable one. Likewise, the staggered conformation of 2-butyne was found to be the most stable one compared to the eclipsed 2-butyne. 1-butyne has only one probable conformation.
In table 3, the theoretical calculated and experimental intramolecular chemical shifts (ΔI) are presented. The carbon atoms are numbered from the end of the molecule where the double or triple bond is located. These chemical shifts were used in the fitting procedure in Igor as a start. In the most cases, these shifts had to be adjusted in the optimization to obtain a better fit. From the table, we can see that the carbon sequence is preserved for all the molecules. The shift differences between theory and experiment varies from 0 to 120 meV, and the average difference between theory and experiment is approximately 40 meV.

6.1.1 1-butene

The photoelectron spectrum of 1-butene is shown in figure 31. The sequence of the ionization energies of the four chemically different carbon atoms was determined theoretically and applied to the spectrum. As we can see, carbon atom number 1 has the smallest ionization energy while carbon 3 has the highest. The interpretation of this, is that carbon 1 is expected to be the most

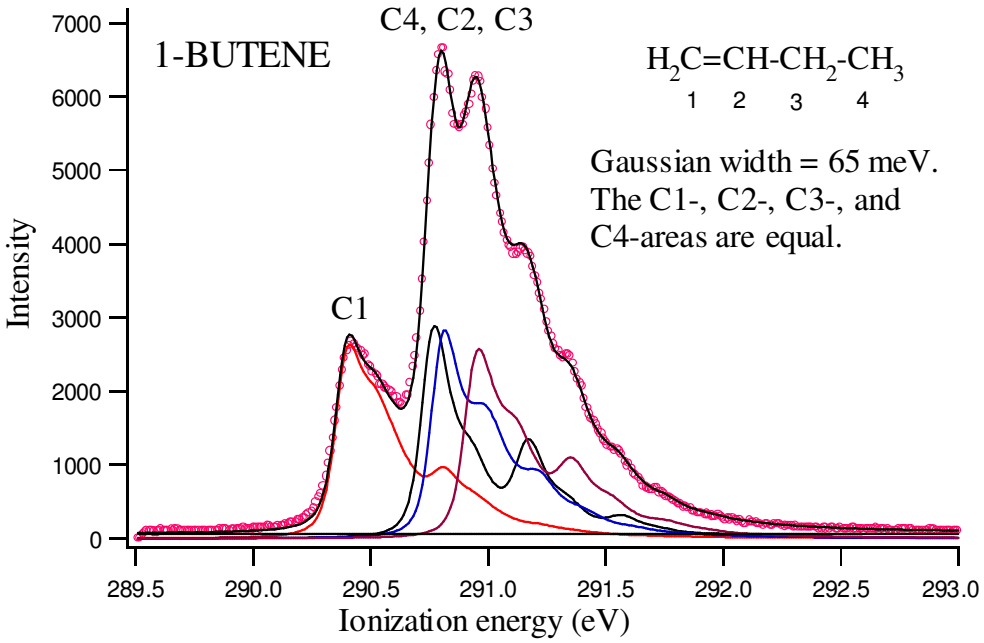

Figure 31: The carbon 1s spectrum of 1-butene.

reactive carbon atom in this molecule.
The life-time of the core hole, the *Lorentzian width*, was fixed to 100 meV (which was used in all the fitting procedures) while the *Gaussian width* (the instrumental resolution) was fixed to 65 meV. The Lorentzian width was taken from [44], while the Gaussian width was taken from [38]. As we shall see, there are examples of other Gaussian widths.
As mentioned in section 5.3, the intensity area ratios between all the inequivalent carbon atoms in the molecule should be approximately equal. The intensity area ratios were also obtained from the fit. In table 8, the adiabatic and vertical energies of each of the four different carbon atoms in 1-butene are tabulated.
The Igor fitting process started out with the carbon sequence shown in table 3. During the fitting of both the position and the intensity of the vibrational profiles to the experimental spectrum, the C1-C4-C2-C3 sequence did not change.
The resultant carbon atom ionization energy sequence (C1-C4-C2-C3) can be explained by the concept of *hyperconjugation* [63], which appears in all the alkenes and alkynes discussed in this thesis.
In valence bond theory, hyperconjugation is a special type of resonance which is used to describe interactions between the π system and substituent groups. Alkyl groups attached to carbon-carbon double bond act as electron donors to the π system, and "no bond" resonance structures are introduced to indicate this electronic interaction. For 1-butene, the hyperconjugation is as shown in figure 32.
A deprotonation of the CH_2 group leads to a localization of an electron pair

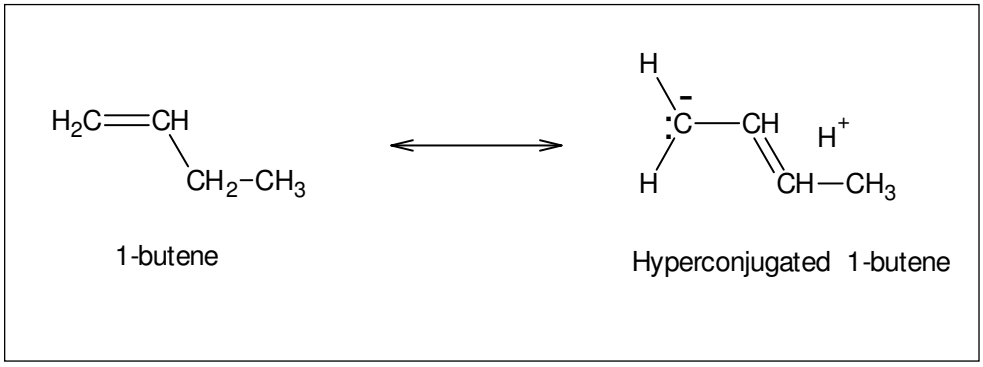

Figure 32: Hyperconjugation of 1-butene.

at the end carbon atom where the double bond was located (transfer of electron density from C3 to C1). The effect of this is that the ground state electron density around the end carbon atom is higher than the electron density around the other carbon atoms in the molecule. This results in a decrease in the energy required to core ionize the end carbon atom. Because of this, the end carbon atom is the one with the lowest ionization energy. When we take a look at the individual vibrational profiles of the four carbon 1s ionizations, we can notice that each profile has a long tail with a shoulder in the high ionization energy range. The appearance of the tails can be explained by the different vibrational excitations that take place in the core-ionization process. Both bending and stretching modes are excited in the core ionization, but it is mainly C-H-stretching modes that is the origin of the shoulders in the high ionization energy range of the profile.
If we compare the intensity areas with the number of hydrogen atoms for each carbon atom in 1-butene, we can find a trend. The more hydrogen atoms connected to a specific carbon atom, the larger the intensity area of the shoulder for the corresponding vibrational profile. This can also be seen in references [64] and [65].

6.1.2 Cis+trans-2-butene

2-butene is a symmetric molecule with only two chemically inequivalent carbon atoms giving only two vibrational profiles in the photoelectron spectrum shown in figure 33.
We can notice a split of 53 meV between the two vibrational profiles of carbon atom number 2. This split appears because of close interaction between the core orbitals of the two unsaturated carbon atoms. The bond length between two carbon atoms decrease in the order $C-C > C=C > C \equiv C$, which means that the triple bond has the shortest bond[17]. Because of the short bond length, the equivalent core orbitals are getting closer and can interact with each other to give a splitting due to incomplete localization of the core

[17]The carbon-carbon single bond is approximately 1.54 Å, the carbon-carbon double bond approximately 1.33 Å, while the carbon-carbon triple bond is about 1.20 Å.

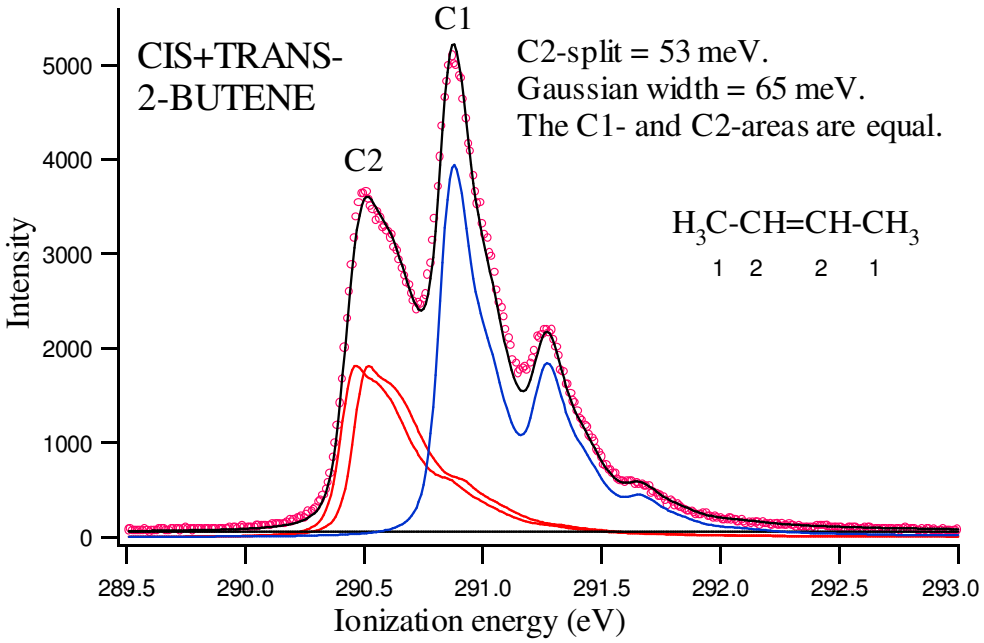

Figure 33: The carbon 1s spectrum of cis+trans-2-butene.

hole (this kind of splitting is further discussed in reference [32] and [66]). The splitting of a symmetric alkyne is therefore normally bigger than for the corresponding alkene.
If the energies of the two core orbitals were significant different, the interaction between the two core orbitals would be very small and the resultant splitting very small independent of the degree of unsaturation. This is the case for unsymmetric molecules. However, if the molecule is symmetric, like 2-butene, the core orbitals have similar energies and can interact to give a significant splitting. In this case, the degree of unsaturation will play a role regarding the magnitude of the splitting.
Table 8 is showing the adiabatic and vertical energies of 2-butene, where carbon 2 is the one with the lowest adiabatic energy.
As we can see, the sequence of the carbon atoms in the fitted spectrum is the same as predicted by theory shown in table 3. This can also be rationalized by using the concept of hyperconjugation.
The C2-split was optimized to 53 meV in the fitting, while the core hole life time and Gaussian width was fixed to 100 meV and 65 meV respectively. The intensity area ratio between C1 and C2 was fixed to 1:1. This was done because we expect the intensities of the different carbon atoms to be stoichiometric similar. In addition, the bigger shoulder in the tail of the vibrational profile of C1 compared to that of C2, can be explained by comparing the number of hydrogen atoms connected to the end carbon atoms with the number of carbon atoms connected to the inner carbon atoms. This ratio is 6:2, which means that the intensity area of the C1-shoulder should be approximately three times bigger than the intensity area of the C2-shoulder.

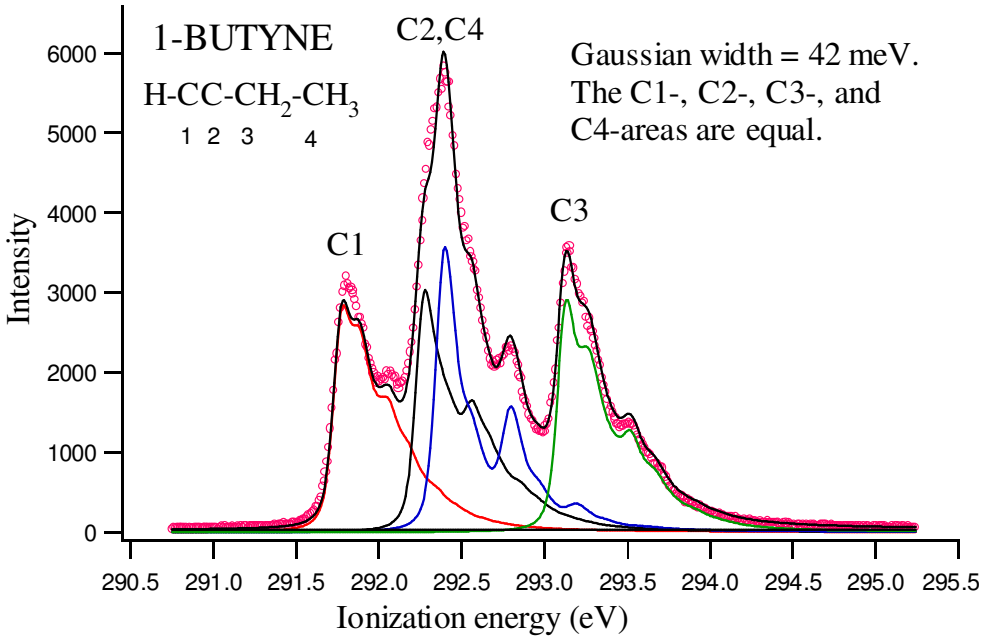

Figure 34: The carbon 1s spectrum of 1-butyne.

As previously noted, these shoulders appears in the spectrum due to excitations of C-H stretching modes.

6.1.3 1-butyne

The obtained experimental adiabatic and vertical energies of 1-butyne are shown in table 8. From this table we can see that carbon 1 is the one with the lowest adiabatic energy, as was the case for 1-butene. The sequence of the carbon atoms (C1-C2-C4-C3) can be explained by hyperconjugation and is the same as predicted by theory.
The carbon 1s photoelectron spectrum of 1-butyne is shown in figure 34. 1-butyne has four chemically inequivalent carbon atoms which give rise to four different vibrational profiles in the spectrum. As expected, C3 and C4 have the broadest shoulders due to C-H stretching vibrations. The Lorentzian and Gaussian width was fixed to 100 meV and 42 meV respectively[18]. The intensity area ratios between the four inequivalent carbon atoms were fixed to be equal. As we shall see for 2-butyne, the intensity area ratio is *not* 1:1. The reason for this is explained in section 6.1.4.

6.1.4 2-butyne

The photoelectron spectrum of 2-butyne is shown in figure 35, and the adiabatic and vertical energies of the two chemically inequivalent carbon

[18]The carbon 1s photoelectron spectrum of 1-butyne and 2-butyne were obtained at ALS in Berkeley (California), USA.

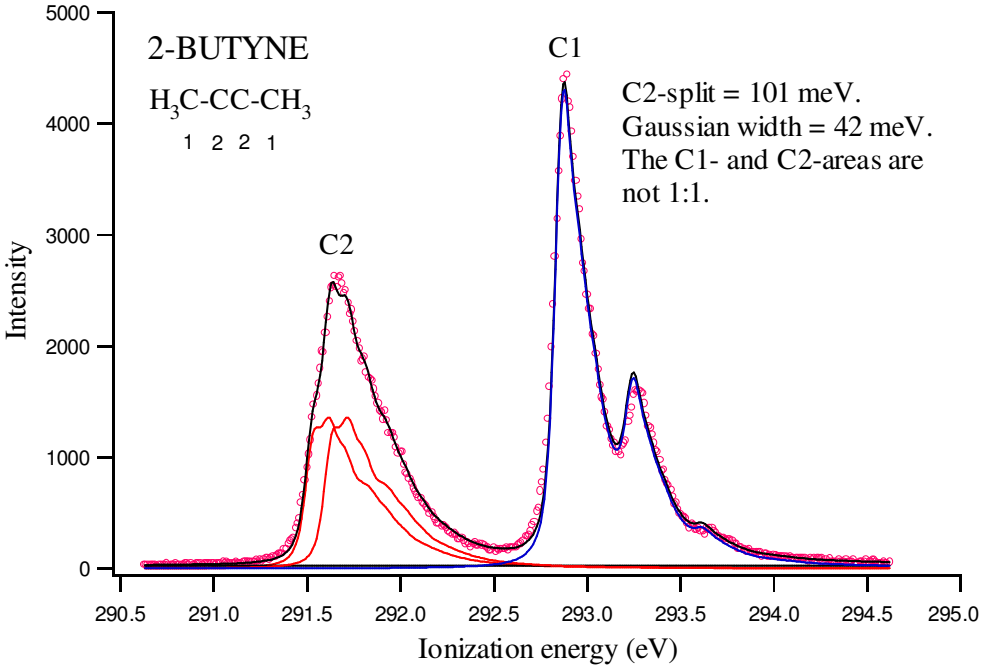

Figure 35: The carbon 1s spectrum of 2-butyne.

atoms are tabulated in table 8.

Two features in the spectrum of 2-butyne are worth mentioning. The first feature is the unequal intensity areas of C1 and C2. It is not shown in the spectrum of 2-butyne, but Igor showed that the intensity area of C2 was *smaller* than the intensity area of C1. This unequality can be explained by taking into account the *shake-up process*. This is a process which frequently occur in symmetric unsaturated molecules. It also occurs in unsymmetric unsaturated molecules, but not to such a significant degree. As described in section 3.4, the shake-up process is a process in which core electrons are excited from the highest occupied molecular orbital (HOMO) to the lowest unoccupied molecular orbital (LUMO). This happens due to the small energy difference between the two MO's. Because of this, low intensity satellites appears in the spectra at positions corresponding to this energy difference, and less of the unaffected core electrons are detected in the analyzer, and the resultant intensity area is smaller.

The second feature is the C2-split of 100 meV (due to incomplete localization of the core hole). We noticed that the C2-split in 2-butene was 53 meV, so what is the reason for the larger split in the case of 2-butyne? The triple bond is shorter than the double bond, so the distance between the core orbitals in the alkyne is smaller than for the corresponding alkene. This allows the core orbitals in the alkyne to interact more than in the alkene, which finally results in a larger splitting in the alkyne compared to the alkene. The intensity area ratio of the two splitted profiles is 1:1.

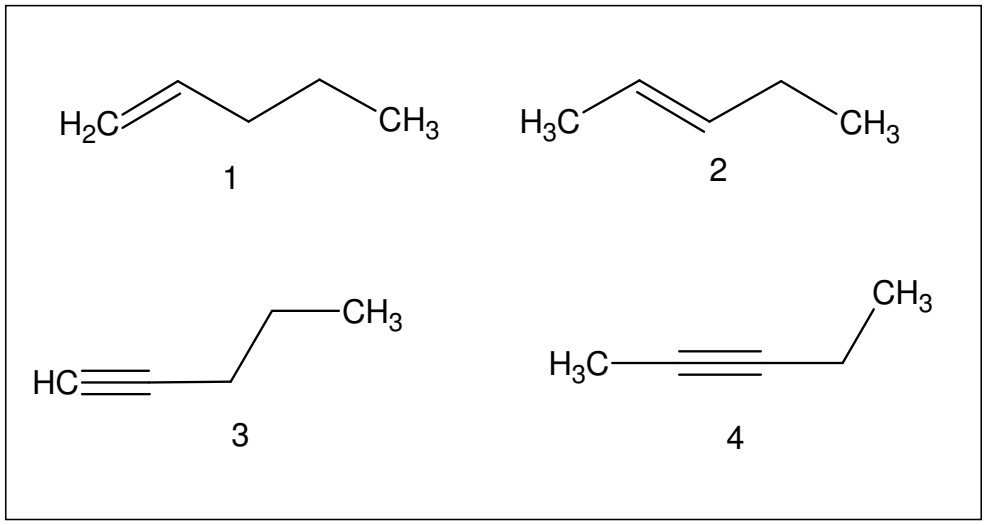

Figure 36: The structure of 1-pentene (1), trans-2-pentene (2), 1-pentyne (3), and 2-pentyne (4).

Table 4: Settings used during the measurements of the pentenes and pentynes.

Pass energy (Ep)(eV)	20
SES-slit	900
Step energy (meV)	10
Time per step (sec)	0.2
Undulator gap (mm)	30.76
Monochromator slit (μm)	5

6.2 The pentenes and pentynes

In this section we will take a closer look at the theoretical and experimental results of 1-pentene, trans-2-pentene, 1-pentyne, and 2-pentyne. The schematic structures of these molecules are shown in figure 36.
All of these molecules were measured at a photon energy of 330 eV at MAX-lab in Lund in Sweden. Some of the settings used during the measurements of these molecules are presented in table 4.
Ab initio calculations were carried out on all 4 molecules. 1-pentyne has two different conformations in the ground state of comparable energy. It is important to know the energy of the possible conformations, because the two conformations may give vibrational profiles that are significantly different.
The calculated and experimental intramolecular chemical shifts of the pentenes and pentynes are presented in table 5. These chemical shifts were used as a starting point in the Igor fitting, and also in this case the fitted chemical shifts were not the same as the starting point. This altering did not change the intramolecular carbon sequence for other molecules than 1-pentene (C3 and C4 switched places). The differences between theory and experiment

Table 5: Theoretical calculated and experimental intramolecular chemical shifts (ΔI) of 1-pentene, skew-1-pentyne, trans-2-pentene, and 2-pentyne.

Molecule	**Atom**	ΔI_{calc} **(eV)**	ΔI_{exp} **(eV)**
1-pentene	C1	0	0
	C2	0.396	0.399
	C3	0.357	0.384
	C4	0.355	0.390
	C5	0.319	0.308
Skew-1-pentyne	C1	0	0
	C2	0.523	0.543
	C3	1.182	1.213
	C4	0.565	0.618
	C5	0.264	0.381
Trans-2-pentene	C1	0	0
	C2	-0.358	-0.422
	C3	-0.452	-0.531
	C4	-0.0627	-0.0490
	C5	-0.128	-0.175
2-pentyne	C1	0	0
	C2	-1.291	-1.309
	C3	-1.345	-1.435
	C4	-0.106	-0.109
	C5	-0.775	-0.767

varies from 0 to 117 meV, while the average difference is approximately 30 meV.

6.2.1 1-pentene

The spectrum of 1-pentene is presented in figure 37. 1-pentene has a double bond located at the end of the carbon chain, and it is numbered from this unsaturated end.

1-pentene has five chemically inequivalent carbon atoms which give five different vibrational profiles in the spectrum. The starting sequence of these profiles in the fitting process, was the one shown in table 5: C1, C5, C4, C3, and C2. This is not the same as the fitted sequence shown in the spectrum which is C1, C5, C3, C4, and C2. C3 and C4 switched places with one another. The chemical shifts of these two carbon atoms are very similar. This means that it is hard to differ between these two carbon atoms with respect to ionization energies both theoretically and experimentally. However, C1 is the

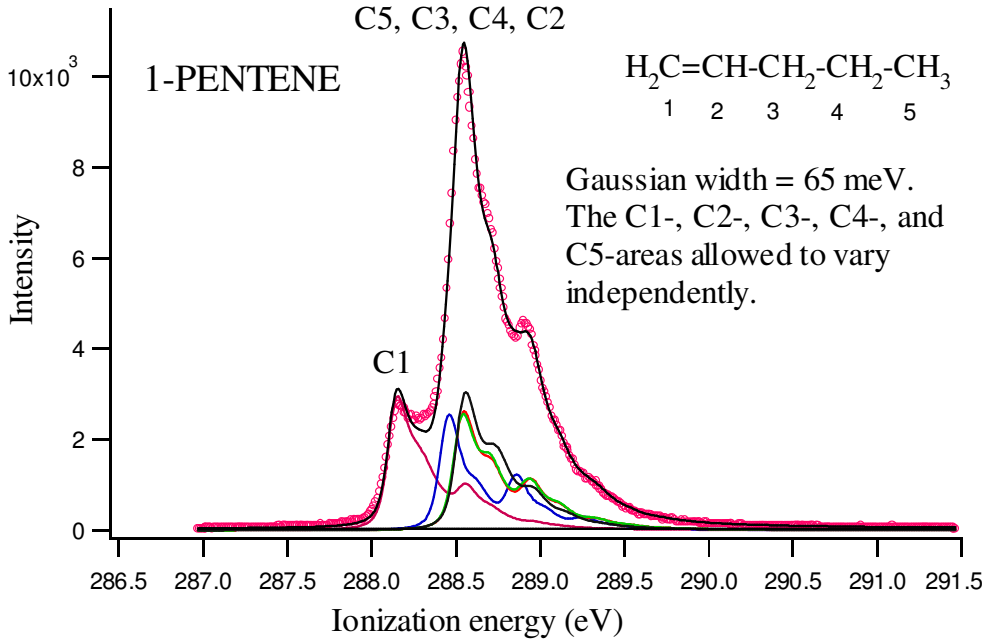

Figure 37: The carbon 1s spectrum of 1-pentene.

first adiabat and has the lowest ionization energy. This can be explained by the high electron density associated with double and triple bonds. Because of this, we expect C1 to be the most reactive carbon atom in 1-pentene.
As mentioned earlier, CH-stretching vibrations can be seen in the spectrum by considering the high-energy "shoulders". The intensities of these "shoulders" are varying according to the number of H-atoms in the CH_n group in the molecule. The more H-atoms, the higher the intensity area of the "shoulder" becomes [64], [65]. The adiabatic and vertical energies of 1-pentene can be seen in table 8. As we can see from the table, C1 is clearly the one with the lowest ionization energy. The sequence of the carbon atoms in the fitted spectrum can again be explained by the concept of hyperconjugation.

6.2.2 Trans-2-pentene

Like 1-pentene, 1-pentyne, and 2-pentyne, trans-2-pentene has five chemically inequivalent carbon atoms. We should therefore expect this molecule to have five different vibratonal profiles in the photoelectron spectrum. The chosen geometry of this molecule is the trans-configuration with the ethyl group (C4 and C5) oriented in a "linear" manner (see figure 38).
The spectrum of trans-2-pentene is presented in figure 39. The carbon atoms are numbered from the unsaturated end. As we can see, C2 and C3 have the lowest ionization energies as expected from the high electron density associated with the double bond. The adiabatic and vertical energies are presented in table 8. The theoretical and fitted carbon atom sequence is the same.

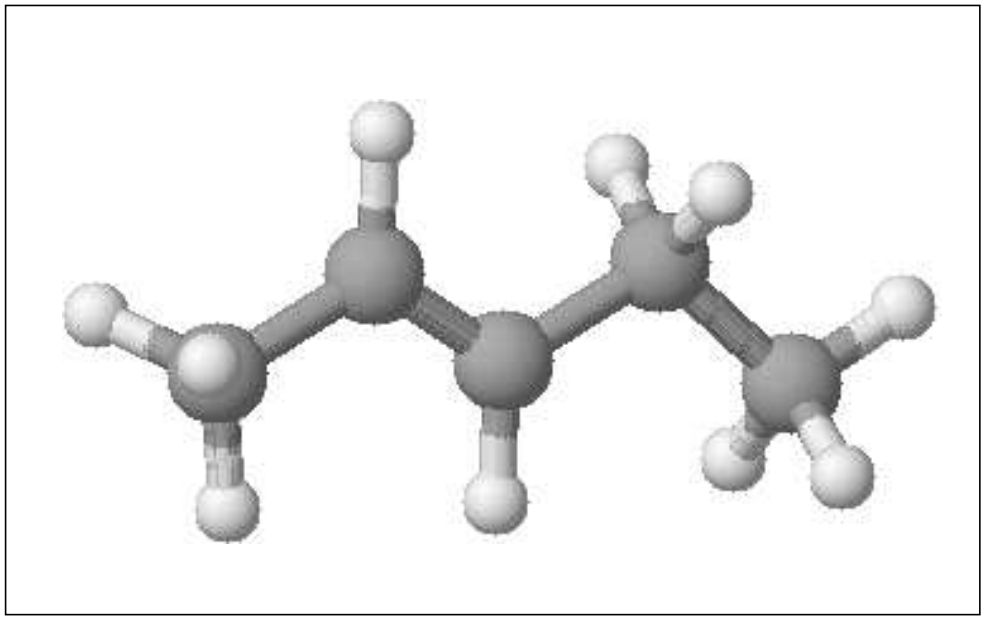

Figure 38: The geometry of trans-2-pentene used in the calculations.

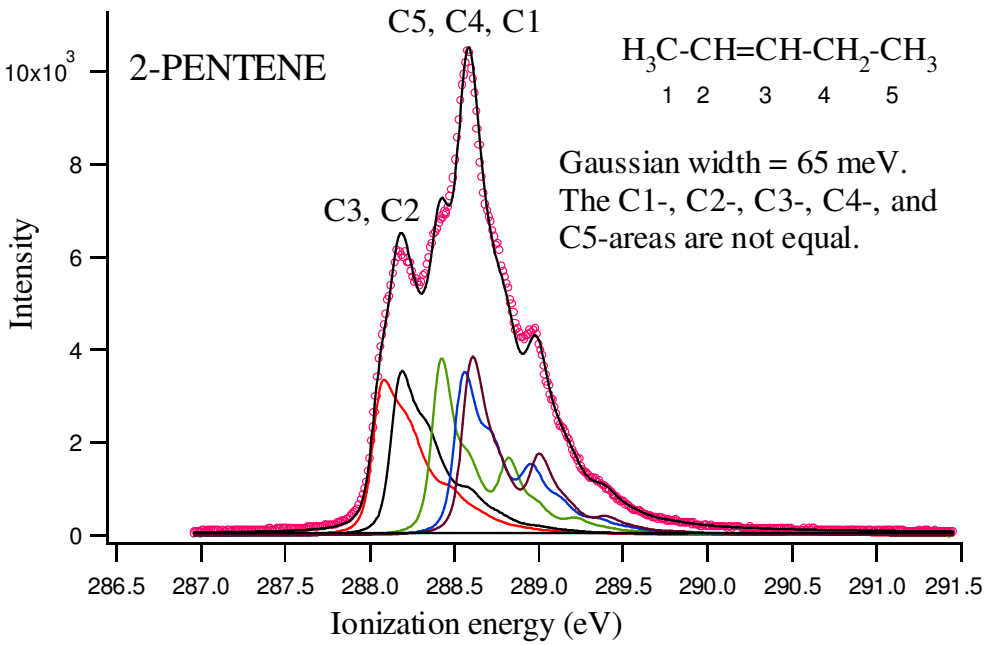

Figure 39: The carbon 1s spectrum of trans-2-pentene.

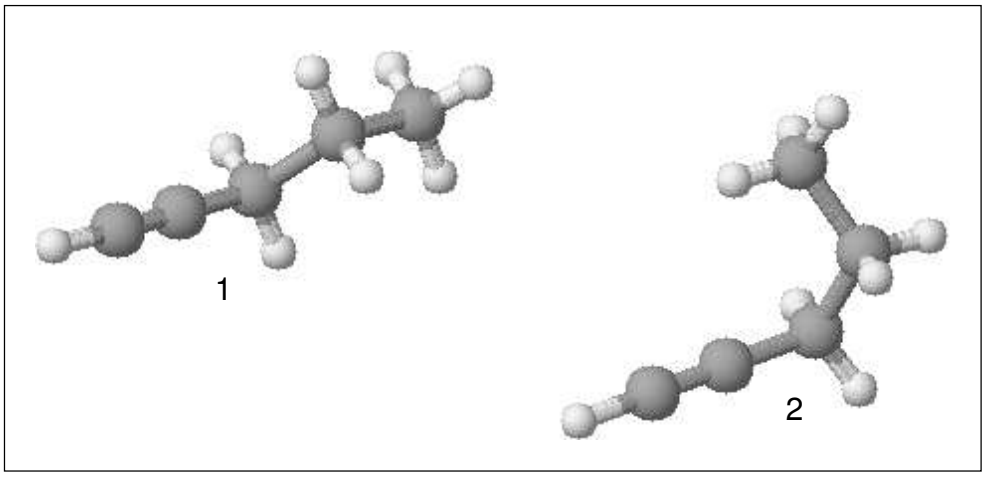

Figure 40: The structure of "trans"-1-pentyne (1) and skew-1-pentyne (2).

6.2.3 1-pentyne

1-pentyne has two conformations in which both could be the most stable one. This is the linear "trans"-1-pentyne and skew-1-pentyne. According to the MP2-calculations, skew-1-pentyne should be the most stable ground state conformation of these two. The MP2-calculations were based on DFT-results which sensationally indicated the opposite (this is also the case for 2-hexyne). Because of a higher accuracy of an MP2-calculation compared to a DFT-calculation, the vibrational profiles were generated from the skew-conformation. There is a possibility of an equilibrium between the skew- and "trans"-conformation, but because of a majority of the skew-conformation (81% skew), only this one was taken into account. The distribution of the conformations was determined by extracting the necessary information from theoretical calculations (the calculations where the distribution is determined, will be shown in more detail in section 6.3.5 where 2-hexyne is discussed). See figure 40 for an illustration of the two conformations.

The shape of the vibrational profiles of the two 1-pentyne conformations were identical, except the C1s ionization of carbon atom number 5 (the methyl group). When both conformations were mixed in the same Igor fitting, no improvement of χ^2 was observed. As we shall see in section 6.3.5, the fitting of 2-hexyne improves when a mixture of vibrational profiles of two different conformations are used.

The carbon 1s spectrum of 1-pentyne is presented in figure 41, and the adiabatic and vertical energies can be found in table 8.

As we can see from table 8, the carbon atoms are clearly separated from one another with different IE's. The theoretical and fitted carbon atom sequence is the same. C1 has the lowest IE and is therefore expected to be the most reactive carbon atom in 1-pentyne.

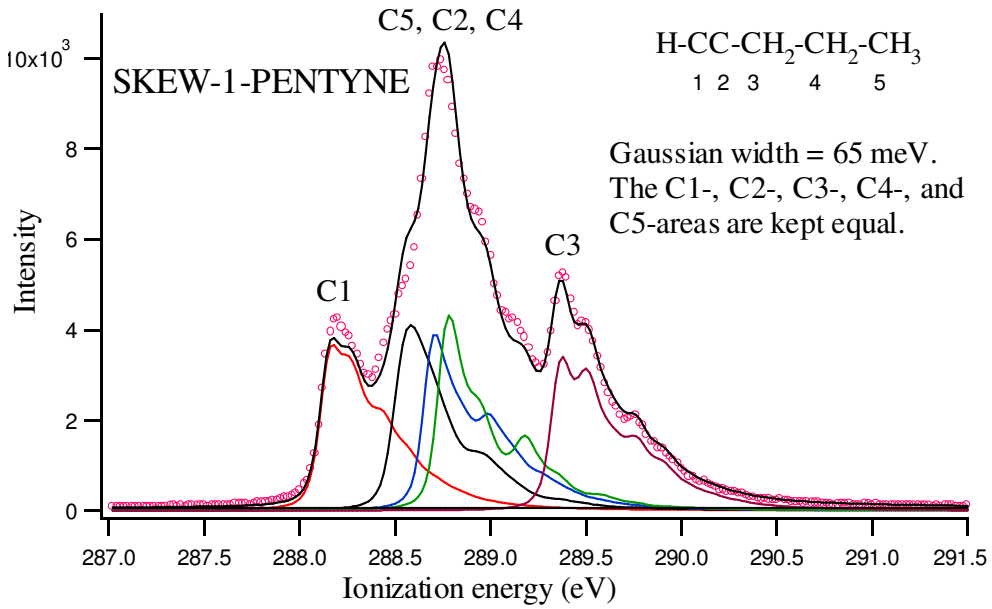

Figure 41: The carbon 1s spectrum of 1-pentyne.

6.2.4 2-pentyne

2-pentyne has only one probable conformation. The carbon 1s spectrum of 2-pentyne is presented in figure 42. In table 8, the adiabatic and vertical energies are listed.
The IE's of the different carbon atoms are also in this case clearly separated, and the "shoulders" that have it's origin from the C-H stretch vibrations of C1 and C5 can easily be seen in the spectrum. As expected, C2 and C3 have the lowest ionization energies because of the high electron density associated with the triple bond in addition to the effect of hyperconjugation.

6.3 The hexenes and hexynes

The hexenes and hexynes discussed in this section are 1-hexene, trans-2-hexene, trans-3-hexene, 1-hexyne, 2-hexyne, and 3-hexyne, which gives a total of six different molecules. Other configurations like cis-2-hexene and cis-3-hexene are possible, but we chose to study the trans-isomers because of their higher energy compared to the corresponding trans-configurations.
As we will see in section 6.3.5, 2-hexyne consists of a mixture of two conformations in its ground state; "trans"-2-hexyne and skew-2-hexyne. For the other hexenes and hexynes, there are several possible conformations which may exist. For each hexene and hexyne, the linear/stretched geometry was used. The vibrational profiles generated from these molecules were well fitted to their experimental spectrums. This indicated that the chosen geometry was adequate to describe the spectrum. Therefore it was not necessary to do calculations on the other possible conformations. Figure 43 shows the structures of the six different hexenes and hexynes.

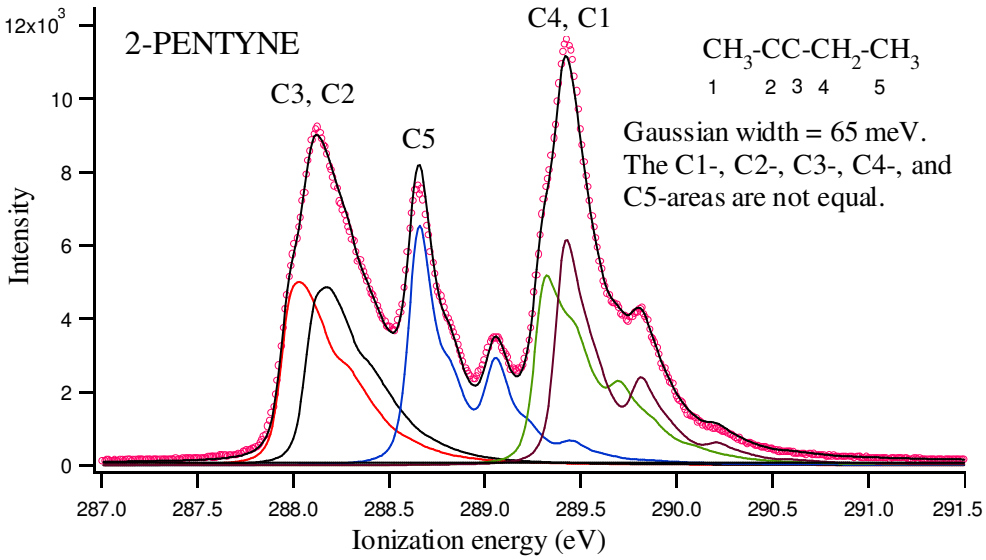

Figure 42: The carbon 1s spectrum of 2-pentyne.

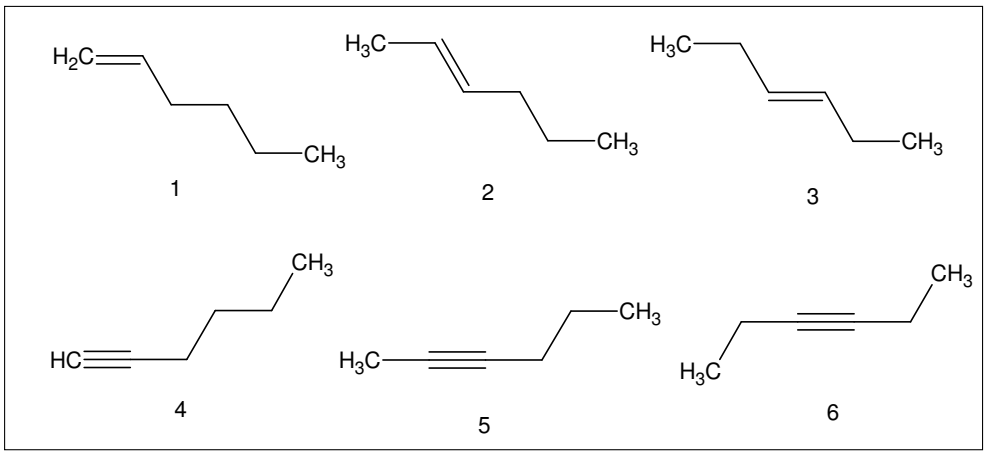

Figure 43: The structure of 1-hexene (1), trans-2-hexene (2), trans-3-hexene (3), 1-hexyne (4), 2-hexyne (5), and 3-hexyne (6).

As for the pentenes and pentynes, all the hexenes and hexynes were measured at MAX-lab in Lund, Sweden. The chosen photon energy was also in this case 330 eV. The settings used in these measurements were the same as those shown in table 4, except a SES slit of 800 instead of 900.
Ab initio calculations were carried out on all six molecules. This was also done for skew-1-hexyne and skew-2-hexyne. The skew-conformations were interesting because they were a good alternative to the corresponding "trans"-configurations with respect to ground-state stability. The MP2-results showed that "trans"-1-hexyne was more stable than skew-1-hexyne, and that skew-2-hexyne was more stable than "trans"-2-hexyne. This will be further discussed in section 6.3.4 and 6.3.5.
The chemical shifts of all the hexenes and hexynes were calculated, and these are presented in table 6. The hexenes and hexynes are numbered from the unsaturated end.
These chemical shifts were used as a starting point in the Igor fitting procedures. From the table, we can see that the experimental chemical shifts are not the same as the theoretical. This shift difference leads to no change in the intramolecular carbon sequence, and it varies from 0 to 132 meV. The average difference is approximately 30 meV (the same as for the pentenes and pentynes).

6.3.1 1-hexene

The core photoelectron spectrum of 1-hexene is shown in figure 44. 1-hexene has six chemically different carbon atoms which results in six different vibrational profiles with different ionization energy. C1 is the one with the lowest ionization energy. Table 9 shows this adiabatic and vertical energy in addition to the energies of the other carbon atoms.
As we can see, the carbon sequences are the same when we compare the theoretical results with the fitted ones. The vibrational profiles were well fitted to the experimental spectrum.

6.3.2 Trans-2-hexene

The core photoelectron spectrum of trans-2-hexene is presented in figure 45. The intensity areas of C2 and C3 are slightly smaller than the intensity areas of the other carbon atoms. The reason for this is the shake-up process. This molecule has six different carbon atoms in which C3 has the smallest ionization energy. The adiabatic and vertical energies are presented in table 9. The carbon sequence in the spectrum is the same as the theoretical one. The vibrational profiles are well resolved and well fitted to the experimental spectrum.

6.3.3 Trans-3-hexene

Trans-3-hexene is an alkene with the possibility of a mirror plane and a C_2-axis as symmetry elements. This makes this molecule (and 3-hexyne) more symmetrical than the other hexenes and hexynes. This means that this

Table 6: Theoretical calculated and experimental intramolecular chemical shifts (ΔI) of 1-hexene, trans-2-hexene, trans-3-hexene, 1-hexyne, 2-hexyne, and 3-hexyne.

Molecule	**Atom**	ΔI_{calc} **(eV)**	ΔI_{exp} **(eV)**
1-hexene	C1	0	0
	C2	0.398	0.420
	C3	0.337	0.365
	C4	0.233	0.218
	C5	0.302	0.360
	C6	0.296	0.302
Trans-2-hexene	C1	0	0
	C2	-0.372	-0.431
	C3	-0.471	-0.550
	C4	-0.194	-0.243
	C5	-0.147	-0.135
	C6	-0.153	-0.189
Trans-3-hexene	C1	0	0
	C2	0.0590	0.131
	C3	-0.378	-0.360
1-hexyne	C1	0	0
	C2	0.538	0.530
	C3	1.172	1.192
	C4	0.456	0.453
	C5	0.469	0.489
	C6	0.415	0.353
2-hexyne	C1	0	0
	C2	-1.321	-1.353
	C3	-1.363	-1.464
	C4	-0.250	-0.278
	C5	-0.796	-0.829
	C6	-1.050	-1.009
3-hexyne	C1	0	0
	C2	0.663	0.646
	C3	-0.639	-0.771

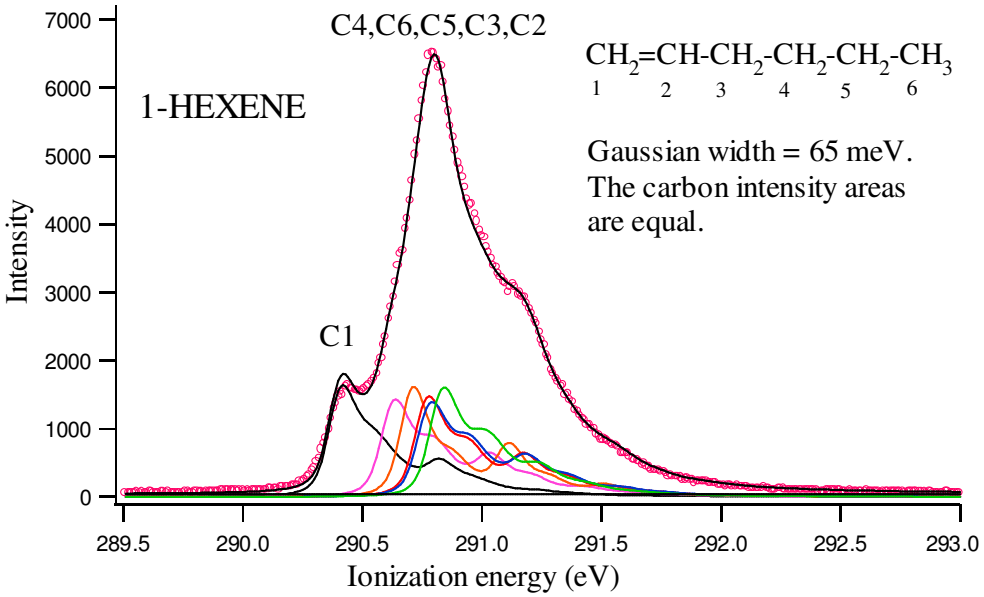

Figure 44: The carbon 1s spectrum of 1-hexene.

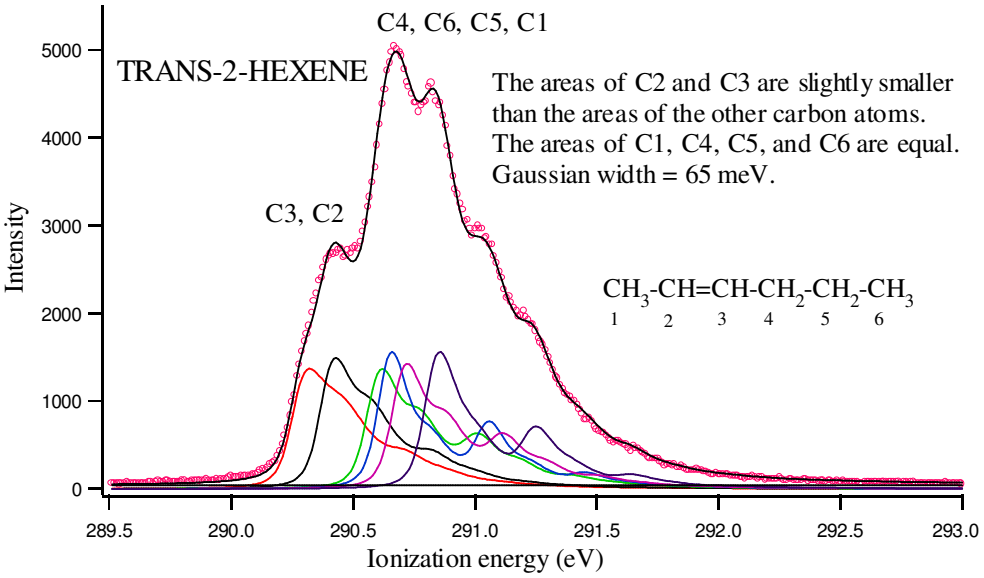

Figure 45: The carbon 1s spectrum of trans-2-hexene.

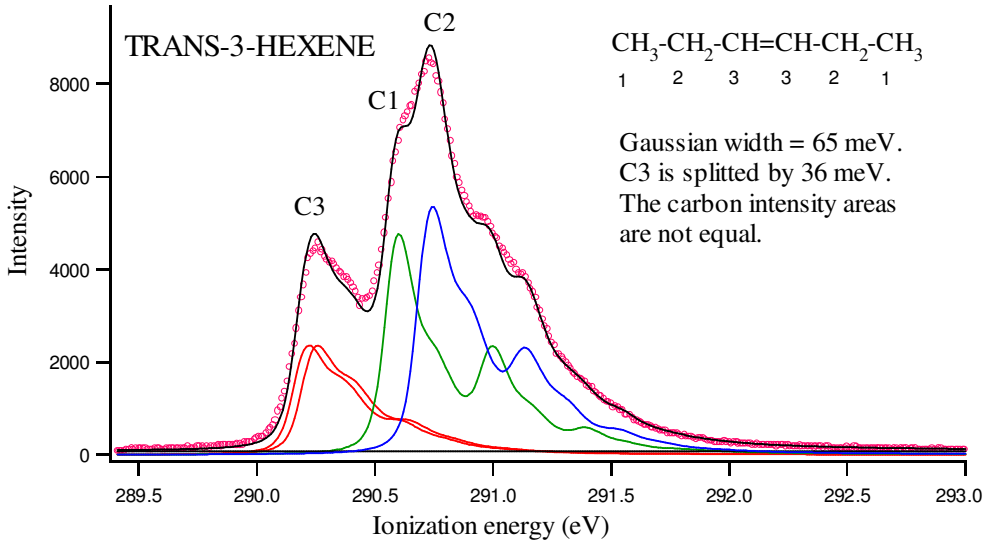

Figure 46: The carbon 1s spectrum of trans-3-hexene.

molecule (and 3-hexyne) belongs to the C_{2h} point group, while the other hexenes and hexynes (except for the skew conformations) only have one mirror plane which leads to the C_s point group. During energy optimizations in Gaussian, the finally optimized molecule often ended up with neither a mirror plane nor a C_2 symmetry element. In this case, the molecules belongs to the C_1 point group. Because of the C_2 symmetry element, trans-3-hexene (and 3-hexyne) has only three chemically inequivalent carbon atoms. Because of the close interaction between the C3 core orbitals in trans-3-hexene, the vibrational profile of C3 is splitted into two separated profiles with a splitting of 36 meV (due to incomplete localization of the core hole). This can be seen in figure 46.
The intensity area of C3 is slightly smaller than for C1 and C2 due to the shake-up process. Since trans-3-hexene only have three different carbon atoms, it is more easy to separate the carbon atoms which in turn makes it possible to relax the restrictions on area ratios. This means that it is not that important to have a carbon intensity area ratio which is 1:1. As expected, C3 is the carbon atom with the lowest ionization energy. The adiabatic and vertical energies of trans-3-hexene are presented in table 9.

6.3.4 1-hexyne

1-hexyne has a triple bond located at the end of the carbon chain and has six chemically different carbon atoms. The spectrum of this alkyne is shown in figure 47.
As mentioned in the introduction (section 6.3), two possible conformations called skew- and "trans"-1-hexyne were investigated. These are illustrated in figure 48.
After performing MP2-calculations on these two conformations, it was found

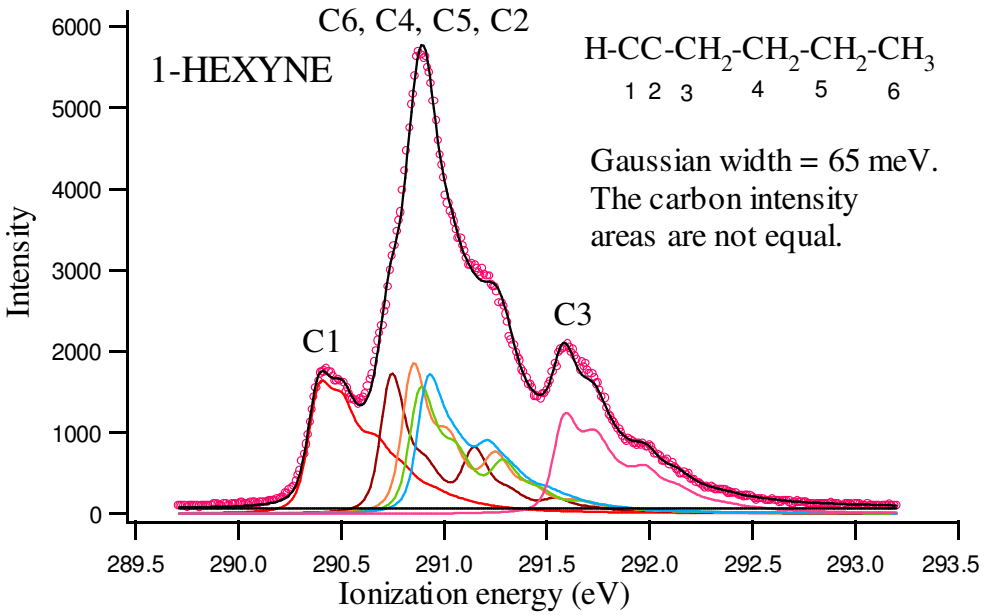

Figure 47: The carbon 1s spectrum of 1-hexyne.

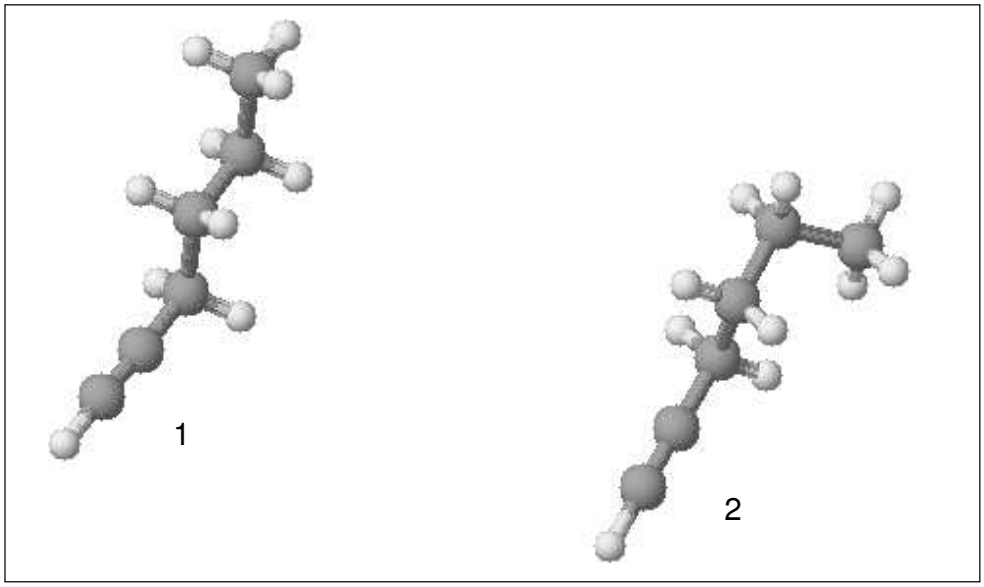

Figure 48: The structure of "trans"-1-hexyne (1) and skew-1-hexyne (2).

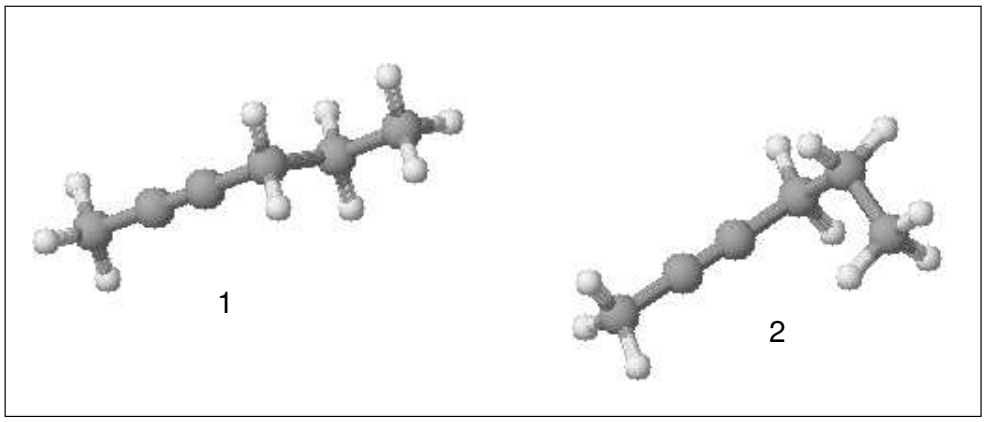

Figure 49: The structure of "trans"-2-hexyne (1) and skew-2-hexyne (2).

that the "trans"-conformation was more stable than the skew-conformation. The MP2-calculations were based on results from DFT-calculations which gave the same results. This was not the case for 2-hexyne and 1-pentyne. The DFT-results indicated that the "trans"-conformation of 2-hexyne should be more stable than the skew-conformation. The MP2-results indicated the opposite.
The difference in ground state energies between these two conformations appear to be so large that the skew-conformation could be eliminated from the fitting of 1-hexyne. The DFT calculations indicated a distribution of 97% of the "trans"-conformation and 3% of the skew-conformation, while MP2 indicated 93% "trans" and 7% skew. Because of this, the vibrational profiles from the "trans"-conformation were the only profiles that were used in the Igor fitting procedure. The resultant adiabatic and vertical energies are shown in table 9.

6.3.5 2-hexyne

Among all the molecules presented in this thesis, 2-hexyne has been the most time-consuming and difficult molecule to calculate and fit. At the same time, it has been the most interesting and special molecule to work with. The work with this molecule is not yet completed, and only preliminary results will be presented.
As mentioned earlier, 2-hexyne has two interesting conformations. These are skew-2-hexyne and "trans"-2-hexyne and are illustrated in figure 49.
The work started out with calculations on the "trans"-conformation followed by generation of the corresponding vibrational profiles. The result of the fitting of this conformation is shown in figure 50.
As we can see, some of the vibrational profiles are not well fitted to the experimental spectrum. The intensity distribution of the vibrational profiles of C2, C3, and C6 is not consistent with the experimental result. What could be the reason(s) for this? Contamination of the test sample during the measurement was one possibility. After doing new measurements with a new

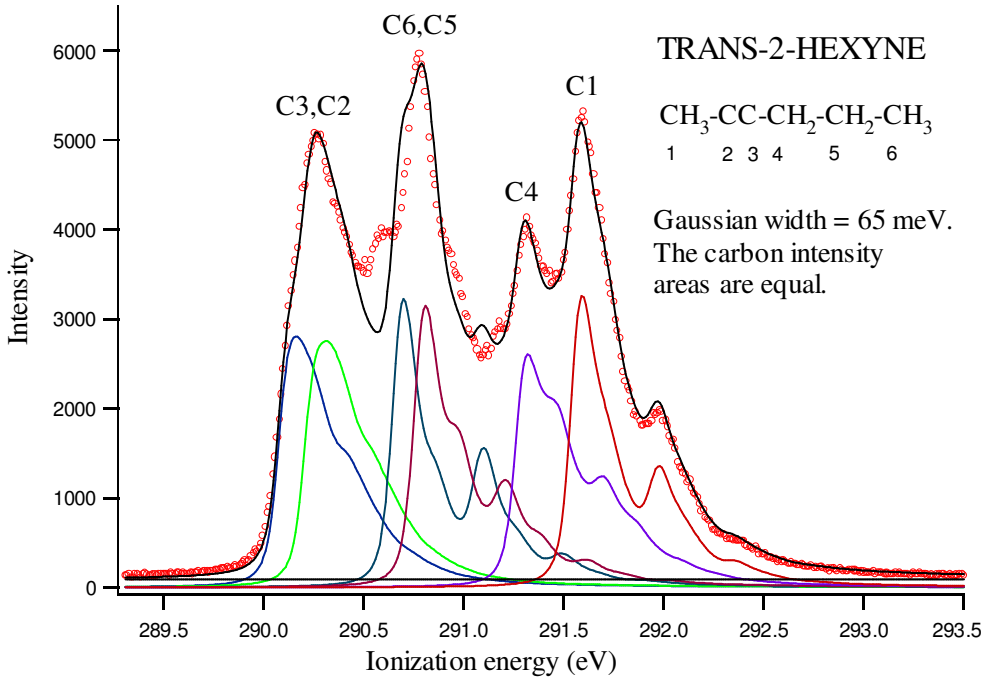

Figure 50: The carbon 1s spectrum of "trans"-2-hexyne.

sample of 2-hexyne from an another production company, the resultant spectrum was identical to the first one. Therefore, there had to be other reasons for this bad fitting.

We then looked at the other possible conformations of 2-hexyne. The other two conformations were skew-2-hexyne and "cis"-2-hexyne. In "cis"-2-hexyne, the ethyl group (C5 and C6) is twisted 180^o from the original geometry of "trans"-2-hexyne. The DFT-calculations showed that the "cis"-geometry was energetically unfavourable, and ended up with the skew-conformation in the energy optimization. Skew-2-hexyne turned out to be the most stable conformation of them all. This was the result of the MP2-calculations based on the DFT results. Therefore, vibrational profiles of this conformation was generated, and the results turned out to be somewhat different compared to "trans"-2-hexyne. The profiles of C2, C3, and C6 did not have the same shape in the two different conformations. In contrast, the profiles of C1, C4, and C5 are unaffected. The spectrum of skew-2-hexyne can be seen in figure 51.

In fact, we can rationalize this difference by taking a look at a model of 2-hexyne. In "trans"-2-hexyne, the distance between C6 and C2+C3 is large and there is little interaction between the protons of C6 and the π bonds of the triple bond. However, when the ethyl group (C5 and C6) in "trans"-2-hexyne is twisted 120^o to a skew-2-hexyne conformation, the distance between C6 and C2+C3 has become smaller, which in turn increases the interaction between the C6 protons and π electrons.

DFT calculations of skew-2-hexyne showed that the distance between the C6 proton and C3 was 2.82 Å in the ground state. This distance was 2.87 Å for

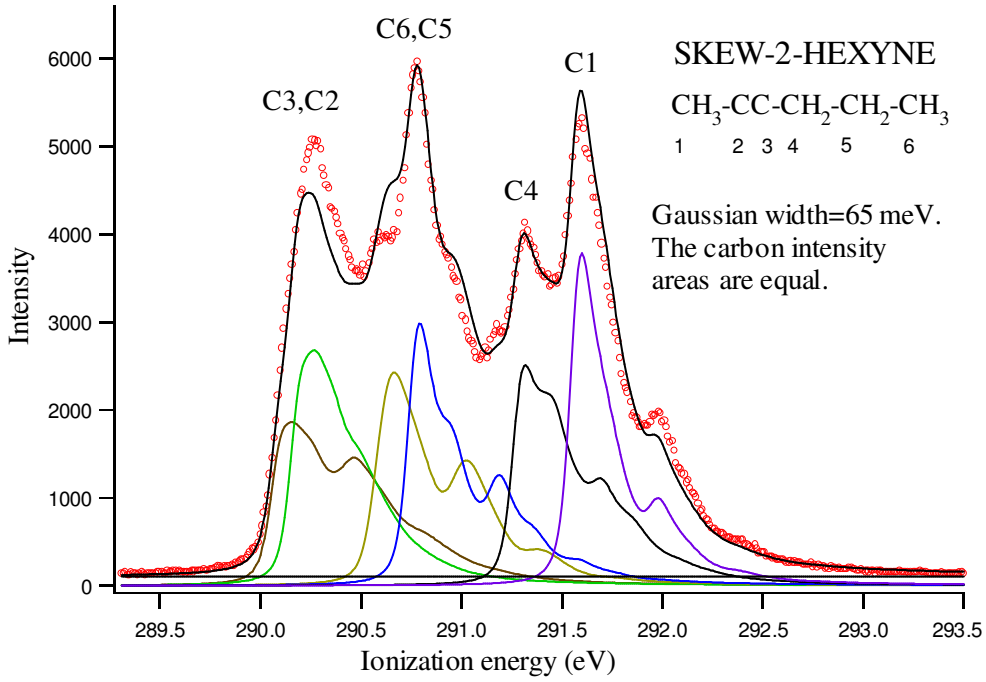

Figure 51: The carbon 1s spectrum of skew-2-hexyne.

the C2 core ionized state, 2.85 Å for the C3 core ionized state, and 2.28 Å for the C6 core ionized state. This result gives an indication of *Lewis* interactions where the π electrons act as a Lewis base and the C6 protons act as a Lewis acid. From these bond distances, this interaction should be largest for the final state in which C6 is core ionized. One important reason for this, is the larger electrostatic attraction between the π electrons and proton attached to the positively charged carbon atom. In the cases where C2 and C3 are core ionized, the positively charged carbon atoms have a higher ability to repel the proton attached to C6. This results in a larger distance between the C6 proton and C3.

The difference between the theoretical spectra can be attributed to the broader vibrational profiles of C2, C3, and C6 of skew-2-hexyne relative to the corresponding profiles of "trans"-2-hexyne. The fitted spectrum of skew-2-hexyne was slightly better than the fitted spectrum of "trans"-2-hexyne, but it was not satisfactory. One way to improve the fit, was to *combine* the vibrational profiles from both conformations in the same experimental spectrum. As we shall see, this gave a good result. This means that the core ionization of C2, C3, and C6 *must* lead to different final-state geometries.

The percentage contribution from each conformation in the same gas mixture was found from theoretical calculations to be 56% skew and 44% "trans". In the following, it is shown how these numbers are calculated. The values used in this calculation is presented in table 7.

To calculate the percentage contribution of the two conformations, we use the

Table 7: Gibbs free energies (G^o), electronic energies from DFT and MP2 levels of theory, and the corresponding Δ values of "trans"-2-hexyne and skew-2-hexyne.

	"Trans"-2-hexyne	**Skew-2-hexyne**	ΔG^o, ΔE **(kJ/mol)**
G^o(DFT)	-234.578076 au	-234.577266 au	2.128
E(DFT)	-234.685925 au	-234.685751 au	0.457
E(MP2)	-233.913389 au	-233.913815 au	-1.119

expression shown in equation 26.

$$\Delta G = \Delta G^o + RTlnQ \tag{26}$$

G is the Gibbs free energy, R is the gas constant and is equal to 8.31 $Jmol^{-1}K^{-1}$, T is the absolute temperature in Kelvin and is equal to 298.15 K, and Q is the reaction quotient. At equilibrium, ΔG is equal to zero, and Q is equal to the equilibrium constant K. This gives us the following expression:

$$K = e^{-\frac{\Delta G^o}{RT}} \tag{27}$$

We assume that there is an equilibrium between the two 2-hexyne conformations:

"Trans"-2-hexyne $\rightleftharpoons$ Skew-2-hexyne

The equilibrium constant K of this reaction can be expressed as $\frac{a_S}{a_T}$ where a_S is the activity of the skew-conformation, and a_T is the activity of the "trans"-conformation. This constant can be related to the fact that: $a_S + a_T = 1$. 1 atomic unit (au) is equal to 2627.38 $kJmol^{-1}$.
The DFT-calculations resulted in a distribution with 70% "trans" and 30% skew. To calculate the percentage distribution of the two conformations from the MP2-results, following expression was used:

$$\Delta G^o(MP2) = \Delta G^o(B3LYP) - \Delta E(B3LYP) + \Delta E(MP2) \tag{28}$$

Using these equations, a distribution with 56% skew and 44% "trans" was obtained. This MP2-result tells us that there is almost an equal distribution of the two conformations in the gas phase.
The next step was to mix the vibrational profiles of the two conformations in the same 2-hexyne spectrum with an intensity area distribution consistent with the percentage distribution calculated from the MP2 level of theory. The calculated chemical shifts were used to find the initial energies. The fitted spectrum is shown in figure 52 on the following page.
We can notice an improvement of the spectrum. Each carbon atom has two different vibrational profiles which gives a total of 12 (2x6) profiles in the spectrum. The shape of the black line (integration of all the vibrational profiles) is the same as the shape of the experimental line (circles). The fitted

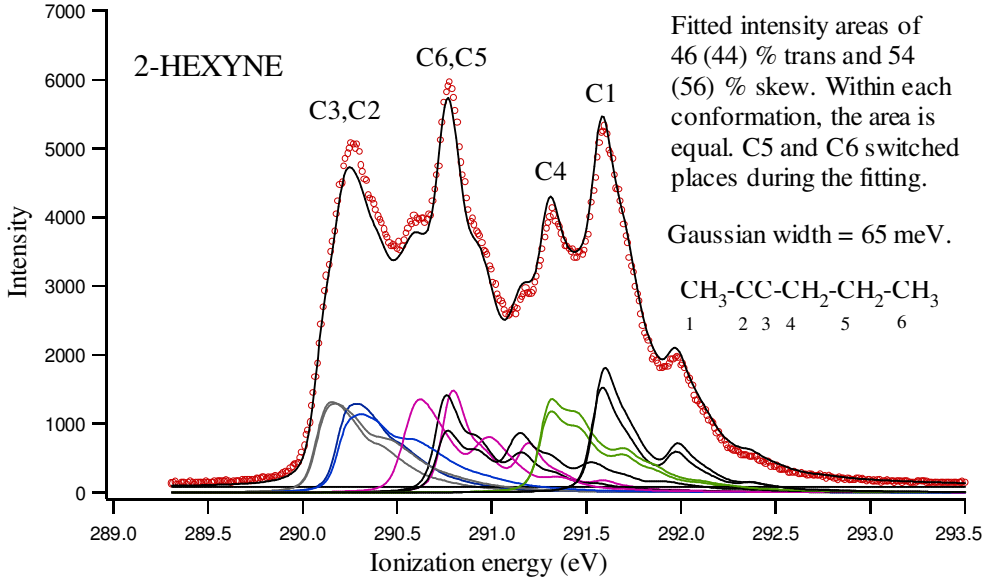

Figure 52: The carbon 1s spectrum of 2-hexyne (a mix of skew and "trans").

percentage distribution of the two conformations is 54% skew and 46% "trans", which is not far away from the calculated.
In order not to loose the control over all the parameters in the fitting procedure, we had to force some of the parameters not to change during the fitting. The intensity areas were forced to be equal in addition to forcing the Gaussian and Lorentzian widths to be constant. The carbon sequence in the spectrum was the same as the theoretical predicted except for C5 and C6; they switched places during the fitting. The finally adiabatic and vertical energies of 2-hexyne are presented in table 9.
Since the vibrational profiles of all the carbon atoms (except C6) of trans-2-hexyne have smaller ionization energies than the corresponding profiles of skew-2-hexyne, the adiabatic and vertical energies were found from the C1-, C2-, C3-, C4-, and C5-profiles of trans-2-hexyne and C6-profile of skew-2-hexyne. The energy differences between these two conformations with respect to the vibrational profiles, vary from 6 to 218 meV. The relatively large value of 218 meV is the C6-difference.

6.3.6 3-hexyne

The carbon 1s spectrum of 3-hexyne is shown in figure 53. 3-hexyne has three chemically different carbon atoms. As we can see, the vibrational profiles are well fitted to the experimental spectrum. The intensity area of C3 is slightly smaller than for the other carbon atoms due to shake-up.
Since the two central atoms in this molecule with a triple bond between them are chemically equivalent, we can expect a splitting of the core orbitals into a *gerade* orbital and an *ungerade* orbital because of the small bond length associated with triple bonds (due to incomplete localization of the core hole).

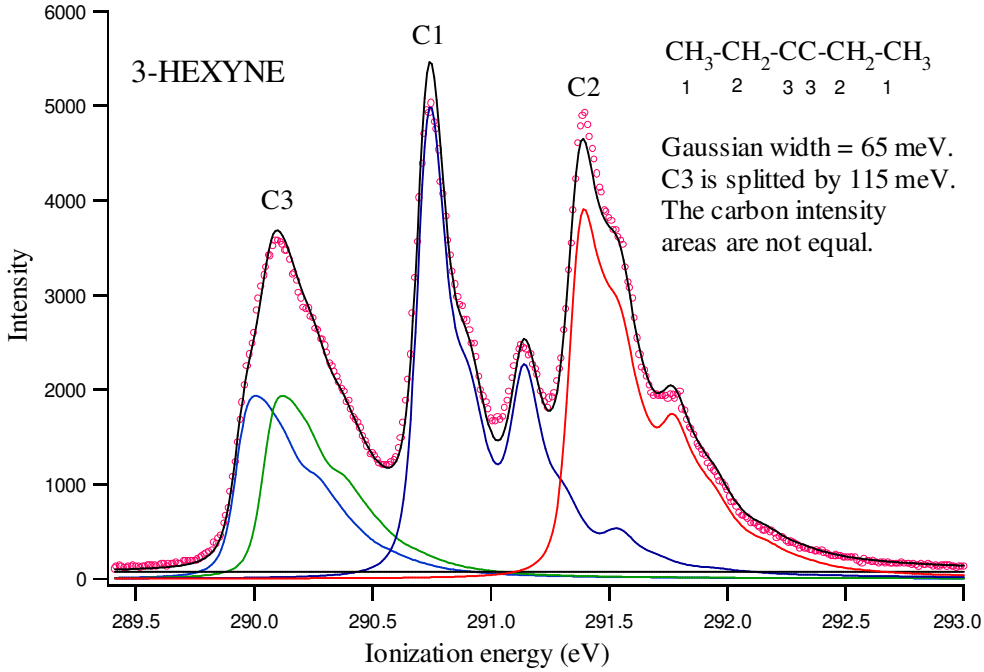

Figure 53: The carbon 1s spectrum of 3-hexyne.

This means that the interaction between the core orbitals should increase with decreasing bond length, and the degree of splitting should therefore increase with decreasing bond length. Triple bonds are shorter than double bonds, which means that the interaction between the core orbitals in 3-hexyne should be greater than for trans-3-hexene. This should result in a larger splitting of C3 in 3-hexyne than for trans-3-hexene. Indeed, this is also the case in the experimental spectra where we can observe a C3-splitting of 115 meV in 3-hexyne compared to 36 meV in trans-3-hexene. The final adiabatic and vertical energies of 3-hexyne are given in table 9 in which the energies of C3 are extracted from the ungerade peak.

Table 8: Adiabatic and vertical energies of the butenes, butynes, pentenes, and pentynes.

Molecule	Atom	Adiabatic energy (eV)	Vertical energy (eV)
1-butene	C1	290.035	290.203
	C2	290.401	290.547
	C3	290.445	290.633
	C4	290.582	290.773
Cis+trans-2-butene	C1	290.502	290.699
	C2	290.115	290.275
1-butyne	C1	290.056	290.219
	C2	290.552	290.732
	C3	291.408	291.586
	C4	290.671	290.850
2-butyne	C1	291.330	291.490
	C2	289.993	290.145
1-pentene	C1	289.996	290.155
	C2	290.395	290.542
	C3	290.380	290.577
	C4	290.386	290.577
	C5	290.304	290.502
Trans-2-pentene	C1	290.469	290.662
	C2	290.047	290.194
	C3	289.938	290.088
	C4	290.420	290.616
	C5	290.294	290.477
1-pentyne	C1	290.007	290.172
	C2	290.545	290.722
	C3	291.217	291.416
	C4	290.605	290.774
	C5	290.410	290.614
2-pentyne	C1	291.229	291.404
	C2	289.920	290.080
	C3	289.794	289.954
	C4	291.120	291.303
	C5	290.462	290.647

Table 9: Adiabatic and vertical energies of the hexenes and hexynes.

Molecule	Atom	Adiabatic energy (eV)	Vertical energy (eV)
1-hexene	C1	289.959	290.117
	C2	290.379	290.527
	C3	290.324	290.528
	C4	290.177	290.379
	C5	290.319	290.513
	C6	290.261	290.460
Trans-2-hexene	C1	290.440	290.633
	C2	290.009	290.155
	C3	289.890	290.051
	C4	290.197	290.406
	C5	290.305	290.504
	C6	290.251	290.454
Trans-3-hexene	C1	290.255	290.460
	C2	290.386	290.582
	C3	289.859	290.014
1-hexyne	C1	289.965	290.129
	C2	290.495	290.671
	C3	291.157	291.354
	C4	290.418	290.600
	C5	290.454	290.642
	C6	290.318	290.510
2-hexyne	C1	291.205	291.380
	C2	289.852	290.009
	C3	289.741	289.899
	C4	290.927	291.135
	C5	290.376	290.561
	C6	290.196	290.427
3-hexyne	C1	290.437	290.598
	C2	291.083	291.266
	C3	289.666	289.854

Chapter 7

7 Chemical reactivity

It is time to use all the data presented in the previous sections to relate this to chemical reactivity. As mentioned in the first chapter, the concept of reactivity is of great importance in chemistry and can be measured experimentally in many ways.
In order to create correlation plots where a given physical parameter of an alkene or alkyne is plotted against the corresponding ionization energies, it is necessary to use experimental data which can give information related to chemical reactivity. Physical parameters used in this thesis are rate constants (k), gas phase basicities (GB), and proton affinities (PA). Since the rate constant k is discussed earlier in sections 1.1.3 and 1.2.2, only gas phase basicity (GB) and proton affinity (PA) will be discussed in the following.
Gas phase basicity is defined as the negative of the Gibbs energy (ΔG^o) change associated with the following reaction in the gas phase [5]:

$$B + H^+ \longrightarrow BH^+$$

Hence, the gas phase basicity of the reacting species B can be written as GB(B) = -ΔG^o.
The proton affinity (PA) of species B is defined as the negative of the enthalpy change ΔH^o for the protonation of B [5]. Therefore, the proton affinity of the reacting species B in the reaction above (same as used for the GB definition) can be written as PA(B) = -ΔH^o. This means that a larger proton affinity and basicity of B corresponds to greater difficulty in removing a proton from BH^+. Since $\Delta G^o = \Delta H^o - T\Delta S^o$ in which ΔS^o is the entropy change and T is the absolute temperature, GB and PA are interconverted with the following relationship:

$$PA = GB - T\Delta S^o \tag{29}$$

In addition to references [67] and [68], reference [69] contributed data which could be used to make correlations with the adiabatic energies. In some of the correlations, the vertical energies were also used to find whether the plots were dramatically changed or not.
As pointed out in reference [67], there are three reaction steps in an acid-catalyzed hydration reaction. The step with the lowest rate determines the magnitude of the rate constant k and the rate of the overall reaction. In this case, the protonation step is the rate determining step. Because of this, we can compare the k values with the ionization energies.
The reactivity data of some alkenes and alkynes in acid-catalyzed hydration reactions at 25^oC, is taken from reference [67] and is presented in table 10.

Table 10: Reactivity data of some alkenes and alkynes in acid-catalyzed hydration reactions at 25^oC.

Molecule	$\mathbf{k}_{H^+}$, $\mathbf{M^{-1}s^{-1}}$	**log** $\mathbf{k}_{H^+}$
1-hexene	$0.432x10^{-8}$	-8.36
1-hexyne	$0.225x10^{-8}$	-8.65
Trans-3-hexene	$0.127x10^{-7}$	-7.90
3-hexyne	$0.568x10^{-8}$	-8.25
1-butene	$0.233x10^{-8}$	-8.63
1-butyne	$0.258x10^{-9}$	-9.54
Trans-2-butene	$0.448x10^{-8}$	-8.35
2-butyne	$0.611x10^{-10}$	-10.21
Propene	$0.238x10^{-8}$	-8.62
Propyne	$0.674x10^{-11}$	-11.17

Proton affinities and gas phase basicities of selected molecules from reference [69] are presented in table 11. These molecules were selected because they could be related to some of the molecules presented in this thesis.
Different plots based on these two tables and the ones presenting the core ionization energies of the different alkenes and alkynes, are correlations between proton affinities, gas phase basicities, adiabatic energies, and vertical energies. The different combinations gives in total four different plots.
The plot in figure 54 on the next page shows a linear correlation between proton affinities and adiabatic energies. The reactivity is expected to increase with increasing proton affinities and decreasing adiabatic carbon 1s ionization energies. This is consistent with the negative slope of the curve in the figure. In addition, we can see that the alkene or alkyne becomes more reactive (larger PA) the longer the carbon chain is. In gas phase proton additions, 2-hexyne is predicted to be the most reactive while ethyne should be the least reactive. Figures 55, 56, and 57 are basically showing the same as figure 54.
In figure 58 the negative logarithm of the rate constant k (-log k) is plotted against the adiabatic energies of different alkenes and alkynes. The k values are measured in the liquid phase in acid-catalyzed hydration reactions at 25^oC. The adiabatic energies are measured in the gas phase.
In this case, a straight line gives a bad correlation. When the correlation line is splitted into two separate lines in which one is representing the alkenes and the other is representing the alkynes, better correlations are obtained. The correlation coefficients are relatively low, but a rough tendency can be seen in these two lines.
The chemical reactivity (in an acid catalyzed hydration reaction) is expected to increase with decreasing activation energies (-log k) and adiabatic carbon 1s ionization energies. The direction of the two curves is consistent with this expectation. Again, the chemical reactivity increases with the number of carbon atoms in the alkene and alkyne. In equation 30, the linear relationship

Table 11: Proton affinities (PA) and gas phase basicities (GB) of different alkenes and alkynes.

Molecule	PA (eV)	GB (eV)
2-hexyne	8.35	8.09
2-pentyne	8.39	8.06
1-hexene	8.34	8.04
1-hexyne	8.28	8.02
2-butyne	8.04	7.72
Propene	7.78	7.49
Propyne	7.75	7.49
Ethene	7.05	6.75
Ethyne	6.64	6.39

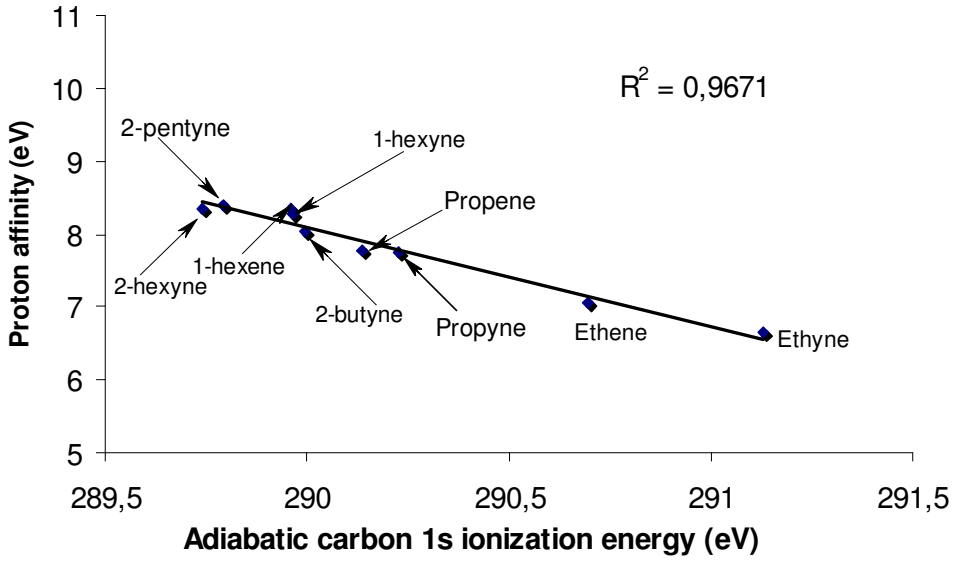

Figure 54: A correlation of proton affinities with adiabatic carbon 1s ionization energies.

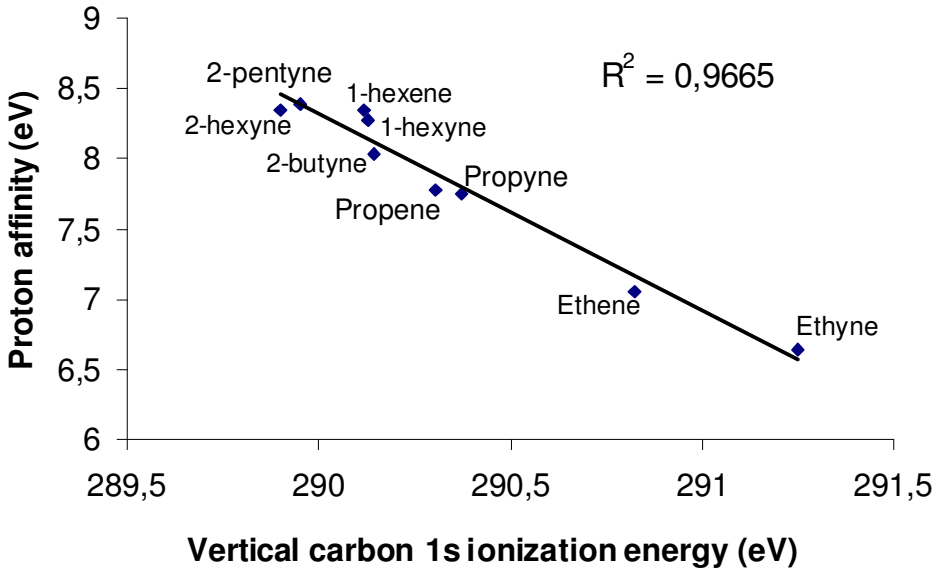

Figure 55: A correlation of proton affinities with vertical carbon 1s ionization energies.

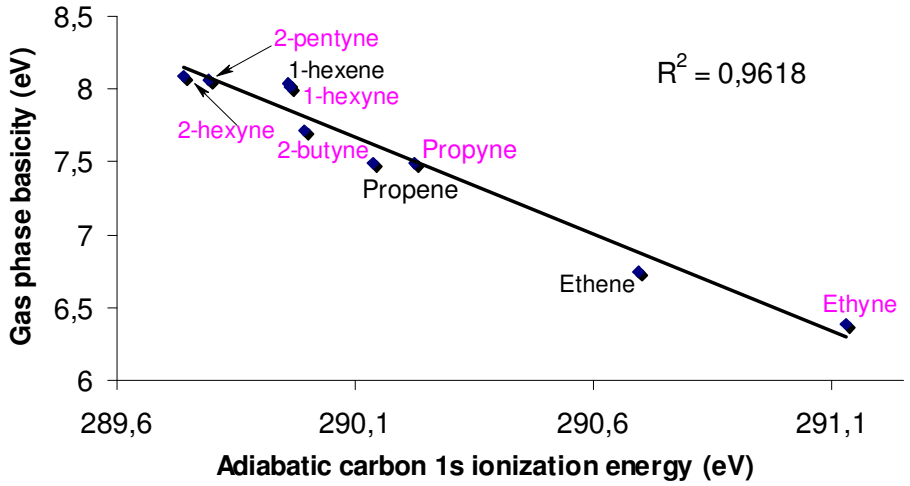

Figure 56: A correlation of gas phase basicities with adiabatic carbon 1s ionization energies.

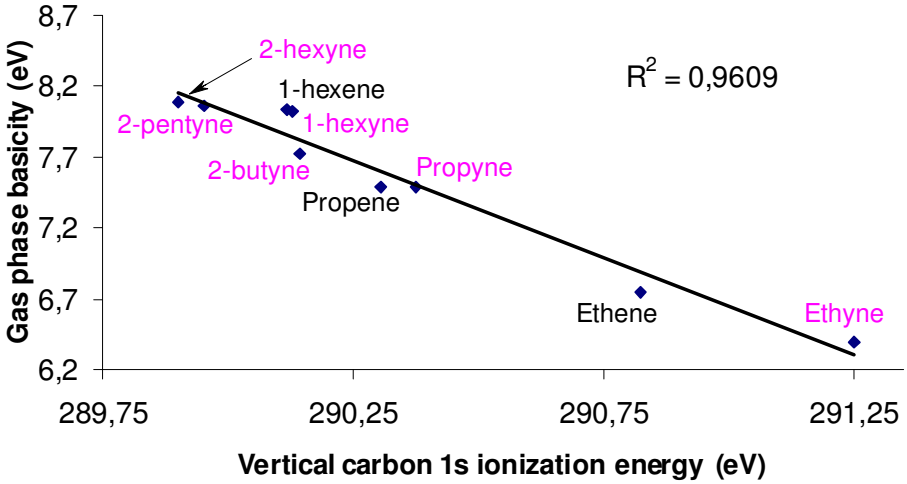

Figure 57: A correlation of gas phase basicities with vertical carbon 1s ionization energies.

between the negative logarithm of the rate constant k (-log k) and the activation energy E_a is shown (derived from the Arrhenius equation, see section 1.2.2 for symbol explanations).

$$-2.303 * logk = \frac{E_a}{RT} - lnA \tag{30}$$

Another point is the different slopes. The alkyne curve has a slightly higher slope than the alkene curve, which indicates that substituent effects on reactivity in acid-catalyzed reactions are *larger* for alkynes than the corresponding alkenes[19]. A possible reason for this difference is the shorter bond length in alkynes compared to alkenes. The triple bonded carbon atoms will be influenced more by the substituents because these carbon atoms are closer to the substituents than is the case for the alkenes.
We can observe that the two curves are clearly separated. One interpretation of this is that the alkenes and alkynes follow different *reaction mechanisms* in the acid-catalyzed hydration reactions. Generally, the alkynes have a higher activation energy (E_a) than the alkenes.
The last important point in this figure is the convergency of the two curves with the increasing number of carbon atoms in the chain. If we extrapolate these two curves, they will cross. This means that the difference in reactivity between an alkene and corresponding alkyne vanishes as the carbon chains gets large enough. It is therefore natural to believe that the reaction mechanisms and substituent effects of the alkenes and alkynes will get more similar.

[19]This is consistent with the results from reference [67] and [68].

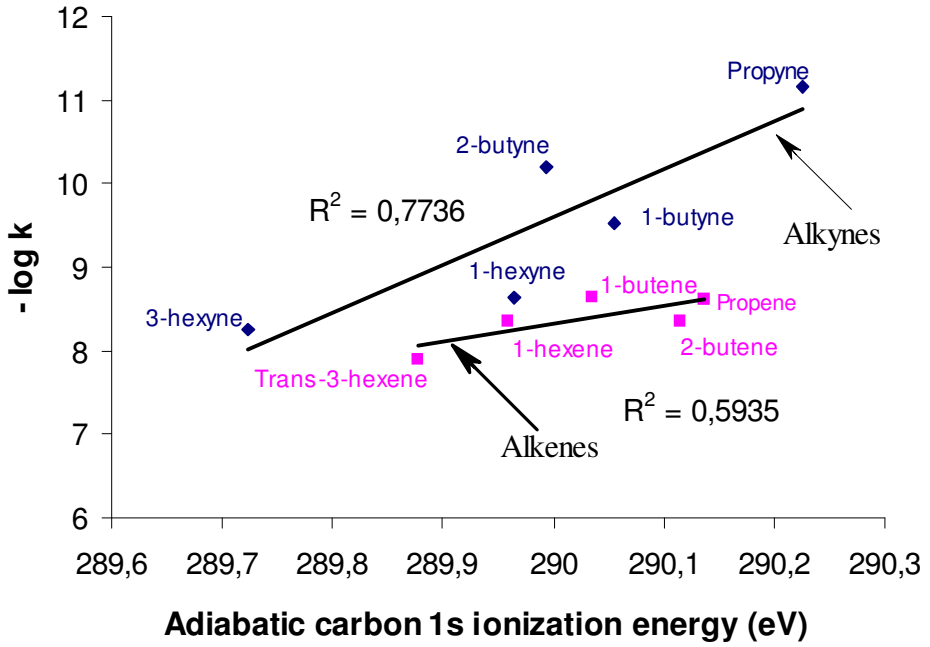

Figure 58: A correlation between activation energies (-log k) and adiabatic carbon 1s ionization energies of some alkenes and alkynes.

In figure 59, activation energies (-log k) are plotted against vertical C1s ionization energies for different alkenes and alkynes. The tendencies in this figure are the same as in figure 58, but there is one point worth mentioning. Since the activation energies are dependent on the transition state geometries of the reacting molecules, it is expected that adiabatic and vertical energies will give different correlations (and correlation coefficients) with the activation energies. For the adiabatic energies the geometry of the molecules is changed, while the geometry is unchanged for the vertical energies. In the transition state of an acid catalyzed hydration reaction, the geometry of the alkene or alkyne is unchanged. Because of this similarity between the vertical and activation energies, we expect these correlations to be better than the correlations which involve adiabatic energies. From figure 59, we can see that the alkene curve has a better correlation while the alkyne curve has a worser correlation. From this, we can not see this effect clearly in these two figures. However, this effect is *not* expected to be seen in the correlations between adiabatic/vertical energies and proton affinities (PA)/gas phase basicities (GB). In this case, there are no transition states and activation energies to take into account. Because of this, it is the same whether the molecular geometry is changed (adiabatic) or unchanged (vertical). When we compare the correlation coefficients of figures 54, 55, 56, and 57, they are very similar. A possible explanation of the trend in the two curves, is to assume all molecules in the two figures to follow the Ad_E2 mechanism as proposed in

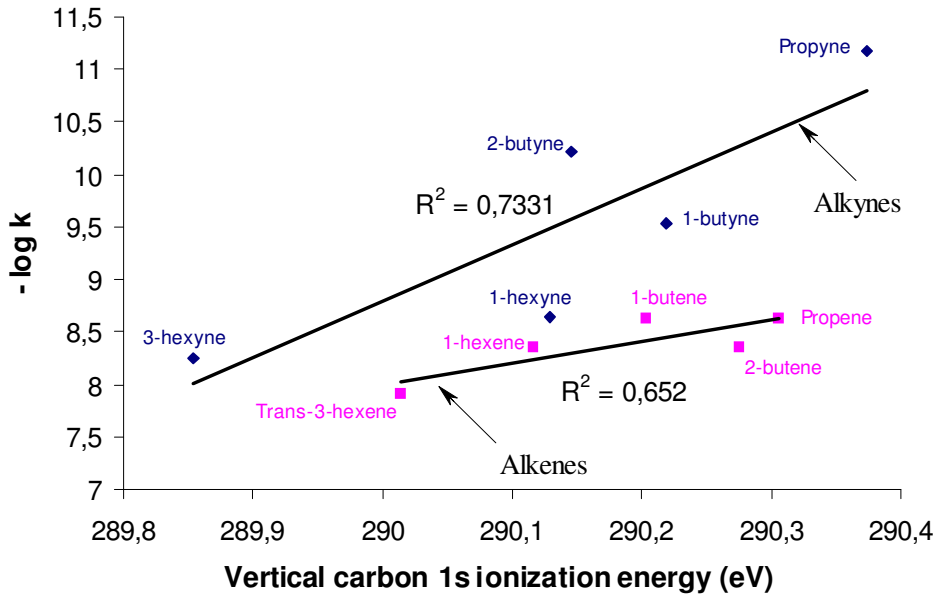

Figure 59: A correlation between activation energies (-log k) and vertical carbon 1s ionization energies of some alkenes and alkynes.

reference [67]. In this model, the relatively higher energy of the vinyl cation intermediate of propyne, 1-butyne, and 2-butyne is the reason for the smaller k value. 1-hexyne and 3-hexyne follow the Ad_E2 mechanism in both interpretations because the vinyl cation intermediates of these alkynes are more stabilized by the larger and electron donating alkyl groups.

A local trend in figure 58 and figure 59 is presented in figure 60. One possible reason for this trend, is that the core ionization energy does not take into account effects that are important in an acid-catalyzed hydration reaction. The *geometrical change* of the molecules that take place in a hydration reaction is one effect. There are geometrical changes of the molecules in a core ionization process also, but these changes can not be compared to the bigger molecular geometrical change in a hydration reaction. Different and uncomparable transition state geometries may also partly explain the trend.

The trend in figure 60, may also partly be explained by a certain difference between the Ad_E2 and Ad_E3 mechanisms. As mentioned in section 1.1.1, an important difference between Ad_E2 and Ad_E3 is that carbocations are formed in Ad_E2 reactions while this is not the case for Ad_E3 reactions. To link chemical reactivity to results from photoelectron spectroscopy, the rate determining step in the chemical reaction must involve a formation of a species with a positive charge. Since this is not the case for the Ad_E3 reactions, we can expect these reactions to be less correlated to ionization energies than Ad_E2 reactions and give an overall worser correlation (if the Ad_E3 mechanism is followed to some extent). This may also partly be one of the reasons for the relatively low correlation coefficients in figures 58 and 59.

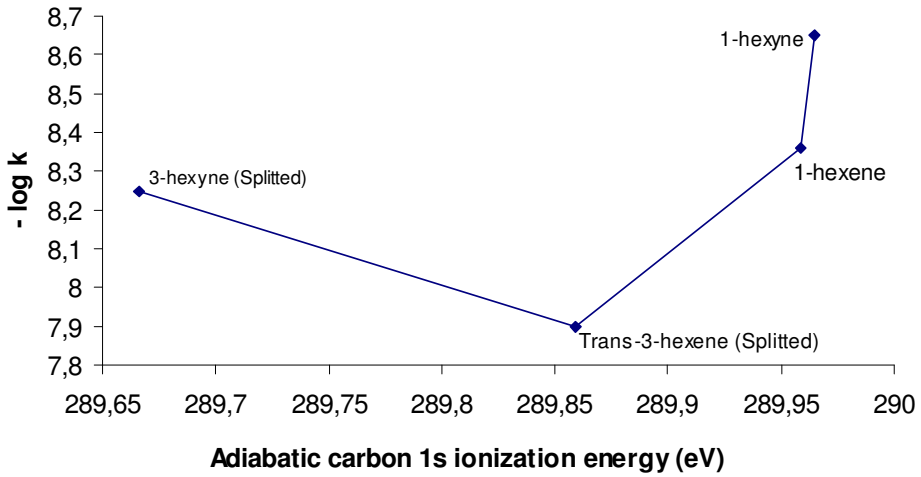

Figure 60: -log k plotted against lowest adiabatic carbon 1s ionization energies of two hexenes and hexynes.

In the following, some correlations where the lowest adiabatic core ionization energies are plotted against the number of carbon atoms in the specific alkene or alkyne.

Figure 61 shows an exponential correlation between adiabatic energies and the number of carbon atoms in the carbon chain of alkenes and alkynes with their double or triple bond located at the end of the carbon chain (C1).

This figure gives the same picture as the one presented in figure 58 and 59. The difference of the adiabatic energies of an alkene and the corresponding alkyne vanishes as the carbon chain gets longer. This means that the expected chemical reactivity difference between an alkene and alkyne should vanish if the carbon chain gets long enough. Generally, the alkene is expected to be most reactive compared to the corresponding alkyne.

In figure 62, the alkenes and alkynes have their double and triple bond located between carbon 2 and 3. In this case, we do not get a convergency of the two curves as the carbon chain gets longer. Instead, the curves are diverging somewhat with increasing number of carbon atoms in the chain. In this case, there are relatively large alkyl groups bonded to both unsaturated carbon atoms. In this group of unsaturated molecules, the plot is indicating that the alkynes should be the most reactive.

In the third plot shown in figure 63, only the symmetrical alkenes and alkynes are used. In this plot, the two curves cross each other going from C2 to C4. This plot shows a cross-over with respect to differences in chemical reactivity going from ethene/ethyne to 2-butene/2-butyne.

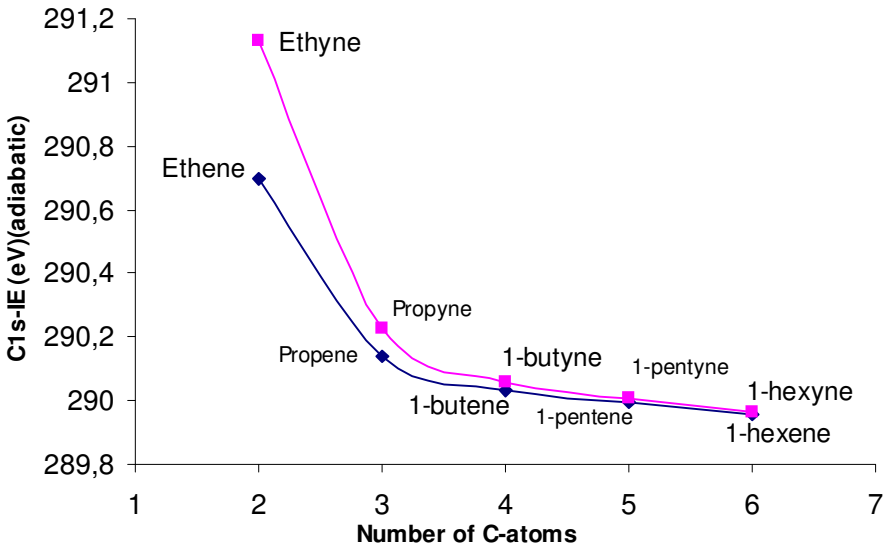

Figure 61: Adiabatic energies plotted against the number of carbon atoms in alkenes and alkynes where the double and triple bond is located between C1 and C2.

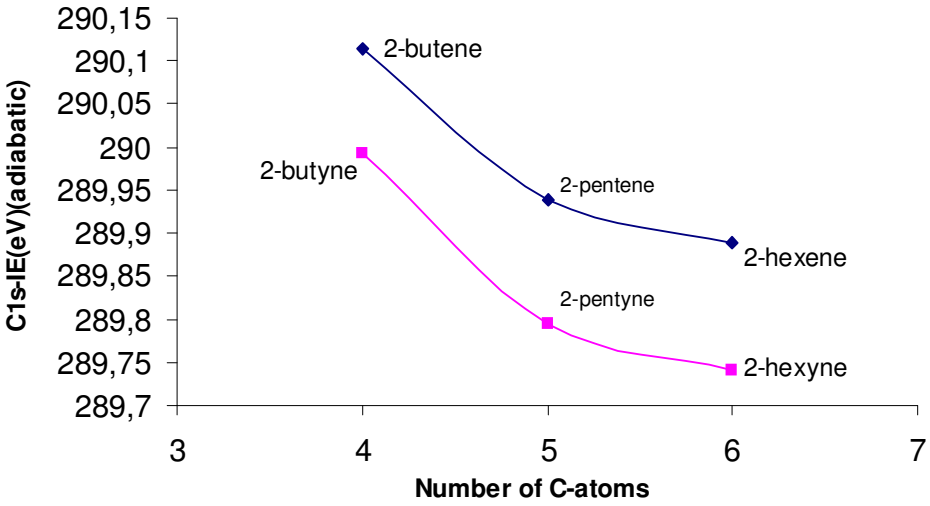

Figure 62: Adiabatic energies plotted against the number of carbon atoms in alkenes and alkynes where the double and triple bond is located between C2 and C3.

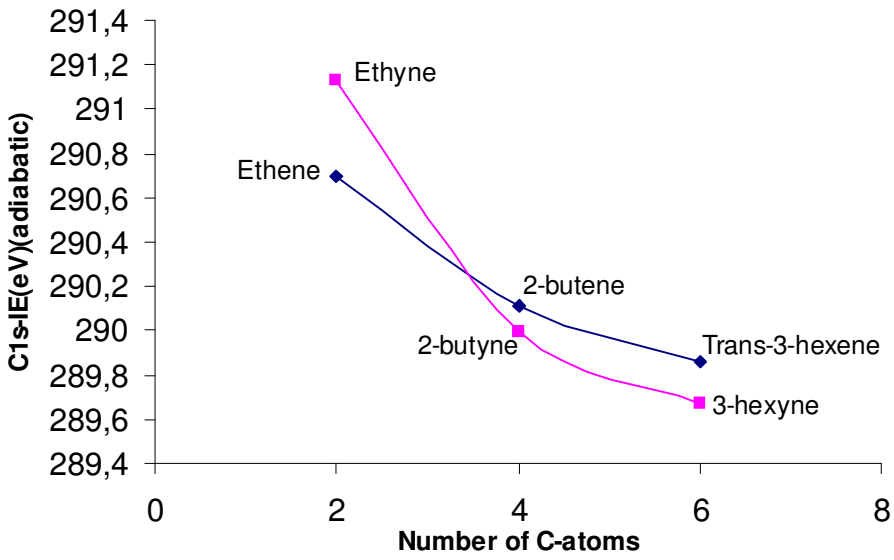

Figure 63: Adiabatic energies plotted against the number of carbon atoms in symmetrical alkenes and alkynes.

7.1 Initial and final state effects

In this section, an outline of how the initial and final state affects the ionization energy (or ΔI) will be given.
We remember from section 4.2 that $\Delta I = \Delta V - \Delta R$. ΔI is equal to the adiabatic energiey from the fitted experimental spectrum and calculated relative to ethene (the adiabatic energy of 290.695 eV [24]). ΔV is found by using the Extended Koopman's theorem, and ΔR is obtained by subtracting ΔI from ΔV (ΔV and ΔR were also calculated relative to ethene). The valence correlated levels of theory used in the calculation of ΔV, were DFT and MP2. The DFT results will be discussed in the following.
In figures 64, 65, and 66, the energy differences of the three parameters $(\Delta R, \Delta V, \Delta I)$ are plotted against the number of carbon atoms in the alkene or alkyne chain[20]. In the first plot, the double and triple bonds are located at the end of the carbon chain (between C1 and C2). The energies from C1 were used to calculate the three parameters. In the second plot, the double and triple bonds are located between C2 and C3. Here, both C2 (butene and butyne) and C3 (pentene, pentyne, hexene, and hexyne) energies were used to calculate the parameters. In the third plot, only symmetrical alkenes and alkynes are used. As for the previous group of alkenes and alkynes, both C2 (butene and butyne) and C3 (hexene and hexyne) energies were used in the parameter calculations. All the plotted values can be found in table 12 on page 93.
The ionization energies used in the three plots correspond to ionized molecules

[20] A similar plot can be found in reference [38].

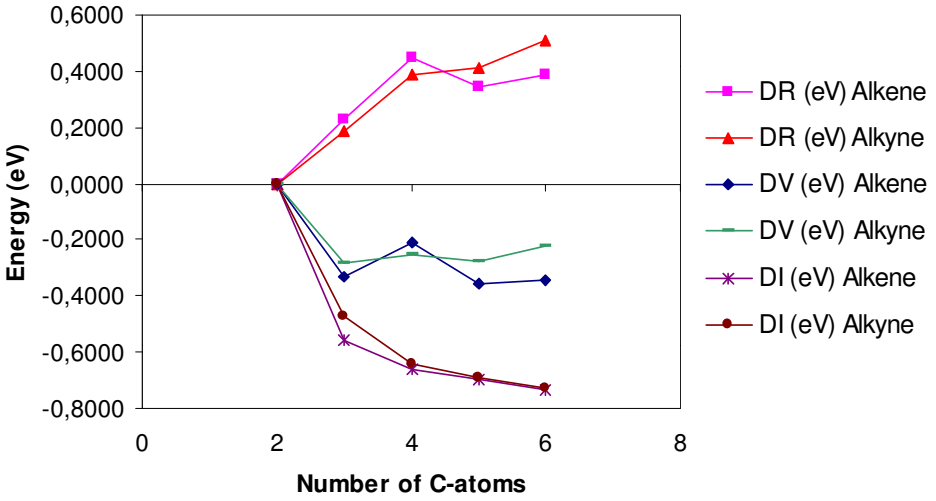

Figure 64: ΔR, ΔV, and ΔI values plotted against the number of carbon atoms in alkenes and alkynes with double and triple bonds located between C1 and C2.

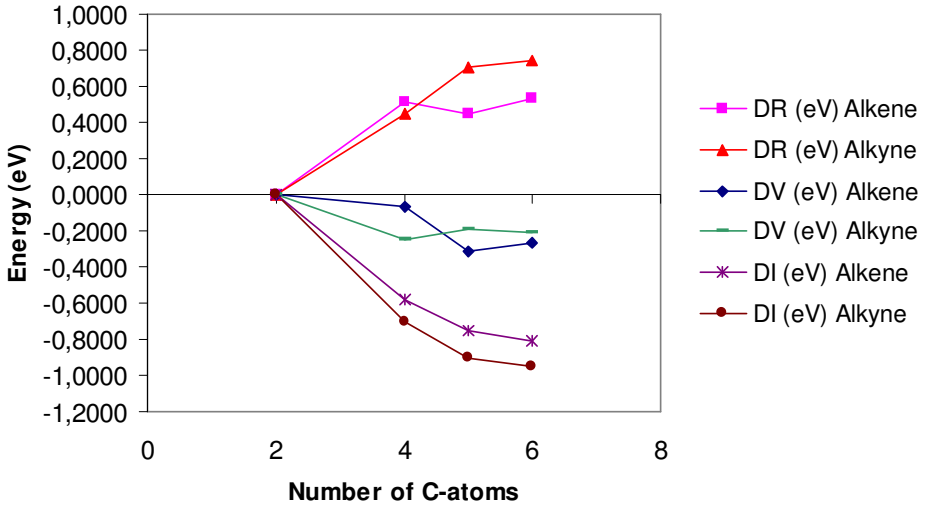

Figure 65: ΔR, ΔV, and ΔI values plotted against the number of carbon atoms in alkenes and alkynes with double and triple bonds located between C2 and C3.

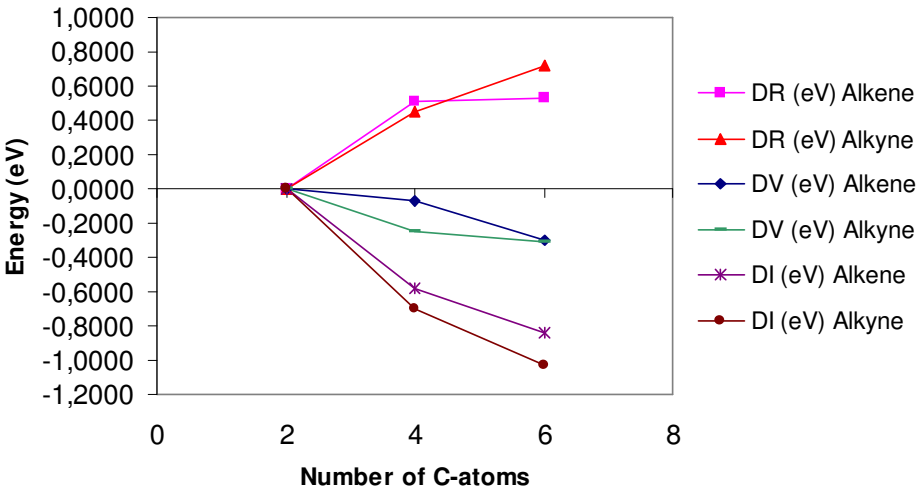

Figure 66: ΔR, ΔV, and ΔI values plotted against the number of carbon atoms in symmetrical alkenes and alkynes.

Table 12: ΔR, ΔV, and ΔI values of different alkenes and alkynes.

Molecule	ΔR **(eV)**	ΔV **(eV)**	ΔI **(eV)**
Ethene	0	0	0
Propene	0.228	-0.331	-0.558
Propyne	0.187	-0.283	-0.469
1-butene	0.450	-0.210	-0.660
1-butyne	0.385	-0.254	-0.639
1-pentene	0.345	-0.355	-0.699
1-pentyne	0.409	-0.279	-0.688
1-hexene	0.390	-0.346	-0.736
1-hexyne	0.507	-0.223	-0.730
2-butene	0.512	-0.0678	-0.580
2-butyne	0.452	-0.250	-0.702
2-pentene	0.445	-0.312	-0.757
2-pentyne	0.709	-0.192	-0.901
2-hexene	0.537	-0.268	-0.805
2-hexyne	0.744	-0.210	-0.954
3-hexene	0.531	-0.305	-0.836
3-hexyne	0.717	-0.313	-1.030

in their *vibrational* ground state. These energies are known as adiabatic energies. This implies that the relaxation energies ΔR include contributions from both electronic and geometric relaxations of the molecule.
The ΔR values increase with increasing number of carbon atoms in the carbon chain, which can be understood by the increasing ability of the molecule to relax electronically and geometrically.
The ΔR values also increase slightly with the position of the unsaturated bond. In figure 64, the lowest adiabatic energies of the alkenes and alkynes originate from carbon atom number 1. The number of surrounding nuclei and the magnitude of the electron density around this carbon atom is smaller than is the case for the carbon atoms localized in the center of the carbon chain. In figures 65 and 66 the lowest adiabatic energies of the alkenes and alkynes have their origin from these central carbon atoms. Because of this, these last mentioned alkenes and alkynes will have a larger total amount of electronic and geometric relaxation in the final state.
From the three figures we notice that all the ΔI values decrease with increasing carbon chain length. This can be rationalized in terms of the increasing electron donating ability of the substituents with increasing number of carbon atoms. The ground state electrostatic potentials ΔV have a shift towards the negative side of the plot, but as the carbon chain length increases, the ΔV values stabilizes.
Since the three parameters ΔR, ΔV, and ΔI of the alkenes and alkynes are calculated relative to ethene, we can compare the values (ΔR, ΔV, and ΔI) of the alkenes with the corresponding alkynes. What we can observe from the three plots, is that the ΔR values of the alkynes are larger than for the corresponding alkenes (except propyne, 1-butyne, and 2-butyne), while the magnitude of the ΔV values is larger for the alkenes compared to the corresponding alkynes (except 1-butene, 2-butene, and trans-3-hexene). In addition, the chemical shift ΔI decreases from the alkenes and alkynes where the double and triple bond is located between C1 and C2 to the alkenes and alkynes where the double and triple bond is located towards the center of the carbon chain. This means that the last mentioned molecules have the lowest ionization energies.
As we can see from figures 65 and 66, the alkynes have the lowest ionization energies as the carbon chain length increases. This is not the case in figure 64. For this group of alkenes and alkynes, the difference in ΔI vanishes as the number of carbon atoms in the carbon chain increases. This is consistent with what we observed in figure 61.
There is one final question that has to be answered. How large is the contribution from ΔV and ΔR to the chemical shift ΔI? In figure 64 on page 92 where the double and triple bond is located between C1 and C2, the magnitude of the ΔV and ΔR values of the alkenes is about the same except 1-butene, where ΔR is larger. It is also about the same for the alkynes, except 1-hexyne. Also for this molecule, the ΔR value is noticeable higher than the ΔV value. In this case, the final state electronic and geometric relaxation is relatively higher than the initial state electrostatic potential effect.
In figures 65 and 66, we can see that this is also the case of 2-butene,

trans-2-hexene, 2-butyne, 2-pentyne, 2-hexyne, and 3-hexyne. The interpretation of this is that the ΔR contribution gets more and more important as the carbon chain length in the *alkyne* increases. This is also the case for the alkenes, but not to such a high degree as the alkynes.

Conclusions

All the calculated vibrational profiles of all the molecules were well fitted to the experimental spectrum. For all the molecules except 2-hexyne, only one conformation of the molecule was used to generate the profiles. According to the theoretical calculations, one conformation of these molecules is dominating. This is not the case of 2-hexyne. This fit was improved by adding profiles from two conformations of the same molecule. This means that 2-hexyne has to exist in an equilibrium between the skew- and "trans"-conformation with comparable amounts in the ground state. The core ionization at one or more atoms must lead to different final-state geometries, and the chemical shift for one or more atoms must be different.
The lowest adiabatic energies are decreasing as the carbon chain length increases. This is true for both alkenes and alkynes. This indicates that the alkenes and alkynes are more reactive in electrophilic addition reactions as the chain length increases. For the smallest alkenes and alkynes like ethene and ethyne and in the cases where the double or triple bond is located at the end of the carbon chain (C1), the alkenes have the lowest adiabatic energies. In cases where the double or triple bond is located between two carbon atoms which both are bonded to other carbons, the alkynes have the lowest adiabatic energies.
The correlation between the gas phase basicities (GB) and proton affinities (PA) data and the ionization energies is very good. These quantities are both measured in the same phase, so this may be one important reason for this good correlation. The correlation between the reactivity data (acid catalyzed hydrations) and the ionization energies is not that good. A possible reason might be that solvent effects will influence the transition states and hamper the correlation with the ionization energies.
The difference between alkenes and alkynes with respect to adiabatic energies vanishes as the carbon chain length increases. This can also be observed in plots where activation energies (-log k) are plotted against the lowest adiabatic and vertical energies. This trend indicates that the increasing size of the electron donating alkyl groups is "masking" the differences between double and triple bonds in aliphatic compounds. This means that the substituent effects and reaction mechanisms in electrophilic addition reactions should become more similar as the carbon chain length increases.
The magnitude of the final state relaxation energy ΔR is increasing as the carbon chain increases. This is true because the larger the molecule gets, the higher ability the molecule has to relax geometrically and electronically when core ionized.
The parameters ΔR, ΔV, and ΔI were calculated from the carbon atoms with the *lowest* ionization energies. All three parameters were calculated

relative to ethene. The magnitude of ΔR is larger for the alkynes than the corresponding alkenes when the number of carbon atoms in the molecule is five and higher. Likewise, the magnitude of the ΔV values of the alkenes are larger than for the corresponding alkynes. In this case, 1-butene, 2-butene, and trans-3-hexene are the exceptions. In general, this means that the alkynes have the largest contribution of ΔR compared to the corresponding alkenes, while the alkenes have the largest contribution of ΔV compared to the corresponding alkynes.
When the contributions of ΔR and ΔV are compared, the ΔR contributions are generally higher than the ΔV contributions. The ΔV values are stabilizing when the carbon chain length increases.
Finally, we can see that the magnitude of the chemical shift ΔI is decreasing as the size of the alkenes and alkynes are increasing. When the double or triple bond is located between carbon atoms C2 and C3, the alkynes have the lowest ΔI values. For the molecules where the double and triple bond is located at the end of the carbon chain (C1), it is the alkenes that have the lowest ΔI values until the carbon chain contains 5 or 6 carbon atoms. Then this difference has diminished, which means that the expected reactivity in electrophilic addition reactions of an alkene and corresponding alkyne is comparable. The reason for this pattern is the distance between the methyl group of the substituent and the core ionized carbon atom in the molecule. When the carbon chain length increases, the distance from the core ionized atom to the methyl group of the added substituent will also increase. When this distance is getting longer, the core ionized atom will experience less electronic interaction from the methyl group of the substituent. Because of this, the ΔI differences vanish.

References

[1] H. M. Weiss, Journal of Chemical Education, **70**, 873(1993).

[2] T. T. Tidwell, Journal of Chemical Education, **73**, 1081(1996).

[3] F. A. Carey and R. J. Sundberg, *Advanced Organic Chemistry, Third Edition, Part A: Structure and Mechanisms*, Plenum Press, New York, pp 341-367, 1990.

[4] Ibid. Part B, pp 167-211.

[5] F. A. Carroll, *Perspectives on Structure and Mechanism in Organic Chemistry*, Brooks/Cole Publishing Company, Pacific Grove, California 93950, pp 548-626, 1998.

[6] T. Åberg, G. Howat, L. Karlsson, J. A. R. Samson, H. Siegbahn, and A. F. Starace, *Corpuscles and Radiation in Matter I*, 1982.

[7] M. N. Piancastelli, *Overview of international SR-research*, Nordic Summer School in Synchrotron Radiation, 3-11 June 2002.

[8] H. D. Young and R. A. Freedman, *University Physics*, Tenth Edition, Addison Wesley Longman, Inc., p 1232, 1999.

[9] `http://www.cmmp.ucl.ac.uk/~ajf/1B23/qm/node4.html`

[10] F. A. Carey and R. J. Sundberg, *Advanced Organic Chemistry, Third Edition, Part A: Structure and Mechanisms*, Plenum Press, New York, pp 258+368, 1990.

[11] S. Werin, *The Accelerators*, Nordic Summer School in Synchrotron Radiation, 3-11 June 2002.

[12] `http://www.accsys.com/history_linacs.htm`

[13] `http://www.maxlab.lu.se/`

[14] D. Attwood, *Soft X-rays and Extreme Ultraviolet Radiation, Principles and Applications*, Cambridge University Press, p 123, 2000.

[15] `http://detserv1.dl.ac.uk/Herald/xray_review_propertiesofsr.htm`

[16] Malcolm R. Howells, Advanced Light Source (ALS), *Diffracting Grating Monochromators*, Nordic Summer School in Synchrotron Radiation, 3-11 June 2002.

[17] `http://www.tasc.infm.it/tasc/lds/aloisa/layout.html`

[18] `http://www.maxlab.lu.se/beamlines/bli411/endstation.html`

[19] S. Svensson, J.-O. Forsell, H. Siegbahn, A. Ausmees, G. Bray, S. Södergren, S. Sundin, S.J. Osborne, S. Aksela, E. Nõmmiste, J. Jauhiainen, M. Jurvansuu, J. Karvonen, P. Barta, W. R. Salaneck, A. Evaldsson, M. Lögdlund, and A. Fahlman, American Institute of Physics, 2149, **67**(1996).

[20] N. Mårtensson, P. Baltzer, P.A. Brühwiler, J.-O. Forsell, A. Nilsson, A. Stenborg, B. Wannberg, Journal of Electron Spectroscopy and Related Phenomena, 117, **70**(1994).

[21] S. J. Osborne, *Synchrotron Radiation Studies of Resonantly and Non-resonantly Excited Electron Spectra of Free Atoms and Molecules*, Department of Physics, Uppsala university, 1997.

[22] `http://www.siu.edu/~cafs/surface/file4.html`

[23] L. Karlsson, *En introduction till fotoelektronspektroskopi*, Fysiska institutionen, Uppsala universitet, Sweden, p 8, 1992.

[24] V. Myrseth, J.D. Bozek, E. Kukk, L.J. Sæthre, T.D. Thomas, Journal of Electron Spectroscopy and Related Phenomena, 57, **122**(2002).

[25] V. Myrseth, *Chemical Reactivity of Methyl-benzenes from Core-photoelectron Spectroscopy and Theory*, Department of Chemistry, University of Bergen, Norway, p 41, 2000.

[26] T. Karlsen, *Fine Structure in Inner-shell Photoelectron Spectroscopy*, Department of Chemistry, University of Bergen, Norway, p 7, 2001.

[27] `http://www.fi.tartu.ee/labs/rsl/resonant_auger_effect.htm`

[28] P.W. Atkins, *Physical Chemistry, 6^{th} edition*, Department of Chemistry, University of Oxford, UK, Oxford University Press, Great Clarendon Street, Oxford OX2 6DP, p 498, 1998.

[29] `http://www.ch.ic.ac.uk/taylor/Born.html`

[30] P.W. Atkins, *Physical Chemistry, 6^{th} edition*, Department of Chemistry, University of Oxford, UK, Oxford University Press, Great Clarendon Street, Oxford OX2 6DP, p 462, 1998.

[31] Ibid. p 501.

[32] K.J. Børve, L.J. Sæthre, T.D. Thomas, T.X. Carroll, N. Berrah, J.D. Bozek, and E. Kukk, Physical review A, 012506, **63**(2000).

[33] C. Enkvist, S. Lunell, S. Svensson, Chemical Physics, 123, **214**(1997).

[34] B. Sjögren, S. Svensson, A. Naves de Brito, N. Correia, M.P. Keane, C. Enkvist, Journal of Chemical Physics, 6389, **96**(1992).

[35] See documentation from Gammadata Scienta AB, Uppsala, Sweden.

[36] V. Myrseth, *Chemical Reactivity of Methyl-benzenes from Core-photoelectron Spectroscopy and Theory*, Department of Chemistry, University of Bergen, Norway, p 38, 2000.

[37] K.J. Børve, *G2FC*, Department of Chemistry, University of Bergen, Norway, 1999.

[38] T. Karlsen, K.J. Børve, L.J. Sæthre, K. Wiesner, M. Bässler, and S. Svensson, J. Am. Chem. Soc., 7866, **124**(2002).

[39] L.J. Sæthre, T. D. Thomas, and S. Svensson, J. Chem. Soc., Perkin Trans. 2(1997).

[40] T. Karlsen, K.J. Børve, J. Chem. Phys., 7979, **112**(2000).

[41] T. Karlsen, K.J. Børve, L.J. Sæthre, N. Berrah, E. Kukk, J.D. Bozek, T.X. Carroll, T.D. Thomas, J. Phys. Chem. A, 7700, **105**(2001).

[42] Spancf (2000)-`http://www.geocities.com/ekukk`. E. Kukk 2000.

[43] P. van der Straten, R. Morgenstern, A. Z. Niehaus, Phys. D, 35, **8**(1988).

[44] T. X. Carroll, K.J. Børve, L. J. Sæthre, J. D. Bozek, E. Kukk, J. A. Hahne, and T. D. Thomas, J. Chem. Phys., 10221, **116**(2002).

[45] J.B. Foresman and Æleen Frisch, *Exploring Chemistry with Electronic Structure Methods*, Second Edition, Gaussian, Inc., Pittsburgh, PA, p 5, 1996.

[46] M.J. Frisch, G.W. Trucks, H.B. Schlegel, G.E. Scuseria, M.A. Robb, J.R. Cheeseman, V.G. Zakrzewski, J.A.Jr. Montgomery, R.E. Stratmann, J.C. Burant, S. Dapprich, J.M. Milliam, A.D. Daniels, K.N. Kudin, M.C. Strain, O. Farkas, J. Tomasi, V. Barone, M. Cossi, R. Cammi, B. Mennucci, C. Pomelli, C. Adamo, S. Clifford, J. Ochterski, G.A. Petersson, P.Y. Ayala, Q. Cui, K. Morokuma, D.K. Malick, A.D. Rabuck, K. Raghavachari, J.B. Foresman, J. Cioslowski, J.V. Ortiz, A.G. Baboul, B.B. Stefanov, G. Liu, A. Liashenko, P. Piskorz, I. Komaromi, R. Gomperts, R.L. Martin, D.J. Fox, T. Keith, M.A. Al-Laham, C.Y. Peng, A. Nanayakkara, M. Challacombe, P.M.W. Gill, B.G. Johnson, W. Chen, M.W. Wong, J.L. Andres, C. Gonzalez, M. Head-Gordon, E.S. Replogle, J.A. Pople, *Gaussian 98*, revision A.9, Gaussian, Inc., Pittsburgh, PA, 1998.

[47] P.W. Atkins and R.S. Friedman, *Molecular Quantum Mechanics*, Third Edition, Oxford University Press, Great Clarendon Street, Oxford OX2 6DP, p 301, p 19, 1997.

[48] P.C. Hemmer, *Kvantemekanikk*, 2. utgave, Tapir akademiske forlag, Trondheim 2000, p 204, 2000.

[49] P.W. Atkins and R.S. Friedman, *Molecular Quantum Mechanics*, Third Edition, Oxford University Press, Great Clarendon Street, Oxford OX2 6DP, p 301, 1997.

[50] J.B. Foresman and Æleen Frisch, *Exploring Chemistry with Electronic Structure Methods*, Second Edition, Gaussian, Inc., Pittsburgh, PA, p 272, 1996.

[51] P.W. Atkins and R.S. Friedman, *Molecular Quantum Mechanics*, Third Edition, Oxford University Press, Great Clarendon Street, Oxford OX2 6DP, pp 164+298, 1997.

[52] Ibid. p 293.

[53] J.B. Foresman and Æleen Frisch, *Exploring Chemistry with Electronic Structure Methods*, Second Edition, Gaussian, Inc., Pittsburgh, PA, p 97, 1996.

[54] V. Myrseth, *Chemical Reactivity of Methyl-benzenes from Core-photoelectron Spectroscopy and Theory*, Department of Chemistry, University of Bergen, Norway, p 37, 2000.

[55] `http://server.ccl.net/cca/documents/basis-sets/basis.txt`.

[56] W.J. Stevens, H. Basch, M. Krauss, J. Chem. Phys., 6026, **81**(1984).

[57] T.D. Thomas, R.J. Shaw Jr., J. Electron Spectrosc. Relat. Phenom., 1081, **5**(1974).

[58] K.J. Børve, T.D. Thomas, J. Electron Spectrosc. Relat. Phenom., 155, **107**(2000).

[59] K. Siegbahn, C. Nordling, G. Johansson, J. Hedman, P.F. Hedén, K. Hamrin, U. Gelius, T. Bergmark, L.O. Werme, R. Manne, Y. Baer, in: ESCA Applied to Free Molecules, North-Holland, Amsterdam, 1969, Chapter 5.4.

[60] L.J. Sæthre, M.R.F. Siggel, and T.D. Thomas, J. Electron Spectrosc. Relat. Phenom., 119, **49**(1989).

[61] T.H. Dunning Jr., J. Chem. Phys., 716, **55**(1971).

[62] K. Raghavachari, J.S. Binkley, R. Seeger, and J.A. Pople, J. Chem. Phys., 650, **72**(1980).

[63] F. A. Carey and R. J. Sundberg, *Advanced Organic Chemistry*, third edition, Part A: Structure and Mechanism, Plenum Press, New York, p 54, 1990.

[64] L. J. Sæthre, O. Sværen, S. Svensson, S. Osborne, T. D. Thomas, J. Jauhiainen, and S. Aksela, Physical Review A, 2748, **55**(1997).

[65] S. Sundin, L. J. Sæthre, S. L. Sorensen, A. Ausmees, and S. Svensson, J. Chem. Phys., 5806, **110**(1999).

[66] V. Myrseth, K. J. Børve, K. Wiesner, M. Bässler, S. Svensson, and L. J. Sæthre, Phys. Chem. Chem. Phys., 2002(In press).

[67] A. D. Allen, Y. Chiang, A. J. Kresge, and T. T. Tidwell, J. Org. Chem., 775, **47**(1982).

[68] G. Melloni, G. Modena, and U. Tonellato, Acc. Chem. Res., 227, **14**(1981).

[69] E. P. Hunter, S. G. Lias, *Evaluated Gas Phase Basicities and Proton Affinities of Molecules: An Update*, J. Phys. Chem. Ref. Data, **27**(1998).

[70] O. Sværen, *Electron Spectroscopy and Chemical Reactivity*, Department of Chemistry, University of Bergen, Norway, p 111, 1997.

A

A short introduction to the analysis part of the scienta program [70]

1. Get started: Open the Esca program in Windows. In DOS you have to open the directory `c:\esca300` and writes esca.

2. Login: Username=SYS Password=SYS

3. Get ready to process the data/take in a spectrum:

   Data Analysis − screen with many options
   Load Spectrum − choose the file you want to watch

   Find your folder and choose the spectrum you want to watch. You can choose the spectrum by using the mouse. Choose the spectrum, and you will come back to the previous screen picture, but now with your spectrum in the lowest window.

4. Comparing spectra/add the spectra together(if the spectra are overlapping): **N**umerics − take you into the part of the program where this is going to happen
   Compare − choose the next spectrum in the series you are going to take a look at (spectrum number 2). When the spectrum is added, you have to push enter before anything else can happen.
   To add the spectra, they have to represent an energy that is as similar as possible. In addition, to do this in the correct way, the size of the spectra must be as similar as possible. This can be done by enlarging the smallest spectrum such that it is as identical as possible with the biggest one:

   Input − by keyboard
   Type of operand − Constant
   Dest. Curve − Current

   Choose the multiplication sign $*$ and write the appropriate value (pure trial and error). Remember to use dots (.) and not comma (,) when using decimals. Try out a value, is it too small or too big, choose the division sign / and write the same value as you just wrote in the multiplication. Now you are back to the beginning and can try again. Keep on doing this until the spectra are as similar as possible in size.

   Now you can see if the spectra are in the same area, or if one of them has to be moved a little bit. If it is overlapping, you just get the spectrum back in its original size, and get in a new one. If it has to be moved, you do the following:

5. Moving a spectrum (remember that the smallest spectrum should be moved to the biggest, and not vice versa):

   Input − by mouse
   Energy shift

   Click with the mouse in a chosen edge of the spectrum that is to be removed, and pull the mouse to the spot where the two spectra should be overlapping, and click ones more. The spectrum should now be moved to the spot you indicated, and you are now ready to add these two spectra together if they are overlapping. IMPORTANT: Before these spectra can be added, the enlarged spectrum has to be reduced back to it's original size. To be assure of getting back the original spectrum, you have to repeat 5 and change input to "by mouse". Do the divition with the value you previous did the multiplication with.

6. Adding two spectrum:

   Input − by mouse
   Type of operand − Curve
   Dest Curve − new

   Choose the biggest spectrum by clicking on the name in the upper right corner. Choose + and click on the spectrum that is to be added. The combined spectrum appears now on the screen and gets the name $< addcurve >$. You are now ready to get in a new spectrum. Follow the same procedure with this spectrum: Enlarge the spectrum, move the spectrum, reduce the spectrum, and add it to the spectrum you made the last time.

7. Saving the combined spectrum:
   Choose the combined spectrum by clicking on the name in the upper right corner. Choose save, and write the name of the spectrum with maximum 8 letters. You may now get the message: file not found. Ignore this message. It is a bug! The spectrum is stored. You can now leave the menu by using the esc-button (this can also be done by clicking the right mouse button, or pushing the little quadrangle in the upper left corner).

   If you get a question where you are asked if you want to store all regions or energy shift, you just answer **n**o! Leave menu? Answer **y**es. This new spectrum can be used in the curve fitting. A tip: It is a good idea to

   take in all the spectra at the same time to figure out which one is the biggest. The disadvantage by doing this is that it is difficult to differ

between the spectra. Alternatively you can see through the spectra in the main window (where you choose Load Spectrum) and see what spectrum in the actual series that got the most counts.

PRINTING:
Choose "**P**rint tables", and the mouse arrow gets another colour while the program is preparing the printing. It starts to blink some places on the printer, and when this blinking stops, you push the blue button on the printer such that the paper is coming out.
To print your spectrum, you push F5, and make sure that the settings are as follows:

Output device – quick
Lower field – no output
Right field – output
Upper field – output
Area size – /1

Push the "**B**egin plot" command. The mouse arrow change it's colour and the printer starts to blink. Do not push escape or any other button at this time, because the program will then respond by shutting down! When the printer stops blinking, you can push the blue button and the spectrum will come out of the printer.

B

Curve Fitting Macro Package for Igor [42]

1) Introduction

The purpose of this macro package is to perform a least-squares curve fitting to an experimental spectrum, using pre-defined (Voigt, PCI, Fano etc.) or user-provided lineshapes, with advanced peak parameter linking arithmetics. The package consists of the following macros:
1) MakeDataWave – selects a part of a spectrum displayed in a graph and creates a new graph from it for curve fitting.
2) Background – allows to define a linear background for the fit.
3) InitPeakTable – Generates a table to show and edit the parameters for the peaks.
4) GraphParEdit – allows to edit peak positions and intensities interactively in the graph.
5) InitFit – calculates and displays the peaks with the parameters as given in the table.
6) Simplex – performs iterative least-squares fitting using Simplex method.
7) LevMarq – performs iterative least-squares fitting using the Levenberg-Marquardt method.
8) AutoRestart – automatically restarts Simplex until the fit converges.
9) RestoreInitial – restores the parameters to the values they had before running Simplex.
10) ResultTable – generates a table with fit results for final printout.
11) Tags – attaches tags to the individual peaks in the graph.
12) SaveFit – saves fit parameters to a file.
13) LoadFit – loads fit parameters from file.
14) Setup – defines some auxiliary parameters.
15) FitErrors – performs error analysis of the fit result.

Igor Pro ver.>3.12 is needed to run these macros. If you have an older version, update it or see the README.txt file for necessary modifications.

2) Getting started

a) At first you need to create an Igor data wave from the spectrum you want to study. This is a standard Igor procedure. You should use the wave's intrinsic x-scaling rather than plotting it vs. another wave.
b) Create a graph displaying your spectrum. Use the cursors to select the region of the spectrum you want to fit. Then run *MakeDataWave* macro. It

creates a new graph showing the selected region and displays a panel which allows you to define the background. By default, the background is kept fixed during the fitting procedure, but it can also be optimised during the fit.
c) Run the *InitPeakTable* macro, which creates a table for defining the initial parameters of the peaks. At this point, you can either enter peak parameters directly into the table or edit them interactively in the graph using *GraphParEdit* macro. This macro is accessible from the menu as well as through the *Edit* button on the graph. For setting up the parameters, see section *Peak Parameters* below.
d) After you have entered your first guess for the peak parameters, run the *Initfit* macro. It calculates and displays the peaks in the graph, together with their sum (black curve) and the difference from the experimental spectrum (dashed curve). The goodness parameter, χ^2, is also displayed.
e) You can always modify your initial guess either by changing the parameters in the table or by interactive editing in the graph. After changing the parameteres in the table, run *InitFit* or click the *Update* button on the graph to bring the fit up to date.
f) Once you have arrived at a reasonably good initial guess, you can start the fitting process by running macro *LevMarq* or *Simplex*. The section *Optimisation* describes, how these routines work and how to use them. There is a shortcut to these macro on the graph - they can be started by clicking the button *Fit*.
e) Finally, when your fit result is satisfactory, you can create a results table using macro...*ResultTable* either from the menu or by clicking on the *Results* button. This macro resolves the linking arithmetics for the linked peaks and also calculates peak areas and widths.
f) You can now add tags to the peaks in the graph by activating the graph and running the macro *Tags*.
g) As the final step, it is a good idea to create a layout where the result table and the fit graph are together. It can then be printed, for example.
h) The fit results can also be saved on disk, using the macro *SaveFit*.

3) Peak parameters

The table *PeakTable* contains the parameters that define the fit. There are two types of parameters - the ones that contain the actual values and the ones that contain the linking information. For a simplest fit one can ignore the linking parameters - just make sure they are all set to 0 - no linked or fixed parameters whatsoever. The meaning of the rest of them is the following:
Label – a short text describing the peak. Useful when there are many peaks and a complex structure.
Shape – defines the analytical shape of the peak. Currently the following shapes are available - p and p0 is a PCI-shape, an asymmetrically distorted Voigt profile, convoluted by a Gaussian. One can use this type as a symmetric shape, by setting the asymmetry parameter to 0 and not allowing it to change. The second, v, defines a pseudoVoigt shape, which is a linear

combination of a Lorentzian and a Gaussian. It is less precise that the first type, obtained by convolutiong shapes, and does not include asymmetry.
The shape f defines a Fano profile. Finally, u, means a user-defined shape (see section 4).
En − stands for the energy (in general, X-value) of the peak maximum.
Int − peak intensity Fwhm(L) and Fwhm(G) − full width at half maximum of the lorentzian and gaussian components of the peak
Asym − asymmetry parameter of the PCI-shape. It can also be negative.

When you generate a 'virgin' table by *InitPeakTable*, the rows will be empty except the first one (No. 0), which has a special meaning. It does not define a peak, but the variations used to initiate the least-squares fitting, which reflect your guess of how much a given type if parameter is going to change when doing the Simplex-type optimisation. It has some preset initial values that you can freely change. More about them under *Optimisation*.

Each of the next rows defines one peak. You can delete, add or copy the rows, should the need be. Take a look at your spectrum in *FitGraph* and determine the number of peaks needed and their approximate parameters. Don't forget the shape and width parameters! You can set the energy and intensities rather arbitrarily and modify them later. Run Initfit. The peaks should now appear in the graph. If they do not, check the parameters! To reposition the peaks, you can either edit the table manually or run *Graphedit*. In any case, try to find a reasonably good-looking match to the spectrum before doing the optimisation −− it'll make life much easier for the fitting routine.

An alternative way of setting up the peaks is provided by the *GraphEdit* macro, which overrides the default mouse functions. When you run this macro, a small panel appears. In here, select the number of the peak you want to modify and click *Change peak*. The selected peak will be displayed in green. You can now select a new position for it by clicking left mouse button at the desired location. You can also change its width by holding down the *Shift* key and clicking the left mouse button at an appropriate distance from the peak maximum. When you create the first peak of the fit, default parameters are assigned to it, but when you add peaks to the existing ones, the parameters for the new peak are copied from the last peak. Note that the *InitPeakTable* macro should be run before you can use the graphical editing features.

The background you defined already at the beginning, after making the data wave. You can always redefine the background by running the *Background* macro again, after which you need to run *Initfit*. Background level can be defined in two ways − from the graph or by typing in the numerical values. The two checkboxes in the background panel define, how it behaves during the fit. You can uncheck the *Fixed* box, "unfreezing" the background so that it will be optimised during the fit. Leaving the *Constant* box checked keeps the background equal across the spectrum, while unchecking it allows the left and

right ends to have different values. The background will always remain linear, however. If you want *Simplex* to do the work and find the best background, don't start by defining zero background, since the initial variations are set to 10% of the background level and would therefore be −− zero.

There is also a possibility to use peak parameters saved to disk by using the *Savefit* macro. It is convenient, if you just want to save the results or to use the to fit a similar spectrum. To use the parameters from a file, you should first run *MakeDataWave*, if you haven't already done so. After that you can retrieve the fitting parameters from a file by using the *LoadFit* macro. Of course, the file must have been created by the *SaveFit* macro only. However, the easiest way to fit multiple spectra is to load all of them in your experiment and, when you are finished with one spectrum, close the *FitGraph, Peaktable* and *Results* windows (after printing them or saving the results, of course), activate the graph containing your next spectrum and start a new − define the desired range by cursors, run *MakeDataWave* etc. Then the result of the previous fit will be used as initial parameters for the new one. Note that you might need to go back to the *root* directory of Igor, as during the fit the active directory is *PeakSpec*.

4) Fitting with user-defined shapes

If you find the pre-defined peak shapes unsuitable, you can define your own. For that, the shape parameter in the peak table must be u. The fitting routine then calls a function UserCurve for which a template is provided in the procedure file *amob.ipf*. You can define any analytical shape in the body of this function, using the energy, intensity, Lorentzian and Gaussian width and asymmetry parameters (of course, their meaning can be redefined). If your formula does not use some of the parameters, they should be marked as fixed parameters in the peak table, so that the fitting routine doesn't waste time trying to optimize them. Note also that if the Gaussian width differs from zero, your peak shape will be convoluted with a Gaussian of that width.

The peak label is passed to the *UserCurve* function as a string parameter. It can be used to fit a numeric (non−analytical) shape to the spectrum. This shape should be contained in a wave and the name of that wave should be given as the label of the corresponding peak. One can then manipulate this wave (shift, multiply) in the *UserCurve* function, after including a line:
`wave w1=$label`
in the body of the function and then operating on the wave w1.

5) Optimisation

Currently, two optimisation algorithms are implemented: Simplex and Levenberg−Marquardt. The latter is the default assigment for the button *Fit*

on FitGraph, but can be changed through the Setup macro. Note that the button *Auto* always starts a Simplex optimisation. Neither of the methods guarantees that the global minimum will be found, so in case your χ^2 landscape is 'bumpy', it might be a good ide to restart the procedure with inital values slightly different than the optimisation result.

The goodness of the fit across the spectrum is reflected in the residual curve. In addition, you can also switch on (from the Setup macro) color coding of the data points according to how significant is their deviation from the fit curve. Points with large deviation are shown in green and points with good fit in black.

a) Simplex

Simplex is the name for a blob on the multidimensional surface of the fit 'goodness' parameter. During the interation process, this blob starts to crawl around, shrink, expand, squeeze or wiggle towards the lowest point on the surfece in its vicinity (NB! not globally). This behaviour gave the algorithm it's name – amoeba. The whole purpose of the game is, of course, to find the lowest spot, that is, to minimize the χ^2 value. The algorithm is not the fastest or best on Earth, but works. In the future it might be replaced by a more effective one. Take a look at row 0 of the table before starting *Simplex*, It determines the initial size of the "blob". The variation is given directly for the energy and intensity parameters – e.g., 0.01 means that *Simplex* starts to vary the energy parameter with the initial step of 0.01 energy units, whatever they happen to be. The variation is given as percentage for the intensity and width parameters – e.g. 0.1 for intensity means that the initial step will be 10 for a peak of the intensity 100, but 1000 for a peak with 10 000 intensity.

Simplex displays information in the command window during the iteration. It shows, how well the iteration converges. If the first values of χ^2 are very large (much more that 100, let's say), but your initial settings were rather good, then it means that you have given too large variations for one or more parameters. *Simplex* might still converge, but might also give strange results. On the other hand, if χ^2 starts to converge very slowly, then maybe the initial step sizes are too small. It will get there, eventually, but it might take very long. So try to increase the variations in row 0.

It seems to be a good strategy to start with rather large variations and run *Simplex* once or twice. When it gets closer to convergence, decrease the variations. There are two conditions at which *Simplex* stops.
1) The χ^2 has converged. To change the convergency limit (minimum change between subsequent iterations), run the *Setup* macro. The second parameter to this macro lets you add a 'virtual' background to the data before χ^2 is calculated. This is useful when dealing with background-subtracted spectra or when you want to obtain a better fit for strong peaks, trading off the quality

of the fit of the weak structures in the spectra. Ideally, χ^2 should be close to unity, if your data contain real counts with Poisson distribution. It is still a good idea to run *Simplex* once more with rather small variations.
2) Maximum number of iterations is performed. The maximum number depends on how many free parameters there is. The condition at which *Simplex* stopped is shown in the command window. If it didn't converge, you definitely have to restart it, maybe with smaller variations, until convergeny is achieved.

The macro *AutoRestart* can be used to restart *Simplex* automatically until the χ^2 converges within the given limit. It is useful for routine fits that take long time to run.

b) Levenberg-Marquardt

The "standard" fitting algorithm. It is much faster than the Simplex method for complicated fits, but seems to be somewhat less robust and less forgiving for the initial settings of the parameters. An odd step can occasionally slip through and cause weird results. If you suspect this to be the case, check carefully the parameter table.

6) Linking

Smart linking of parameters is absolutely essential for a good fit. With all paraters free, an excellent match to the data is usually achieved, but the results do not necessarily make any sense physically. One should use all available knowledge about the spectrum to be analyzed in order to reduce the number of free parameters to minimum.

There is a number of special columns in the "PeakTable". Different parameters can be linked in a different way, so that it makes sense physically. Firstly, and most commonly, the width and asymmetry parameters can be set equal to the corresponing value of another peak. To do this, insert the number of the peak you want to link to into the "L/F" column of this parameter. For example, to set the Lorentzian widths of all peaks equal, link all "Fwhm(L)" parameters starting from peak 2 to peak 1. The width and asymmetry parameters can be also kept fixed by inserting the number "99" in their "L/F" column. Note that multiple linking (linking to a parameter that has already been linked to another parameter etc.) is allowed, but only upwards in the peak definition table.

The linking of the energies ad intensities is much more complex. They have 4 columns each for linking/fixing infromation. Inserting "1" in the "F" column fixes the corresponding parameter and the next 3 columns will be just ignored. Therefore, to use linking, make sure that "F" contains "0" (Note

that the width and asymmetry parameters did not have separate "F" column and therefore the odd "99" encoding of the fix was used. This was done in order to keep the number of columns as small as possible).

There are two types of linking you can use depending of what kind of infromation is available.
1) Let's say you have 2 peaks and you know that they are exactly 1.5 eV apart and that the intesity of peak 2 is 50% of peak 1. But you don't know the absolute energies and intensities. Then give the parameters for peak 1 as free. For peak 2, enter 1.5 in the "En" column and 1 in the "+P" column, telling the fitting routine that
En(peak 2)= 1.5+ En(peak 1)
For the intesity of peak 2, type 0.5 in the "Int" column and 1 in the "∗P" column, meaning that
Int(peak 2)= 0.5∗ Int(peak 1)
One can as well link peak 1 to peak 2, which will be kept free. The coefficients would then be −1.5 for energy and 2.0 for the intensity.
2) Let's now assume that you have 4 peaks and you know that the spacing between peaks 3 and 4 must be the same as the spacing between peaks 1 and 2, but you don't know, how much this spacing is! Same for the intensity − you know that the ratio of peak 3/peak 4 equals peak 1/peak 2, but don't know beforehand, what is this ratio. An example would be a photoelectron spectrum af a molecule with two spin-orbit split components both with the same vibrational progressions. In this case, a more advanced linking arithmetics has to be used. For the energies, keep peaks 1−3 free. For peak 4 it is then known that its energy must be
En(peak 4)= $En(peak3) + (En(peak2) -$ En (peak 1)).
To do this, enter 0 in the "En" column of peak 4 and then enter 3, 2, and 1 in the first "+P", $second$"+P" and in the third "−P" column, correspondingly. You can also enter a value different from 0 in "En", in which case the peak is shifted from its calculated position by that value. For the intensities, the same logic applies −$keeppeaks$1−3 free and the intensity of peak 4 must be
Int(peak 4)= $Int(peak3) * (Int(peak2)/$ Int(peak 1)). Enter 1 in the "Int" column and 3, 2, and 1 in the "∗P"," ∗ P"and"/P" columns, correspondingly. By entering a number other than 1 in "Int", the calculated intensity is multiplied by this coefficient.

7) Extra features

The fit program contains features that are specific for some particular application and are probably of no interest whatsoever for the general user. Currently such features include:
1) Fitting with peaks that have energy-dependent Gaussian widths. This is useful when the energy resolution is not constant but depends linearly on the energy positions of the peaks. To activate this feature, you need two reference peaks that will define the width-energy dependency function. These peaks

must be next to each other in the peak table. If any of the following peaks then has the Gaussian link parameter $(-)$(*number of the second peak*) , its Gaussian width will be calculated by extrapolating a line that goes through the two reference peaks in width vs. energy coordinates. The "$-$" sign just tells the program that this is not the ordinary linking. Maybe the following example clarifies things a bit:
Let's define peaks 1 and 2 with
En[1]=1 Fwhm(G)[1]=0.10 "L/F"=0
En[2]=2 Fwhm(G)[2]=0.15 "L/F"=0
these will be the reference peaks. If we now add a third peak as
En[3]=5 Fwhm(G)[3]=0 "L/F"$= -2$
then its Gaussian width will be calculated as
Fwhm(G)[3]=Fwhm(G)[1]+k$*$En[3]$-$En[1],
where the slope k=Fwhm(G)[2]$-$Fwhm(G)[1]/En[2]$-$En[1].
The result: Fwhm(G)[3]=0.3
The numerical values will change once the fitting procedure starts, but the relationship between them remains defined by the above equations. If you fix the width of the first reference peak, then only the slope k can change. If you fix both of the reference peaks, then the widths of all the energy-dependently linked peaks will remain fixed.
2) A modification of the PCI lineshape, using the full analytical form$*$, which is suitable also very close to the ionization threshold. The *shape* parameter for this type is 'p0'. In most cases, it is almost identical to the 'p' shape, but is much slower to calculate.

$*$ as defined by van der Straten et al., Z. Phys. D, vol. 8, p. 35 (1988).

8) Error analysis

Sometimes it is important to obtain error bars for the energies, intensities and other fit results. There are various methods for error analysis. The macro *FitErrors*, which is a part of this package, uses Monte-Carlo simulated data sets to perform error analysis. Its advantage over other methods is that it works well with strongly correlated parameters. However, due to the nature of the method, it is rather slow.

The macro is contained in the file *FitErr.ipf*, which you can load either manually or, if you plan to use it regularly, can be copied to the *Igor Procedures* folder, from where it loads automatically. Before running the macro, however, you should generate a fit curve that represents the measured spectrum as well as possible. It might be necessary to temporarily release some linked or fixed parameters or even add new peaks. The idea here is to create a template for the spectrum, that represents all its features but is free of statistical noise. After generating such a fit, type on the command line:
duplicate/o d, noiseless

After this, revert back to your original fit settings (remove extra peaks etc.) and run a fit once. Then start *FitErrors*. It takes one parameter, *nloops* - the number of Monte-Carlo spectra to generate from the template and fit. It then calculates standard deviations of the *nloops* values of each fit parameter, so use your own judgement of how many values are satisfactory. In general, nloops shouldn't be <25. If the macro takes too long to run, you can increase the convergency limit somewhat, running *Setup*.

After quite a while, a table is generated with error bars (standard deviations) for each parameter. In addition, in the last column there is a coefficient showing how many times is the error of the peak area larger than the square root of the area. For well-defined single peaks, this should be close to 1, whereas strongly overlapping peaks or peaks with high background can have quite large coefficients. Small peaks which are linked by other parameters (such as widths) to stronger peaks, can have this parameter less than 1.

Appendix

The formula for the PCI shape 'p' is:

$curve =$
$int/(1+4*(x+de-en)^2/fwhml^2)*exp(2*asym*atan(2*(x+de-en)/fwhml))$,
where

$de = asym * fwhm/2$

and *fwhml* is the Lorentzian width. This shape is then convoluted by a Gaussian. Note that the energy parameter refers to the actual peak maximum position, which is shifted by the amount of *de* due to PCI.

The formula for the Fano profile 'f' is:

$curve = int * ((qpar + 2 * (x - en)/fwhml)^2/(1 + (2 * (x - en)/fwhml)^2))$,

where

$qpar = asym/(1 - abs(asym)), (-1) < asym < 1.$